DOI: 10.1002/ (adma.201707271-accepted manuscript)
Article type: Review

Energy Harvesting Research: The Road from Single-source to Multi-source

Yang Bai*, Heli Jantunen, and Jari Juuti

Dr. Y. Bai, Prof. H. Jantunen, Dr. J. Juuti
Microelectronics Research Unit, Faculty of Information Technology and Electrical Engineering, University of Oulu, FI-90014, Finland
E-mail: yang.bai@oulu.fi

Keywords: hybrid energy harvesters, multi-source energy harvesting, piezoelectric, pyroelectric, photovoltaic; photoferroelectrics

Abstract:

Energy harvesting technology may be considered an ultimate solution to replace batteries and provide a long-term power supply for wireless sensor networks. Looking back into its research history, individual energy harvesters for the conversion of single energy sources into electricity were developed first, followed by hybrid counterparts designed for use with multiple energy sources. Very recently, the concept of a truly multi-source energy harvester built from only a single piece of material as the energy conversion component has been proposed. This review, from the aspect of materials and device configurations, tells the entire story with a wide scope to give an overview of energy harvesting research. It covers single-source devices including solar, thermal, kinetic and other types of energy harvesters, hybrid energy harvesting configurations for both single and multiple energy sources and single-material, multi-source energy harvesters. It also includes the energy conversion principles of photovoltaic, electromagnetic, piezoelectric, triboelectric, electrostatic, electrostrictive, thermoelectric, pyroelectric, magnetostrictive and dielectric devices. This is one of the most comprehensive reviews conducted to date, focusing on the entire energy harvesting research scene and providing a guide to seeking deeper and more specific research references and resources from every corner of the scientific community.

1. Introduction

Renewable energy, in the forms of light, heat, fluid, motion, etc., can be converted into electricity. This can make a valuable contribution to solving the issues of the expected fossil fuel shortage in the near future as well as to reduce emissions and toxic waste into the environment. Among the potential next-generation energy sources for green electricity production, solar and wind (or other fluids e.g. ocean waves) are the most popular.[1] Such energy sources are promising to fulfil the mission of converting and generating macro-scale (> W level) power for industrial or domestic use. However, the relevant research topic of focusing on the micro-scale (< W level, usually nW to mW) was not realized until the first investigation of using a device to convert micro-kinetic energy into electricity in 1984.[2] The modern concept of energy harvesting (or power harvesting, energy/power scavenging) was then systematically proposed and reviewed in the 2000's.[3, 4] It is defined as the process by which environmental energy, including but not limited to light, thermal and kinetic energy, which otherwise would be dissipated and wasted, is harvested and converted into usable micro-power electricity to supply wireless sensor networks (WSN).[4-6] The device realizing the energy harvesting function is called an energy harvester. The idea was initiated in order to replace batteries and avoid redundant wiring. It is well known that batteries have issues of safety (risk of explosion at high temperatures or under severe shock), reliability (risk of failure at low/high temperatures and after a long operation time) and environment (tens of billions of batteries containing non-environmentally friendly elements are disposed of annually). Furthermore, with the rapid development of smart systems, the number of WSN will soon become too large to cope with. For instance, the number of WSN (e.g. smoke detectors, thermostats, smart light switches, etc.) installed in a single office building could easily reach 10,000. Meanwhile, more WSN will be operating in remote/harsh/isolated environments. In these situations, the workforce for battery recharging/replacement, rather than the batteries themselves, will be unsustainably costly. Therefore, unlike macro-scale power generation where electricity is usually produced in an

energy-rich place and is then transported to end users in another place, energy harvesting technology features cable-less, battery-less (although in some cases temporary energy storage e.g. capacitors, supercapacitors and fast charging/discharging batteries is needed) and on-site electricity generation.

Nowadays, energy harvesting technology is considered to be the ultimate solution to replace batteries (or at least to be a supplement to batteries) thus providing a long-term (over 10-20 years) power supply to WSN. Energy harvesters integrated with the WSN enable them to convert ambient/environmental/waste energy existing in their working environment into electricity, and autonomously power themselves without the need for maintenance. Conventionally, an energy harvester is designed for only one particular type of energy source. For instance, photovoltaic harvesters can only harvest light; piezoelectric, electromagnetic, electrostatic, triboelectric, etc. harvesters are only designed for kinetic energy; and pyroelectric and thermoelectric harvesters are usually specially made for harvesting thermal energy. However, in many cases, the output power of single-source energy harvesters cannot completely fulfil the power requirements of the WSN, partly because the energy source may not always be stable or continuously available in reality. For instance, a kinetic energy harvester is usually expected to harvest machinery vibration or human movement. However, the machine may not operate constantly and a person will have to rest. In these situations, the input kinetic energy provided to the kinetic energy harvesters may be insufficient. According to the law of conservation of energy, a lower or unstable input energy means a drastic drop in an energy harvester's collected energy and average output power. Therefore, the kinetic energy harvesters may not be able to generate sufficient output power to drive the WSN. Similar situations also occur with thermal and photovoltaic energy harvesters when there are fewer temperature fluctuations/gradients and significant cloudy days/dark environment, respectively.

However, in most situations, a variety of energy sources co-exist. For instance, kinetic and thermal energy typically co-exist in machines and human bodies. Solar energy provides not

only a source of visible light energy but also provides thermal energy from different wavelengths. In some case, e.g. a human performing outdoor activities, light, thermal and kinetic energy sources co-exist simultaneously. In these situations, single-source energy harvesters cannot harvest all of the energy sources and ‘‘waste’’ a significant amount of the harvestable energy, thus hindering the maximization of their energy harvesting capability. Therefore, hybrid energy harvesters which are able to harvest multiple energy sources have been developed by some researchers. Among the hybridization of light, kinetic and thermal energy harvesters, structural optimization is the most used methodology. Different energy conversion materials and configurations responsible for different energy sources are integrated into a hybrid structure. The number of harvestable energy sources for the hybrid energy harvesters is increased and the output power is significantly improved when the harvesters suffer instability of a particular energy source(s), compared to the case for previous single-source energy harvesters.

Apart from the method of structural optimization, the discovery and development of multi-functional materials to achieve multi-source energy harvesting has recently started to attract attention. Compared to the structural optimization method, where different energy conversion materials need to be physically combined in a complex configuration, a single multi-functional material is able to harvest multiple energy sources, thus avoiding the complex structures of conventional hybridization. Multi-functional materials require the different energy conversion mechanisms to co-exist in the same material for them to be comparable to single-functional energy harvesting materials. It is also important that the energy conversion effects can occur simultaneously and do not counteract or cancel each other. Therefore, it needs a great effort for the materials’ development.

A number of high-quality reviews from single-source energy harvesting already exist including photovoltaic, piezoelectric, pyroelectric, triboelectric, electrostatic, elastomers, thermoelectric, etc. Therefore, in this review they are briefly summarized to provide clues for further reading,

with only the latest progress being discussed. However, after decades of development, there is no single article summarizing the entire research field of energy harvesting, covering both single-source and multi-source harvesters. This review provides an overview of this entire subject. The focus of this review is on the multi-source energy harvesters – hybrid energy harvesters through structural optimization and multi-functional materials. The review will further focus on the multi-functional materials, especially the perovskite structured materials which have been found to be promising candidates for the simultaneous harvesting of light, kinetic and thermal energy sources.

It should be pointed out that this review involves two of the three main aspects of energy harvesting research topics – materials and devices. The other aspect – power management circuitry – which is closely related to the subject of electronics – is not in its scope. Readers who are interested in power management can refer to references[7, 8] for information. Meanwhile, some of the pure modeling works have also been cited in this paper. These works are considered to provide novel device designs, although they were not experimentally validated. A recent comprehensive review is available for professional information relevant to pure modeling works related to energy harvesting.[9]

In the following content, Section 2 presents the development of single-source energy harvesters, including photovoltaic energy harvesting materials and solar cells (Section 2.1), kinetic energy harvesting materials and devices (Section 2.2), thermal energy harvesting materials and devices (Section 2.3) and others (Section 2.4). In Section 2.2, triboelectric, electrostatic, electromagnetic, piezoelectric, electrostrictive and magnetostrictive energy conversion effects are presented successively. Thermoelectric, pyroelectric and other indirect effects are covered in Section 2.3. Section 3 presents hybrid energy harvesters, including hybrid structures for single-source (Section 3.2) and multi-source (Section 3.3) harvesting. Different energy source combinations are presented in Section 3.3. Section 4 discusses the development of multi-

functional materials for multi-source energy harvesting in detail. Section 5 concludes this review and gives the perspectives for further research in the field.

2. Development of single-source energy harvesters

2.1. Photovoltaic energy harvesting materials and solar cells

The photovoltaic effect is the only principle enabling direct conversion of solar (light) energy into electricity. It has been rapidly developed and commercialized during recent decades. The advantages of photovoltaic energy harvesting include large power densities (up to 39 mW cm^{-2}) under sufficient outdoor sunlight, easy integration with host structures and a steady working status without noise or emissions.[10, 11] The photovoltaic energy conversion efficiency (under ''one-sun'' illumination, corresponding to 1 kW m^{-2} according to ASTM G-173-03, International standard ISO 9845-1, 1992) and the band gap are the crucial criteria by which to judge the energy harvesting capability of photovoltaic materials and devices. Compared to the efficiency which can be optimized by tuning the structure of the entire device[12], the band gap is an intrinsic property of the photovoltaic materials. It determines the Shockley-Queisser (S-Q) limit, i.e. the theoretical maximum photovoltaic energy conversion efficiency that a single-junction solar cell can achieve. Each band gap corresponds to an S-Q limit. The band gap of 1.34 eV gives the largest possible S-Q limit of 33.7 %.[13] Research into photovoltaic materials strives to approach as closely to this limit as possible.

To date, many efficient photovoltaic materials have been developed, including conventional monocrystalline and multicrystalline Si, GaAs, InP, GaInP, $Cu(In,Ga)(Se,S)_2$ (CIGS), CdTe, etc. as well as emerging dye-sensitized TiO_2, thin-films, organics, quantum dots, $Cu(Zn,Sn)(S,Se)_2$ (CZTS), organic-halide perovskites, etc. Among these photovoltaic materials (single-junction cells), GaAs holds the record for $\boldsymbol{\eta_{photo}}$ of > 28 %, and Si also provides a very high $\boldsymbol{\eta_{photo}}$ of 20-27 %. There are many comprehensive reviews focusing on the development

of photovoltaic materials, including general reviews of all materials[14-17], conventional Si[18], dye-sensitized materials[19-22], organic materials[23-31] and quantum dots[32].

Very recently (since 2009), perovskite structured organic halide materials have been researched for photovoltaic applications. The chemical formula of these materials can be expressed as $MANX_3$, $EANX_3$ or $FANX_3$, where MA means methylammonium ($CH_3NH_3^+$), EA means ethylammonium ($CH_3CH_2NH_3^+$), FA means formamidinium ($NH_2CH{=}NH_2^+$), N represents Pb^{2+}, Sn^{2+}, Ge^{2+}, etc, and X can be F^-, Cl^-, Br^-, I^-, etc. Among all the photovoltaic materials, the organic-halide perovskites have shown a great potential to surpass the conventional Si and GaAs materials. The $\boldsymbol{\eta_{photo}}$ of the organic-halide perovskites has been increased by more than 7 times from about 3 % in 2009 when they were firstly reported to more than 22 % within a relatively short research period of 8 years, compared to decades for Si. The record $\boldsymbol{\eta_{photo}}$ of the organic-halide perovskites has been reported by Yang et. al., where 22.1 % and 19.7 % were achieved in small cells and in 1 cm^2 cells, respectively.[33]

The advantage of the organic-halide perovskites is that they have a high charge carrier mobility.[34] This implies that the charge carriers in these materials, i.e. the light-generated electrons and holes, are able to transit a distance which is large enough for them to be extracted as current, rather than losing their energy as heat. Furthermore, these perovskites use cost-effective elements and consume less energy for manufacture compared to conventional photovoltaic semiconductors which require rare elements (e.g. tellurium, gallium, indium) and high-temperature fabrication processes (typically 300-600 ˚C). There have also been many comprehensive reviews focusing on perovskite photovoltaic materials/solar cells.[35-44]

On the other hand, the organic-halide perovskites suffer from the issue of instability. They usually degrade very rapidly compared to conventional Si and other solar cells due to thermal/chemical instabilities, phase transformations, exposure to visible/UV light, moisture and oxidation.[42, 45, 46] For instance, during the 1000-hour accelerated aging test under different

conditions, i.e. under light soaking at 60 ˚C and 85 ˚C, in 85 ˚C thermal and 85 relative humidity cycling, and under UV light exposure, crystalline Si solar cells only lose 5 % of their initial performance.[47] By contrast, those organic-halide perovskite solar cells which exhibit comparable efficiency to that of the Si cells (~ 20 %) lose significantly more than 10 % (the threshold for commercialization) of their initial performance.[45] In most cases, the data of concerning the stability of organic-halide perovskite materials or solar cells are not reported in the literature. However, this is as great a challenge obstructing the path of the organic-halide perovskites towards commercialization as it is for their Si-based counterparts.

The mechanisms of degradation of the organic-halide perovskite solar cells are not yet fully understood. There are updated reviews discussing the hypotheses and methods to improve the stability of these solar cells.[44, 45, 48] Both the organic-halide perovskite materials and other components (e.g. electrodes) in the devices can cause instability. For instance, in high humidity and/or under light, the $MAPbI_3$ cells are likely to decompose. When exposed to oxygen and moisture, oxidation of both the metal electrodes and the organic components may occur. In terms of the material stability, FA-based organic-halide perovskites are more thermally stable than their MA-based counterparts. Thus, a mixed MA/FA-based composition may show improved stability. For instance, a $0.05MAPbBr_3$-0.95α-$FAPbI_3$ composition is reported to maintain > 93 % of its initial performance (> 22 % efficiency) after about 13 months of storage at ambient conditions.[33] In addition, partially replacing the halide with pseudohalogen (e.g. SCN^-) and the development of 2D perovskites may help to improve the material stability in high humidity and under illumination.[44] In terms of the device stability, Chen et al. used highly doped inorganic charge extraction layers in planar organic-halide perovskite solar cells. This helped to achieve rapid carrier extraction thus eliminating local defects. Over 90 % of the initial performance (> 15 % efficiency) was retained after a 1000-hour light soaking test, indicating a significantly improved stability with less sacrifice of the initial performance.[49] Recently, the elimination of hole transport materials and metal cathodes (e.g. using carbon materials as an

alternative) in organic-halide perovskite solar cells has also shown potential for inducing high stability.[48]

The organic-halide perovskites presented above mostly contain Pb, which is a toxic element both for humans and the environment. As a consequence, the European Union has introduced legislation to replace Pb (together with other hazardous substances) with alternative safe elements/materials.[50, 51] In photovoltaic modules (and piezoelectric components as presented below), Pb is currently allowed. However, the research for lead-free perovskites is very much motivated by a long-term consideration of the legislation, human health and the environment. Several Pb-free perovskites for photovoltaic applications have been developed, including Sn-based compositions with record efficiencies of 3.6 % for $CsSnI_3$[44], 6.4 % for $MASnI_3$[52], 4.8 % for $FASnI_3$[53] and 8.1 % for $(FA,MA)SnI_3$[54], and Bi-based compositions such as $MABi_3I_9$, $CsBi_3I_9$, Cs_2AgBiX_6 (X = Br, Cl), $(MA)_2KBiCl_6$, etc. with improved stability compared to $MAPbI_3$ but with low efficiencies (~ 1%)[44]. The developed lead-free perovskite solar cells have not shown efficiencies competitive with those of Si-based and Pb-based counterparts.

Alongside the organic-halide perovskites, ABO_3 structured perovskites have also been investigated for photovoltaic applications. **Figure 1** shows the schematics of the unit cells of the ABO_3 and organic-halide perovskites. The difference between these two types of perovskites can be clearly seen in the figure. In Figure 1 (a), the A site atoms occupy the eight corners of the cubic unit cell; the B site atom occupies the center; and the oxygen atoms sit at the six face centers thus forming an oxygen-octahedral. There are many elements which can fit into the ABO_3 type unit cells to form perovskite structures. Representatives are Pb, Ba, K, Na, Sn, Bi for the A site and Zr, Ti, Nb for B site. Details of the ABO_3 perovskite structure can be found in reference[55]. In Figure 1 (b), there are two types of I (or X for a generic chemical formula) atoms. I1 atoms sit between two Pb (or N) atoms and are connected with $–CH_3$ and $–NH_3$ groups. I2 atoms are only connected with Pb atoms. The I1 and I2 atoms form an I- (or X-) octahedron.

Although the ABO_3 type perovskites have not been reported to achieve as a high $\boldsymbol{\eta_{photo}}$ as those of their organic-halide counterparts, they still have attracted much attention for use as light absorbers and energy harvesters because of their stability compared to that of the organic-halide perovskite compositions. Unlike the instability issue presented above, the ABO_3 structure has proved its stability and reliability over a long history. For instance, the $PbTiO_3$ (PT), $Pb(Zr,Ti)O_3$ (PZT) and $BaTiO_3$ (BTO) based compositions have been known for more than 50 years and have been widely used in industry for decades as dielectric, ferroelectric, piezoelectric and pyroelectric materials. In addition, the ABO_3 perovskites have shown a widely tunable range of band gaps (1.1-2.0 eV) which are suitable for visible light absorption and harvesting.[56] More recently, it has been found that an ABO_3 perovskite – BTO – is able to exhibit a $\boldsymbol{\eta_{photo}}$ which exceeds the S-Q limit, despite the fact that the band gap of BTO is greater than 3 eV so that less than 10 % of the energy in the solar spectrum is absorbed.[13] This is because the bulk photovoltaic effect (BPVE) in non-centrosymmetric crystals, e.g. tetragonal BTO, results from the photo-exited non-thermalized electrons losing their energy and descending to the bottom of the band.[13, 57] In comparison, in conventional solar cells the high $\boldsymbol{\eta_{photo}}$ relies on strong absorption of the energy in the solar spectrum to promote the carrier movement in the band.[13] Details will be given below in Section 4.

Another reason for the research interest is that the ABO_3 type perovskites with asymmetric unit cell structures (e.g. tetragonal, orthorhombic, rhombohedral) were initially found to be good ferroelectric materials. This strong ferroelectricity enables them to generate strong piezoelectric and pyroelectric effects. By contrast, although the organic-halide perovskites may have the potential to exhibit piezoelectricity, whether they are ferroelectric and pyroelectric or not is still controversial.[58, 59] Considering their potential to be piezoelectric, pyroelectric and photovoltaic simultaneously, the ABO_3 type perovskites have very recently become popular candidates for the multi-functional materials in multi-source energy harvesters.[60] This will also be discussed

in detail in Section 4 below. **Table 1** summarizes the representative examples of photovoltaic energy harvesting materials and devices in terms of materials, configuration, output voltage, power, power density and energy conversion efficiency. More detailed data can be found in reference[10].

2.2. Kinetic energy harvesting materials and devices

2.2.1. Overview

In principle, kinetic energy is everywhere because all matter on earth vibrates due to its internal chemical or physical activities. Kinetic energy includes (but is not limited to) fluid motion, vibration, stress and strain. It is as common a source of energy in the environment as light. The earliest kinetic energy harvesting dates back to that the first hydroelectric power scheme was demonstrated in 1878 and the first battery charging using wind turbines was carried out in 1887. Nowadays, fluid and wind energies are converted into electricity at macro-scale power levels (> W) by mature technologies. However, most recent research related to kinetic energy harvesting refers to micro-scale power levels (< W). Usable kinetic energy which can be effectively harvested usually exists within a host, e.g. buildings/constructions such as roads and bridges vibrating at their eigenfrequency, operating machines, human bodies in daily activities or sports, etc. Together with light source energy harvesting, kinetic energy harvesting is another popular research topic, with over 8,500 academic research papers published in the last 10 years. The biomechanical energy generated from a human's daily life has been considered an attractive source to be harvested in order to power wearable smart devices.[61] The first publication regarding the scavenging of biological motion reported the integration of an energy harvesting system with an animal's ribs.[2] This idea has encouraged a large amount of research to investigate the possibility and feasibility of harvesting human biomechanical energy. Representative examples include shoe-mounted generators in the heel or sole[62-66], medical implants[67-70], wearable devices harvesting head, wrist and arm motion[71-74] and backpack

shoulder straps[75-77]. There are comprehensive reviews available which focus on such biomechanical/human energy harvesting.[78-82]

In addition to the biomechanical energy harvesting, vibrational energy harvesting on machines and constructions has also been emphasized because their conditions need to be continuously monitored in the light of increasing safety concerns and for well-timed maintenance breaks. As the built machines and constructions become aged, together with the fact that the number of newly built structures is drastically increasing, any hidden or potential damage in the structures could put residents or users at risk. In terms of the sensors to be used for such monitoring, the necessary power supplies would represent a large proportion of the expense due to tedious wiring and costly battery recharging/replacement requirements once the sensors have been embedded in the structures. Harvesting vibrational energy dissipated from these structures could solve these issues. To date, many energy harvesting powered structural monitoring systems have been reported, including those for asphalt pavement[83-87], oil pump[88], vehicle suspension[89-91], bridge[92-97], vehicle tire[98-104], railway and train[105-112], aircraft and spacecraft[113-118]. There are also plenty of comprehensive reviews discussing the topic of vibrational energy harvesting.[9, 119-126]

Representative kinetic energy harvesters are summarized in Table 1 in terms of materials, configurations, output voltage, power, power density and energy conversion efficiency.

2.2.2 Triboelectric energy harvesting

The triboelectric effect is the phenomenon where a material becomes electrically charged after being contacted by a different material in a friction motion.[127] However, it being considered a negative effect causing unpleasant experiences in daily life, it was not used for modern kinetic energy harvesting technology until Z.L. Wang's group published their extensive research in triboelectric nanogenerators in 2012.[128] There are already a number of comprehensive reviews summarizing the materials and configurations of triboelectric energy harvesters.[127, 129-139]

In addition, it is worth pointing out that recently Seung et al. has made a significant advancement for triboelectric energy harvesters. Unlike previously developed triboelectric energy harvesters in which pure polymers (e.g. PDMS (polydimethylsiloxane), PTFE (polytetrafluoroethylene), etc.) were used, Seung et al. spread BTO ($BaTiO_3$) nanoparticles in a copolymer matrix – P(VDF-TrFE) (poly(vinylidenefluoride-co-trifluoroethylene) – to form a nanocomposite.[140] **Figure 2** (a) shows the schematic structure, in which 5 wt. % of the BTO nanoparticle addition gave the optimum output voltage and current. The introduction of the ferroelectric-phase BTO significantly improved the charge-trapping capability because of the presence of the high-permittivity dielectric ceramic nanoparticles. As indicated in Figure 2 (b), the poled BTO contributed to the boost of output compared to non-poled pure P(VDF-TrFE) and BTO-P(VDF-TrFE) nanocomposite as well as poled pure P(VDF-TrFE). Their triboelectric energy harvester made from such a nanocomposite showed a 150 times higher output power (6.4 mW) and 22 times higher power density (710 μW cm-2) than those of the pure polymer-based counterpart. This has solved the issue of low output current in conventional triboelectric energy harvesters made from pure polymers, and thus demonstrating the capability of charging a smart watch. Figure 2 (c) compares the charging capability of the triboelectric energy harvesters made from pure PTFE and BTO-P(VDF-TrFE) nanocomposite, where the latter is about 20 times more efficient than the former. It should be noted that both BTO and P(VDF-TrFE) are ferroelectric materials and have the potential to exhibit piezoelectric and pyroelectric effects. This may provide an opportunity to develop a hybrid energy harvester.

2.2.3 Electrostatic energy harvesting

In principle, the triboelectric effect is included in the broader electrostatic effect. Differing from the triboelectric generators, which require the contact and friction of two materials, electrostatic energy harvesters work in a contactless mode. Meanwhile, for electrostatic energy harvesters, an external voltage source is always necessary to maintain the electrical potential.

This is likely to increase the complexity of the energy harvesters, and consequently they are sometimes criticized as not representing true energy harvesting technology (which assumes independence of external electric sources).

However, there is an exception – electrostatic energy harvesters made with electrets. An electret is a type of dielectric material with quasi-permanent charges. It is similar to a charged capacitor, but due to the low leakage and intrinsic dipole polarization, the charges can be retained for many years (quasi-permanent charge storage).[141] The working principle of electret-based energy harvesters is similar to that of the conventional electrostatic ones but without the need for the external voltage source. There are two groups of electret materials – inorganic electrets e.g. SiO_2 based materials[142, 143] and polymer electrets e.g. PTFE (also called Teflon)[144-146], FEP (fluorinated ethylene propylene)[147], CYTOP (amorphous perfluorinated polymer)[148, 149], parylene[150-153], etc. Inorganic electrets exhibit a high surface charge density but also an instability in the long term. Polymer electrets have better long-term stability but a lower surface charge density. There are only a few reviews focusing on electret-based energy harvesters.[125, 141] Some novel representative works which are not included in the published reviews are introduced here.

Lu et al. reported a flexible, paper-based energy harvester made from 3 layers of electret films, i.e. PVDF-PTFE nanofibers covered by parylene C. A peak output power and maximum power density of 46 μW and 7.3 μW cm^{-2}, respectively, were generated with a maximum force of 0.5 N.[153] Xiao and Chen et al. developed flexible bipolar electret membranes, PTFE/THV/PTFE and FEP/THV/FEP where THV referes to a termolymer (tetrafluoroethylene (TFE)-hexafluoropropylene (HFP)-vinylidene (VDF)). A peak output power of 4.7-14.4 μW and maximum power density of 34.8-50 μW cm^{-2} were achieved under different kinetic input conditions.[146, 147] Ahmed et al. proposed a SiO_2 electret-based energy harvester with an angular electrode structure and matched power management circuitry. Driven by the kinetic input which is compatible with the *in-vivo* vibration source, e.g. artery pulse and heartbeat, the harvester

could generate an output power and power density of 9.6 μW and 109.7 μW cm^{-2}, respectively.[154] Bi et al. designed a freestanding-electret rotary generator which gave the record output power density and energy conversion efficiency in electrostatic energy harvesters. **Figure 3** shows the design and working principle. The disc-shaped rotary generator consisted of a rotor (a PMMA (poly(methyl methacrylate) layer and a PTFE layer) and a stator (a Cu layer and an FR4 (a composite of woven fiberglass cloth and an epoxy resin binder) layer) stacked together with an air gap in between (Figure 3 (a)). With the rotation rate of 750 rpm, the harvester delivered an average output power of 10.5 mW, power density of 420 μW cm^{-2} and efficiency of 56 %.[155]

Eectrostatic energy harvesters can be easily fabricated into micro-scale and integrated with micro-systems (e.g. MEMS (microelectromechanical systems)). This ease of miniaturization utilizing a range of microfabrication techniques is an important advantage compared to other energy harvesters. However, in recent years, due to the development of the piezoelectric energy harvester, which can also be easily miniaturized but does not require an external voltage source, electrostatic energy harvesters have attracted less attention compared to a decade ago. There is only one review solely focusing on electrostatic energy harvesting.[125] Other relevant reviews are usually included in those of comprehensive kinetic energy harvesting.[9, 119]Most of the recently developed electrostatic energy harvesters are electret-based, as presented above.

2.2.4. Piezoelectric energy harvesting

Piezoelectricity is defined as the phenomenon where charge displacement (or electric potential) is generated across a material when it is strained under an applied force (direct piezoelectric effect), while, conversely, strain of the material will be induced when it is placed in an external electric field (converse piezoelectric effect). Piezoelectric energy harvesting employs the direct piezoelectric effect, converting kinetic energy input (e.g. strain, stress, vibration, impact, etc.) into electricity. It is a very straightforward method to convert kinetic energy into electricity,

meaning piezoelectric energy harvesters neither require external voltage sources as in the electrostatic and electrostrictive counterparts (to be presented below) nor two relatively moving parts as in the triboelectric and electromagnetic counterparts (to be presented below). In principle, a piece of piezoelectric material is able to complete the energy conversion process. This enables the piezoelectric energy harvesters to be miniaturized easily and to be made/integrated into complex shapes/structures. As a result, among all the kinetic energy harvesting research, most have been carried out on piezoelectric energy harvesters, with nearly 5,000 publication in the last 10 years (approximately 60 % of the total number of all kinetic energy harvesting publications).

The maximum electrical energy ($\boldsymbol{u}$) that can be generated in a piezoelectric energy harvester is expressed by **Equation 1**. In the equation, $\boldsymbol{k}$ is a dimensional constant determined by the shape and structure of the piezoelectric energy harvester, $\boldsymbol{d}$ is the piezoelectric charge coefficient, $\boldsymbol{g}$ is the piezoelectric voltage coefficient, $\boldsymbol{F}$ is the input force applied to the piezoelectric harvester, and $\boldsymbol{\varepsilon_{33}^{\sigma}}$ is the permittivity along the polarization direction in the unclamped state.

$$\boldsymbol{u} = \frac{1}{2}\boldsymbol{k}(\boldsymbol{d}\cdot\boldsymbol{g})\boldsymbol{F^2}; g = \frac{d}{\varepsilon_{33}^{\sigma}} \quad (1)$$

It can be clearly seen in Equation 1 that the electrical output of a piezoelectric harvester is dominated by the $\boldsymbol{d}\cdot\boldsymbol{g}$ term (defined as the piezoelectric figure of merit), if the dimensions, structure and input energy remain unchanged. Therefore, the fundamental research for piezoelectric energy harvesters is the exploration of the highest possible piezoelectric figure of merit. Soft PZT (e.g. PZT-5H) is the most frequently used composition for piezoelectric energy harvesting research. However, soft PZT is most suitable for sensors and actuators and does not necessarily have the highest figure of merit. To the current state of the art, some particularly tuned and doped PZT-based compositions have shown the highest $\boldsymbol{d}\cdot\boldsymbol{g}$ values. Seo et al. reported the compositions of $0.68Pb(Zr_{0.47}Ti_{0.53})O_3$-$0.32Pb[(Ni_{0.6}Zn_{0.4})_{1/3}Nb_{2/3}]O_3$ and $0.65Pb(Zr_{0.45}Ti_{0.55})O_3$-$0.35Pb(Ni_{1/3}Nb_{2/3})O_3$ which exhibited the $\boldsymbol{d_{33}\cdot g_{33}}$ values of $2\text{x}10^{-11}$ m^2

N^{-1} and $1.65x10^{-11}$ m^2 N^{-1}, respectively.[156, 157] Jeon et al. achieved a similar level of $\boldsymbol{d_{33}\cdot g_{33}}$ value of $2.03x10^{-11}$ m^2 N^{-1} with the composition $0.72Pb(Zr_{0.47}Ti_{0.53})O_3$-$0.28Pb[(Zn_{0.45}Ni_{0.55})_{1/3}Nb_{2/3}]O_3$.[158] These values are much larger than PZT's 0.73-1.68 $x10^{-11}$ m^2 N^{-1}. By developing a lead-free piezoelectric composition, $(Na_{0.5}K_{0.5})_{0.94}Li_{0.06}NbO_3$+2 mol% Mn^{2+}, Zheng et al. obtained a $\boldsymbol{d_{33}\cdot g_{33}}$ value of $0.93x10^{-11}$ m^2 N^{-1}.[159] As for the Pb-based organic-halide perovskites presented in Section 2.1, the substitution of non-toxic elements for the toxic Pb in conventional PZT based piezoelectric compositions is also one of the ultimate research topics in almost all piezoelectric related subjects. Details of the lead-free piezoelectric research can be found in some specific articles.[55, 160] Beside these ceramic compositions, semiconductors of ZnO and AlN (e.g. in the forms of thin-films, nanowires, etc.)[161-164], polymer PVDF (polyvinylidene fluoride) and its copolymers[162, 165] and macro-fiber composites[166, 167] have also been used in piezoelectric energy harvesters.

Apart from the tuning of the material composition, the rest of the piezoelectric energy harvesting research has focuses on the structural design and optimization for different applications. The most popular structures used in piezoelectric energy harvesters include cantilever[73, 168-192], stack[193] cymbal configuration[194-203], diaphragm configuration[112, 204-214] and shear mode configuration[215-224]. The cantilever structure is suitable for low input force, small acceleration and mid-high frequencies (tens of Hz or above), but it allows large amplitude/deformation. The stack structure can effectively increase the output. The cymbal configuration is able to withstand significantly higher loads and is suitable for low working frequencies (several Hz). The diaphragm configuration is suitable for working with high accelerations or in fluctuating pressure environments. In these structures/configurations, the polarizations of the piezoelectric components are perpendicular to the electrodes. In comparison, for the shear mode configuration the polarizations are parallel to the electrodes. The piezoelectric response of the shear mode is even higher than that of the typical

electromechanical coupling modes used in other configurations[215, 216] although the fabrication of the materials (e.g. poling, re-electroding) may become complex.

In piezoelectric energy harvesting configurations, pre-stress is a method used to increase the output power and widen the working frequency range. For instance, a pressure energy harvester made with pre-stressed piezoelectric discs has provided an output power density of > 10 mW cm^{-3} which is the record for the energy harvesters made of piezoelectric ceramics, especially for conventional PZT.[66] There are many publications available for the topic of pre-stressed piezoelectric energy harvesters.[66, 112, 211, 225-231]

In the recent decades, nanostructured piezoelectric energy harvesters, usually called piezoelectric nanogenerators, have attracted the research community's attention and experienced a period of intensive research activity. These harvesters are made with piezoelectric thin-films[232, 233], nanoparticles[234], nanowires/rods/fibers/tubes[235-238] and nanocomposites[239, 240] consisting of the above mentioned piezoelectric nanostructures and polymer matrix. Although the microstructures of the piezoelectric nanogenerators are nano-sized, the entire device can be macroscopic. Compared to the counterparts made of piezoelectric ceramics which require high-temperature processing and are rigid, the piezoelectric nanogenerators feature low-temperature fabrication and flexibility. The earliest and most researched piezoelectric nanogenerators to date are built with ZnO nanowires which are relatively simple to fabricate.[161, 235] Later on, fabrication methods of the nanostructure of piezoelectric ceramic compositions including PZT, BTO and other lead-free based materials were advanced and nanogenerators made from these compositions were developed.[241-244] In spite of a relatively short history compared to other piezoelectric energy harvesters, piezoelectric nanogenerators have attracted a large amount of research investigating tens of structures/configurations. Therefore, piezoelectric nanogenerators are actively and regularly reviewed with comprehensive collections of relevant publications.[81, 139, 161-165, 245-249]

Together with the majority of piezoelectric energy harvesting research for vibration, strain, pressure, impact, etc., researchers have also explored the possibility and feasibility of harvesting the kinetic energy carried by wind or other types of airflow and fluid. The idea was raised due to the difficulty and complexity of miniaturizing the conventional electromagnetic wind turbine. There are several configurations designed to convert wind/airflow into electricity via the piezoelectric effect. **Figure 4** shows some representative configurations of piezoelectric windmills. One of them is the contact/impact cantilever structure[250-256], as shown in Figure 4 (a). In such a configuration, a rotor driven by the wind will rotate thus inducing impact on the piezoelectric cantilevers embedded around the rotating shaft. As the contact between the rotor and cantilevers causes wear, thus shortening the lifecycle of the entire harvester, the contactless configuration[257-263] was then developed, as shown in Figure 4 (b). This design replaces the mechanical contacting force applied between the rotor and cantilevers with the magnetic force. Permanent magnets are attached on the rotor shaft and tips of the cantilevers. When the rotor is rotated by the wind, a magnetic attractive and/or repulsive force will be applied to the piezoelectric cantilevers periodically, inducing them to bend. The contact/impact and contactless configurations adopt similar concepts of conventional wind turbines whilst replacing the electromagnetic generator with piezoelectric energy harvesters. Beside these, there are other configurations of galloping[264, 265] and piezoelectric polymers/films/cantilevers/membrane[266-278] excited by the direct blowing force or vortex induced by wind. These configurations introduce some novel concepts such as energy harvester trees[266] or grass[278]. It should be noted that the initial purpose of developing the piezoelectric windmills is to overcome the miniaturization issue of the conventional electromagnetic wind turbine configuration as well as to achieve low-speed airflow harvesting, although not all the research works are beneficial for such purposes. Therefore, careful assessment for a certain case is needed to compare and evaluate the advantages of piezoelectric and conventional techniques. In addition, the configurations employing the piezoelectric effect to harvest fluidic energy are

based on concepts similar to those of wind/airflow piezoelectric energy harvesters. Details can be found in references[279-283].

As shown in Equation 1, the maximum electrical energy that can be generated by a piezoelectric energy harvester ($\boldsymbol{u}$) is proportional to the square of the input force ($\boldsymbol{F^2}$). As the effective input forces applied to the micro-scale piezoelectric energy harvesters through proof mass, pressure, impact, etc. are small, the output power stays at the μW to mW level. However, it can easily be predicted that with an increase of the input force/energy, the increase of the output power will be squared. This has raised some interest in recent years to investigate the feasibility of using piezoelectric energy harvesters for macro-scale energy conversion. The most common large forces in daily life are vehicular loads and vehicle induced vibration. With the combination of a number of piezoelectric energy harvesters, macro-scale output power (~ W level) can be generated by harvesting under-road or roadside kinetic energy. Two configurations, i.e. piezoelectric bulk materials (e.g. discs)[84, 284, 285] and cantilevers/beams or multilayer stacks[86, 286-288], have been used for such macro-scale energy harvesting. The bulk materials are used to harvest vehicular loads (large stress) while the cantilevers (or multilayer stacks) are used to harvest strong vibrations (with high frequency and/or large acceleration) induced by moving vehicles. There is also a review[289] and an article[290] available comparing different harvester configurations.

With the largest number of research and publications, there are also plenty of reviews written about piezoelectric energy harvesting. Readers can refer to the reviews focusing on materials[291-294], devices[11, 64, 121, 292, 293, 295-297] and structural miniaturization[122, 298, 299]

2.2.5 Electromagnetic energy harvesting

Electromagnetic energy conversion is a conventional technology being used in dynamos for macro-scale electricity generation. Conventional wind and water turbines were invented based on this effect. Modern electromagnetic energy harvesters with micro-scale electrical output are

designed to harvest other forms of kinetic energy, e.g. vibrations. One of the popular configurations of an electromagnetic energy harvester is based on a cantilever structure.[300]

Figure 5 shows a novel electromagnetic energy harvester designed for application on a bicycle handle bars.[301] Differing from the popular cantilever configuration which has been used in most electromagnetic energy harvesting research, a magnetic suspension structure was created. As shown in Figure 5 (a), two end magnets were fixed on both ends of a cylindrical tube, whilst a moving magnet was placed in the tube and suspended by the repulsive magnetic forces on both sides, i.e. north (N) to north and south (S) to south. The cylinder was wrapped by four groups of coils as shown in Figure 5 (a) and (b). It was then mounted on the bicycle handle bar thus utilizing the lateral oscillation (weaving motion) of the bicycle frame. The weaving motion is generated in reality because the rider shifts the center of gravity when increasing the pedaling force or accelerating quickly. The harvester was able to generated 6.6 mW output power, equivalent to 0.1 mW cm^{-3} output power density, from normal road riding.

There are reviews published recently which give a comprehensive collection of the representative research results of electromagnetic energy harvesters.[302-304]

Just as conventional electromagnetic energy conversion has achieved success in macro-scale, the modern electromagnetic energy harvester is the only commercialized kinetic energy harvester to date. Perpetuum and EnOcean are the two representative and leading companies specializing in electromagnetic energy harvester powered WSN for the smart structural health monitoring of trains and smart wireless control, respectively.[305, 306] Compared to other types of kinetic energy harvesters, the electromagnetic energy harvesters have advantages in output current but disadvantages in output voltage. Meanwhile, as they contain magnets and coils which occupy much space, they cannot easily be miniaturized. Therefore, they are more suitable for larger-scale energy harvesting where the devices and power supplies in the systems can be large without strict space limits. Other kinetic energy harvesters, e.g. triboelectric and piezoelectric, usually suffer issues of small output current but they typically have large output

voltages compared to the electromagnetic harvesters. Consequently, some hybrid energy harvesters have been developed based on triboelectric/piezoelectric and electromagnetic effects.[307-311] In these hybrid harvesters, the advantages and drawbacks of the different energy conversion mechanisms compensate each other. Such hybrid harvesters will be discussed in detail in Section 3.

2.2.6. Electrostrictive energy harvesting

Electrostrictive energy harvesters are made of electrostrictive polymers (e.g. elastomers) to which are applied DC bias electric fields to induce statics or polarizations within materials. The electrostrictive energy harvesters work as either electrostatic or pseudo-piezoelectric energy harvesters. Compared to other kinetic energy harvesters, electrostrictive energy harvesters have advantages in terms of stretchability and flexibility because of their use of polymers. Their disadvantage is the necessity for an external voltage source, similar to that of electrostatic energy harvesters. The important factors affecting their energy harvesting capability and applicability are the dielectric properties (e.g. permittivity, the higher the better) of the electrostrictive polymers and the operating voltage (external bias DC voltage, the lower the better), respectively.[312] Developed composites made of polymer matrix and dielectric or other fillers[313-319] are typical ways to pursue. There are reviews for electrostrictive energy harvesting.[246, 312, 320, 321] There are also some recent representative works which are not included in the reviews. Yin et al. reported a plasticizer modified electrostrictive terpolymer. An energy conversion efficiency of 34 % and output power density of 4.31 mW cm^{-3} could be achieved with a DC bias electric field of 300 kV cm^{-1}.[322] Tugui et al. developed a highly stretchable free-standing electrode, PDMS-carbon black. By integrating such electrodes with a commercial silicone elastomer (Elastosil), an energy density of 1.1 mJ cm^{-3} was achieved under 200 % strain.[323]

2.2.7. Magnetostrictive energy harvesters

The magnetostrictive effect is the phenomenon where ferromagnetic materials change their shape during magnetization, i.e. with the variation of orientation or intensity of an external magnetic field. Magnetostrictive materials can be combined with piezoelectric materials and permanent magnets and used for vibration energy harvesting. The general process is that the vibration of permanent magnets causes shape changes in the magnetostrictive materials, and then applying the resulting stress or strain to the piezoelectric components. There is a newly published review of this particular topic.[324] As this is a two-stage energy conversion – kinetic to magnetic to electric energy, extra energy loss during the process may decrease the output and efficiency. On the other hand, it enables two energy sources – magnetic field and kinetic energy – to be harvested simultaneously.

2.3. Thermal energy harvesting materials and devices

2.3.1. Overview

Beside solar and kinetic energies, thermal energy is another energy source commonly existing in ambient environments. Thermal energy exists in temperature gradients and fluctuation, e.g. geothermal energy, machine/vehicle waste heat, temperature difference between human body/skin and the atmosphere, etc. Thermoelectric and pyroelectric effects are those mostly used for thermal energy harvesting. In addition, some indirect effects, e.g. via the piezoelectric effect by properly designing thermal coupling configurations, can also be used to harvest thermal energy.

2.3.2. Thermoelectric energy harvesting

Thermoelectric materials, based on the Seebeck effect, are able to directly convert a temperature gradient into electricity in the steady status (without any moving parts as in most kinetic energy harvesters). **Equation 2** defines the thermoelectric figure of merit (***ZT***), where ***S*** is the Seebeck

coefficient, $\boldsymbol{T}$ is temperature, $\boldsymbol{\lambda}$ is the electrical conductivity, and $\boldsymbol{\kappa}$ is the thermal conductivity. A higher $\boldsymbol{ZT}$ will induce a higher thermoelectric energy conversion efficiency.

$$\boldsymbol{ZT} = \frac{\boldsymbol{S^2 \cdot \lambda}}{\boldsymbol{\kappa}} \cdot \boldsymbol{T} \quad (2)$$

There are some potential ways to maximize the $\boldsymbol{ZT}$. Tan et al. have written a comprehensive and deep review[325] to discuss the theoretical and practical methods including the enhancement of carrier effective mass, modulation doping and carrier mobility improvement, the reduction of lattice thermal conductivity, etc. In practice, the nano-structured bulk thermoelectric materials[325, 326] have gained the most success in recent years in terms of achieving $\boldsymbol{ZT}$ values of around or above 2. The nanostructures in bulk thermoelectric materials, i.e. nano-sized grains, lattice distortion, nano-sized point defects, etc., are able to increase the phonon scattering independently, thus decreasing the lattice contribution of the thermal conductivity.[327-338] Comprehensive information on the development of bulk thermoelectric materials can be found in plenty of reviews over the last 10 years.[325, 326, 339-360]

Apart from bulk thermoelectric materials, low-dimensional thermoelectric materials such as thin-films/superlattices/quantum dots[361, 362], composites[363] and polymers[364-371] have also been developed. A supperlattice is a structure containing periodically repeating nanometre-thick layers. Thin-films and superlattices enable the miniaturization of thermoelectric energy harvesters.[372] Meanwhile, they are classified as nanostructured thermoelectric materials which help to increase the phonon scattering thus decreasing the thermal conductivity independently of the electrical conductivity and improving $\boldsymbol{ZT}$.[373-376] For instance, Karppinen et al. recently carried out works on thermoelectric superlattices and thin-films. Pristine ZnO and ZnO-organic superlattices were deposited on cotton textiles via the ALD (atomic layer deposition)/MLD (molecular layer deposition) method.[377] The ZnO-organic superlattice showed two orders of magnitude lower thermal conductivity than the pristine ZnO thin films. Meanwhile, the cotton textile substrate provided the flexibility for application in wearable thermoelectric energy

harvesters, compared to the conventional inorganic, rigid substrates. In addition, Al-doped ZnO/Y_2O_3 multilayer thin-films were deposited by pulsed laser deposition on Al_2O_3 single crystals.[378] The thermal conductivity was one third of the typical value of bulk Al-doped ZnO. Thermoelectric composites usually consist of a polymer matrix and thermoelectric particles (including CNT (carbon nanotubes)/graphene[379]) as the fillers.[363] These composites, as well as thermoelectric polymers, have attracted much research interests recently also by featuring their flexibility which is suitable for application in wearable devices.[380] Thermoelectric polymers typically have the smallest $\boldsymbol{ZT}$ compared to other counterparts, whilst the composites' properties sit between polymers and other thermoelectric materials.[381] The thermoelectric composites should not be confused with thermoelectric nanocomposites, where the former contain a polymer matrix while the latter are the combination of two or more nano-sized thermoelectric compositions which typically do not involve a polymer matrix.[326]

The performance of thermoelectric materials is temperature dependent. The optimum $\boldsymbol{ZT}$ values of different materials are achieved at different temperatures. Thermoelectric materials are classified into different groups according to their optimum working temperature ranges: low temperature up to 200 ˚C (e.g. Bi_2Te_3, Sb_2Te_3), medium temperature from 200 ˚C to 600 ˚C (e.g. PbTe, $CoSb_3$, $CeFe_4Sb_{12}$) and high temperature above 600 ˚C (e.g. SiGe, $Yb_{14}MnSb_{11}$). Plenty of reviews are available from medium/high temperature[336, 382-391] to low temperature[340, 341, 343-345, 347, 348, 350, 388, 389, 391-394] thermoelectric materials.

For the same materials with similar ZT values, the output power depends on the temperature difference ($\Delta\boldsymbol{T}$) between the cold and hot sides, i.e. the larger $\Delta\boldsymbol{T}$ the higher output power. Therefore, the conventional thermoelectric energy harvesters are used in space stations, spacecraft, satellites, missiles, etc.[355, 395, 396] where the $\Delta\boldsymbol{T}$ is large enough to generate decent electricity, even when the $\boldsymbol{ZT}$ values of the thermoelectric materials are not high. They are also proposed to be used to harvest the waste heat in automobiles' engines/exhausting system and heat pipes[397-399]. This is despite the fact that their development has not been very successful

due to their inability to generate suitable output power to match the rapid progress of the electrification of vehicles.[400] However, the development of high $\boldsymbol{ZT}$ thermoelectric materials provides space for a compromise on $\Delta \boldsymbol{T}$.[401] This releases the potential of thermoelectric energy harvesters in e.g. wearable electronics[380] and the internet of things (IoT)[402]. There are also plenty of reviews focusing on the development of thermoelectric energy harvesters from the device aspect.[381, 389, 402-409]

2.3.3. Pyroelectric energy harvesting

While the thermoelectric effect is used to harvest temperature gradient, the pyroelectric effect can be used to harvest temperature fluctuation, i.e. instantaneous or continuous temperature changes. All pyroelectric materials are polar, meaning spontaneous polarizations are present in the materials even without electric fields being applied. When a pyroelectric material is subject to an increased temperature, the polarization will become mis-aligned or less aligned, leading to a reduction in the number of charges bound to the surface thus inducing an electric potential (open-circuit) or current (short-circuit). When cooled down, the initial alignment of the polarization will recover, resulting in the surface being albe to attract/bind more charges and thus inducing an electric potential or current in the opposite direction. An AC output can thus be generated from temperature fluctuation using pyroelectric energy harvesters.

It is worth pointing out that one may easily confuse the concepts of ferroelectricity, piezoelectricity and pyroelectricity. It is important to clarify their differences here as this will be relevant to the fundamentals of Section 4. Ferroelectricity is defined as the phenomenon where the spontaneous polarizations present in the materials that have unit cells in 10 special crystal point groups switch their orientation under an applied external electric field. All ferroelectrics are pyroelectrics; however, this is not true *vice versa* as the orientation of polarizations can be switchable (ferroelectric pyroelectrics) or non-switchable (non-ferroelectric pyroelectrics). Similarly, all pyroelectrics are piezoelectric, but it is not true *vice*

versa. Despite such differences, the strongest piezoelectric and pyroelectric properties are exhibited by poled ferroelectric materials. The corresponding responses of non-ferroelectric pyroelectrics and non-ferroelectric/non-pyroelectric piezoelectrics are relatively weak.[291, 410]

Equation 3 and **4** define the output current ($\boldsymbol{i_{pyro}}$) and figure of merit ($\boldsymbol{FOM_{pyro}}$) of a pyroelectric energy harvester, respectively.[410] In the equations, $\boldsymbol{p}$ is the pyroelectric coefficient, $\boldsymbol{A}$ is the material surface area, $\boldsymbol{T}$ is temperature, $\boldsymbol{t}$ is time, P_s is the spontaneous polarization, and $\boldsymbol{c_V}$ is the volume specific heat. A larger $\boldsymbol{FOM_{pyro}}$ implies a larger amount of generated energy for a given enthalpy input.

$$\boldsymbol{i_{pyro}} = \boldsymbol{p} \cdot \boldsymbol{A} \cdot \frac{\boldsymbol{dT}}{\boldsymbol{dt}};\ p = \frac{dP_S}{dT} \tag{3}$$

$$\boldsymbol{FOM_{pyro}} = \frac{\boldsymbol{p^2}}{\boldsymbol{\varepsilon_{33}^{\sigma} \cdot c_V^2}} \tag{4}$$

Typical pyroelectric materials include the ferroelectric families – TGS ($(NH_2CH_2COOH)_3H_2SO_4$), PMN-PT ($(1-x)Pb(Mg_{1/3}Nb_{2/3})O_3$-$xPbTiO_3$) single crystals, PZT based materials, $LiTaO_3$, BNT-BTO ($(1-x)Bi_{0.5}Na_{0.5}TiO_3$-$xBaTiO_3$) based, KNN ($(K_{0.5}Na_{0.5})NbO_3$) based, PVDF and its copolymer P(VDF-TrFE); and the non-ferroelectric family – AlN, GaN, CdS, ZnO.

Although there is a large amount of research focusing on pyroelectric materials compared to thermoelectric and other sources' energy harvesting, the amount of research into pyroelectric energy harvesters is much less. Bowen et al. has written a comprehensive review[410] about pyroelectric materials and energy harvesters. Therefore, only the pyroelectric works carried out after that review are mentioned below.

In terms of the further development of pyroelectric materials and energy harvesting configurations, a PZT/CFO ($CoFe_2O_4$) multi-layered nanostructure[411] was reported to achieved an energy density of 47.4 J cm^{-3} per temperature fluctuation cycle between -173 ˚C and 27 ˚C. La- or Nb-doped $Pb(Zr,Sn,Ti)O_3$ ceramics[412], single crystals[413] and antiferroelectric films[414, 415] were investigated and achieved a maximum energy density of 4.0

J cm^{-3} per cycle. The compositions of PMnN-PMS-PZT ($Pb[(Mn_xNb_{1-x})_{1/2}(Mn_xSb_{1-x})_{1/2}]_y(Zr_zTi_{1-z})_{1-y}O_3$)[416-418] were also developed, with a maximum output power density of 5.82 mW cm^{-3}. All these materials perform better than conventional PZT-5H (a type of soft PZT). The lead-free compositions such as $LiNbO_3$[419], CSBN ($Ca_{0.15}(Sr_{0.5}Ba_{0.5})_{0.85}Nb_2O_5$)[420], CSAW ($((Ca_{1-x}Sr_x)_8(AlO_2)_{12}WO_4$)[421], BTO based[422] and BNT-BTO based[423] are not necessarily better than PZT for pyroelectric energy conversion, but they are better than conventional lead-free counterparts e.g. ZnO. PZT with aligned porosity proved to have a substantial increase in energy density compared to dense PZT.[424] Modified electrodes, e.g. graphene laminate[425] and meshed electrodes[426], also helped to boost the energy harvesting capabilities of pyroelectric energy harvesters. Recently, pyroelectric energy harvesting with the use of multiferroics and magnetoelectic heterostructures was exploited, which showed much better performance than those with sole ferroelectric pyroelectrics.[427] Multiferroics are materials exhibiting any two or all of ferroelectricity, ferromagnetism and ferroelasticity.

As a larger pyroelectric output power requires a rapid temperature change according to Equation 3, it is relatively difficult to find a proper application in reality for the pyroelectric energy harvesters compared to their kinetic and solar counterparts. On the other hand, unlike in thermoelectric energy harvesters where a heat sink has to be integrated to act as the cold side, pyroelectric energy harvesters only need a piece of pyroelectric material to be present in principle. One of the possibilities where pyroelectric energy harvesters can be used is harvesting the heat in solar, infrared or other environmental radiations.[428-433] By properly designing the configuration, wind energy can also be harvested via the pyroelectric effect.[434] A flexible polymer-on-polymer structure, i.e. PVDF as the pyroelectric material and PEDOT (poly(3,4-ethylenedioxythiphene) as the electrode, was published for harvesting the waste heat from human inhalation and exhalation.[435] Harvesting the waste heat in hot lubricating oil[436], which is widely found in manufacturing industries, has been proposed. Modelling and characterization works have carried out for harvesting human body heat for wearable electronics.[437-439]

Oscillating heat pipes can be another waste heat source for pyroelectric energy harvesting.[440] In addition, the electric energy generated by pyroelectric energy harvesters was found to be practical for water splitting applications.[441]

2.3.4. Indirect thermal energy harvesting

Apart from the direct conversion of thermal energy with thermoelectric and pyroelectric effects, indirect conversion methods such as the piezoelectric effect in combination with ferromagnetic structures[442-444], and the electromagnetic effect in combination with magnetic shape memory alloy (MSMA) structures[445, 446] or ferromagnetic materials[447], can also be used for thermal energy harvesting. **Figure 6** shows the schematics of a configuration combining the electromagnetic effect and MSMA. As shown in the figure, coils and MSMA film are attached on the tip of a polymide (PI) cantilever. When the MSMA film contacts the heat source its temperature will increase and the magnetization will correspondingly change. This causes an attractive force between the film and the permanent magnet, as shown in the figure. The coil and magnetic flux will move relatively to each other when the cantilever bends towards the magnet. The MSMA film will then cool down whilst the attractive force vanishes and the elastic force of the PI cantilever pushes the system to recover the initial status. This energy harvester can give an average output power density of 0.5 mW cm^{-3} with a temperature change of 10 ˚C, which reaches the range of thermoelectrics.

Similarly, in a structure combining the piezoelectric effect and ferromagnetic material, a PZT sheet is placed under one end of a Gd (ferromagnetic) beam. The other end is placed between the cold (ice water, 0 ˚C) and hot (room temperature) surfaces. A NdFeB permanent magnet is placed at the hot side, and the ice water is at the cold side. The Gd possesses a Curie temperature between 0 ˚C and room temperature. In the initial state, the Gd beam is touching the cold side, and is thus able to be attracted by the permanent magnet. When the beam bends towards the

magnet due to the attraction, it applies a strain to the PZT sheet. When the beam and magnet contact each other, the ferromagnetic beam becomes hotter than its Curie temperature, thus causing its transition to paraelectric. The permanent magnet loses its attraction to the beam, which then recovers to the initial state and releases the strain on the PZT sheet. An output power density of 62.9 pW cm^{-3} was obtained with a temperature difference of 20 °C.[442]

In these ways the temperature gradient is transferred, first to kinetic energy and then to electricity – a two-stage energy conversion. These energy harvesters suffer from the issues of slow cyclic operations (or low duty cycle) as well as extra energy loss during the two-stage energy conversion process and hence give a low overall electric output. On the other hand, they provide an opportunity to harvest kinetic (or magnetic) and thermal energy simultaneously.

2.4. Harvesting of other energy sources

2.4.1. Electromagnetic wave and acoustic energy

In the modern world, people are exposed to pervasive electromagnetic waves including radio-frequency (RF) waves emitted by wireless communication devices (GHz frequencies), broadcast waves (MHz frequencies), power line dissipated waves, etc. Such radiation sources have become as widespread as solar, kinetic and thermal energies. The electromagnetic waves can also be harvested to power micro-scale electronics. An antenna is needed and its dimensions need to be tailored to match the different wave-lengths.[448] Most of the research on electromagnetic wave energy harvesting can be merged with research on antennas in terms of design/dimensions, bandwidth, working frequency, limit of space, circuitry, etc, For a deep knowledge and details, readers can refer to the well-developed antenna research which is related to communications technology and is outside the scope of this review. Nevertheless, relevant reviews and evaluation articles with the particular consideration of energy harvesting are available.[448-452] Typically, an output power density of up to 1 μW cm^{-2} can be provided by an RF energy harvester. The harvestable energy is distance dependent.

Apart from those focusing on typical antennas, one unconventional research is worth mentioning where the human body was used as an antenna to harvest low-frequency ambient electromagnetic waves which can easily be put in application to mobile devices.[453] An interesting application of RF energy harvesting is the concept of eWALL – a system of intelligent services which can be placed in any corner of the homes or health institutions, aiming to facilitate the extension of the active life expectancy of those with special needs, e.g. elderly or disabled people.[454]

Acoustic energy associated with sound in different frequencies is equivalent to vibration energy presented in Section 2.2. Therefore, it can be harvested by the electromagnetic or piezoelectric method. A piezoelectric acoustic energy harvester is able to provide a wide range of output power (0.68 pW to 30 mW), whilst an electromagnetic one can provide 1.5-1.96 mW.[455] There are updated comprehensive reviews for acoustic energy harvesting.[295, 455, 456]

2.4.2. Others

Other potential micro-energy sources for energy harvesting can also be considered, although they may have been only rarely investigated or they are too distant from real applications. Piezoelectric and magnetostrictive materials can be combined to harvest magnetic field variations[457], in addition to harvesting vibrations as introduced in Section 2.2.7. Energy emitted by radioactive materials (i.e. radioisotopes) can be harvested through the piezoelectric effect by combining a piezoelectric cantilever with a charge collector.[458, 459] In this type of energy harvester, a radioisotope source such as tritiated silicon emits particles that results in an electrostatic force between the source and a collector which traps the particles. Continuous charge-discharge cycles are then generated by the electrostatic force through driving the charging and actuating cycles of the piezoelectric cantilever. The radioactive source is transferred to mechanical vibration and is harvested via the piezoelectric effect.

2.5. Summary

Table 1 summarizes representative single-source individual energy harvesters together with either their record output voltage, power, power density or energy conversion efficiencies. As already mentioned, each energy conversion effect and its corresponding type of energy harvester has major physical problem(s) to overcome. For photovoltaic materials, although commercialization has been realized for a long time, ways must be found to break the physical limit of the single-junction energy conversion efficiency (S-Q limit, 33.7%). BPVE can help to break this limit. However, the band gaps of the materials exhibiting BPVE are too wide to allow the practical efficiency to exceed those of the Si-based or organic-halide perovskite counterparts. Narrow band gap BPVE materials need to be discovered. In terms of organic-halide perovskite solar cells, the material and device stability is the major challenge. Meanwhile, the efficiencies of Pb-free compositions are too low to be of any practical use. More chemical research needs to be carried out to discover Pb-free compositions with stability comparable to that of Si-based counterparts whilst exhibiting high efficiencies.

Triboelectric, piezoelectric and electret-based energy harvesters have the major physical issue of low output current, which hinders the maximization of output power. Designing proper composites can be an effective way to partially solve the issue. Electromagnetic energy harvesters are difficult to miniaturize. Electrostatic (non-electret) and electrostrictive energy harvesters need external voltage sources. These are non-solvable physical issues due to the nature of the working principles. Therefore, suitable applications need to be defined where the space is not limited (for electromagnetic) or an external voltage source is accessible (for electrostatic and electrostrictive). Magnetostrictive energy harvesters suffer extra energy loss for sole kinetic energy conversion. They need to harvest magnetic and kinetic energy sources simultaneously in order to make them reasonably efficient. For all the kinetic energy harvesters, the narrow bandwidth of the working frequencies is commonly their major physical challenge due to their linear spring-mass configuration. Introducing nonlinearity can be an effective way

to solve the issue. Although nonlinear systems are extensively investigated[460-472], further work still needs to be done to cover each case of the numerous designs or to find a universal solution which can be adapted to every case.

The thermoelectric figure of merit is much too low to meet all the practical requirements. Compositional and microstructural optimizations of the thermoelectric materials to boost the figure of merit should be the core of all thermoelectric energy harvesting research. Pyroelectric energy harvesters can only be practically efficient with rapid temperature change. Therefore, discovering suitable applications and tuning the Curie temperature to fit the application temperature ranges, as well as increasing the change of polarization within the pyroelectric materials around the Curie temperature, are ways to further develop these pyroelectric energy harvesters. Other indirect thermal energy harvesters suffer extra energy losses. Designing hybrid energy harvesters for multi-source operation is their future.

Because there are many physical challenges for individual, single-source energy harvesters, hybridization of different individual harvesters can provide a solution to overcome individual drawbacks by exploiting other advantages.

3. Hybridization of energy harvesters

3.1. Overview

Various single-source energy harvesting technologies are expected to be able to provide substantial electricity to WSN with the stable and ideal input energy experienced under laboratory conditions, making them promising candidates as substitutes for batteries in the future. However, with more realistic input profiles, e.g. random vibration, indoor light, unstable thermal source, etc., the output power from single-source energy harvesters suffers a drastic decrease. For instance, with random inputs the output power of a piezoelectric EHer can be less than 1 % of that with a stable and ideal input, no matter whether a nonlinear structure is introduced or not.[73, 473] Under indoor lighting or on a cloudy day the output power of solar

cells can be only about 0.04-1 % of that under bright sunlight.[3] Because of this, the current single-source energy harvesters have not become fully competitive with batteries in practice. Therefore, hybrid energy harvesters need to be developed in order to enable either increased efficiency by embedding two or more energy conversion effects to harvest single-energy sources, or an increase in total energy by employing different principles to harvest multiple energy sources.

3.2. Hybrid energy harvesters for single-source harvesting

The idea of the hybridization of two or more energy conversion effects for single-source energy harvesting was raised because each effect introduced in Section 2 has its own efficiency limit. The use of two or more energy conversion effects simultaneously to harvest the same type of energy source can help to decrease the overall energy loss during the conversion process and thus increase the efficiency and output power. The most effective such hybridization is for kinetic energy, as there are several methods to harvest kinetic energy but each method has clear advantages and drawbacks. Different kinetic energy conversion methods in combination are able to compensate each other, thus boosting the output power. Various types of kinetic (including fluidic) hybridization involving two energy conversion effects have been developed, including piezoelectric-electromagnetic[89, 311, 474-492], electrostrictive-electrets[493-496], piezoelectric-triboelectric[187, 497-501], electromagnetic-triboelectric[310, 502-512], piezoelectric-electrostatic[513, 514], triboelectric-electrostatic[515] and piezoelectric-electrostrictive[516]. Hybridization involving three kinetic energy conversion effects, piezoelectric-electromagnetic-triboelectric[307], has also been reported. Another benefit of these hybrid energy harvesters is that different effects can be made to respond to different input frequencies and/or create a nonlinear structure to deal with wideband or random vibrations, whilst not compromising the peak output of any of the integrated energy conversion processes. Usually, in a nonlinear single-source energy harvesting structure the peak output is reduced compared to that of the

corresponding linear structure. Several reviews are available for hybrid kinetic energy harvesters.[162, 517-519] The performances of representative examples are listed in Table 1.

Beside kinetic hybridization, thermoelectric and pyroelectric effects have also been integrated in the same energy harvester to simultaneously harvest temperature gradients and fluctuations.[520, 521] Although this is still a single-source (thermal) hybrid harvester, it slightly differs from the concept of the kinetic hybrid harvesters because in reality thermal energy usually consist of the two above-mentioned sub-forms and they have to be harvested by two different energy conversion effects. In comparison, any kinetic energy can be harvested by any of the energy conversion effects introduced in Section 2.2 in principle. Therefore, the two sub-forms of thermal energy can be treated as different energy sources. The thermoelectric-pyroelectric hybrid energy harvesters are actually multi-source harvesters. This will be discussed in Section 3.3 as follows.

3.3. Hybrid energy harvesters for multi-source harvesting

3.3.1. Temperature gradient and fluctuation

The two sub-types of thermal energy – temperature gradient and fluctuation – usually co-exist in reality, e.g. in human bodies. A wearable hybrid thermal harvester was developed[520], where a thermoelectric harvester in a circular mesh and a circular shaped pyroelectric harvester were packed together. The thermoelectric harvester enabled the harvesting of the temperature difference between the human body and extreme environments (cold and hot weather), whilst the pyroelectric harvester became functional when the evaporation heat of the human body causes thermal fluctuations. About 1.5 μW m^{-2} output power density was achieved with a temperature difference of 6.5 ˚C and a temperature change rate of 0.62 ˚C s^{-1}.

The hybridization can not only be achieved through the device combination as in the above example, but also via microstructural modification of the materials. For instance, another novel thermoelectric-pyroelectric hybrid energy harvesting structure based on PZT (pyroelectric) and

CNT (thermoelectric)[521] was also reported. The CNT acted as the core material in the structure, whilst the PZT was wrapped outside as the shell material. This novel structure can be scaled down to the nanometer level and can be used for harvesting thermopower waves. The benefit of this hybrid structure is that the average output voltage peak and duration were amplified and elongated by a factor of 2 and 60, respectively, compared to those of thermoelectric counterparts without the integration of the pyroelectric effect.

3.3.2. Solar and thermal energy

As mentioned in Section 1, solar energy is usually accompanies with thermal energy. Therefore, the sole use of solar energy harvesters more or less wastes the thermal energy. In fact, how to dissipate the heat generated by the sun and thus cool the solar panels down is an issue in the photovoltaic industry. As shown in **Figure 7**, in the solar irradiance spectrum, a substantial part of the incident energy is wasted if only solar cells alone are used for the harvesting.[522] Hybrid solar-thermal energy harvesters are not only able to help to harvest the heat but also to improve the output power and efficiency of either the solar or the thermoelectric energy harvester. **Figure 8** shows two photovoltaic-thermoelectric hybrid energy harvesting structures. The hybridizations were implemented at the device (structural) level (Figure 8 (a)) and the material (microstructural) level (Figure 9 (b)), respectively. In Figure 8 (a), a polymer solar cell made from P3HT/IC60BA (poly(3-hexylthiophene)/indene-C_{60} bisadduct) is combined with a conventional thermoelectric cell in a laminated structure including other functional (e.g. electrodes) and supportive layers.[523] At the bottom of the figure is a close-up of the thermoelectric cell (TE). This hybrid energy harvester first harvested the solar energy on the top of the structure via the photovoltaic effect. The thermal energy that accompanied with the solar radiation then heated the top thermoelectric cell thus creating a temperature gradient, which was harvested via the thermoelectric effect. Improved output power was proved by the

fact that with both the energy conversion effects being functional, an LED bulb could be illuminated but with either effect working individually the same bulb could not be lit.

Figure 8 (b) shows a simplified lamination structure in the nano-scale.[524] In the structure, the p-type CdTe nanorod array and n-type Bi_2Te_3 nano-layer formed a heterojunction solar cell. A close-up of the structure observed under SEM (scanning electron microscope) is shown at the bottom of the figure. When solar energy was applied to the bottom surface of the hybrid harvester, as shown in the figure, the p-n junction acted as a solar cell. Meanwhile, the thermal energy generated a heat flow in the Bi_2Te_3 layer which acted as a thermoelectric cell. This structure is more advanced than the laminated structure of conventional solar and thermoelectric cells because it combines the photovoltaic and thermoelectric structures into the same cell by creating a p-n junction. The functions of the two energy conversion effects overlap in the junction area, making it to be multi-functional through the materials, rather than a simple assembly of different structures. With this solar-thermal hybrid energy harvester, an efficiency increase of about 23 % was achieved. Total efficiency was 2.49 % after 1-minute illumination, consisting of 2.02 % contributed by the solar cell and 0.47 % by the thermoelectric cell.

Apart from the micro- and nano-scale structures, a photovoltaic-thermoelectric hybrid system was also built on a larger scale.[525] A solar spectrum splitter was introduced in the hybrid system in order to separate the short and long wavelengths in the solar radiation. The short wavelength radiation was used to generate electricity via the photovoltaic effect with a conventional solar cell, whilst the long wavelength radiation was used to generate heat for the conventional thermoelectric cell. With this hybrid system, a 30 % output power improvement was realized compared to the single use of solar cells.

3.3.3. Solar and kinetic energy

The hybridization of solar and kinetic energy harvesters has induced some novel concepts of energy harvesting solutions in reality. One of the representatives is the hybrid photovoltaic-

triboelectric harvester for individually or simultaneously harvesting solar energy and kinetic energy in the form of raindrops.[526-528] This concept was proposed to deal with the drastically reduced photovoltaic efficiency of solar cells on rainy days. **Figure 9** (a) and (b) shows the structure and working mechanism, respectively, of such a solar-raindrop hybrid energy harvester, respectively. As shown in Figure 9 (a), the conventional protection (from environmental damages and corrosions) layer of a Si solar cell was replaced by a layer of transparent triboelectric nanogenerator made from PTFE, ITO (indium tin oxide) and PET (polyethylene terephthalate) layers. In the working mode, as shown in Figure 9 (b), the hybrid energy harvester was placed at an angle between the surface of the harvester and the horizontal plane. The raindrops carrying charges had a triboelectric interaction with the surface of the hybrid harvester, thus converting the kinetic energy of the raindrops into electricity. This compensated the reduced photovoltaic efficiency of the solar cell on a rainy day. On sunny days, the solar cell became fully functional with its optimum efficiency. This structure was proved to be able to generate 16 mW m^{-2} solely by harvesting the raindrops, thus providing a solution to compensate the photovoltaic energy generation. The surface of a conventional solar cell can also be modified with PDMS[527] and polyaniline-graphene/PtCo[528] to provide a self-cleaning feature (feasibility consideration in practice) and improved efficiency. For instance, the polyaniline-graphene/PtCo modified solar-raindrop hybrid cell reached a photovoltaic efficiency of 9 % under sunlight and that of about 26 % in the dark and in the rain.

When the rainfall is significantly heavy, raindrops may become water flow. The solar cells may also be installed in coastal areas or even at sea, where ocean waves may be accessible. Therefore, apart from raindrops, water flow[529] (e.g. the transverse motion of the ocean waves[510]) can also be harvested together with solar energy. A 2D hybrid nanogenerator was developed based on a graphene/silicon van der Waals Schottky diode.[529] **Figure 10** shows the structure and working principle. An asymmetric internal potential profile was built into the graphene channel, enabling solar energy harvesting (Figure 10 (a)). Under illumination, an extra voltage was

added to the output when water flowed over the graphene surface (Figure 10 (b)). Rather than the typical triboelectric effect, the water flow energy harvesting in this hybrid structure is due to a reversible wetting and de-wetting effect which induces an additional charge transfer in the graphene channel (Figure 10 (c)). Beside the nano-scale, a macro-scale hybrid system integrating a triboelectric nanogenerator, electromagnetic energy harvester and solar cell was built to harvest solar energy and ocean waves.[510] By employing two kinetic energy conversion principles, as mentioned above, the advantage of this system was its wide working frequency range when harvesting the ocean waves, in addition to the solar energy. The energy harvesting capability of this system was proved by lighting up 102 LED bulbs when simultaneously harvesting the two energy sources.

Kinetic energy does not only exist within raindrops and water flow but also in the forms of acoustic and vibration energies which are pervasive. Acoustic energy can also be concurrently harvested concurrently with solar energy in a hybrid structure.[530-532] **Figure 11** shows a hybrid structure integrating the photovoltaic and piezoelectric effects.[530] The structure contained a dye-sensitized solar cell and a ZnO nanowire nanogenerator. The solar energy was applied to the top of the hybrid harvester and was harvested via the photovoltaic effect. The ultrasonic wave was spread on the bottom surface and was harvested by the piezoelectric effect. A 6 % increase in the optimum output power was observed with the introduction of the piezoelectric nanogenerator. Other solar-acoustic hybrid energy harvesters include nanowire-quantum dot[531] and nanopillar-PVDF[532] structures. Both structures have a similar concept to the dye-sensitized-ZnO nanowire counterpart. In the nanowire-quantum dot structure, CdS and CdTe quantum dots were located between ZnO nanowires, where the quantum dots were responsible for the photovoltaic effect and the nanowires for the piezoelectric effect. Sunlight and acoustic waves were applied on the top and bottom surfaces of the hybrid harvester, respectively. In the nanopillar-PVDF structure, Si was fabricated into nanopillars which were stacked with a PVDF

nanogenerator. The harvester was able to harvest solar energy and sound vibration simultaneously via the Si nanopillars and PVDF, respectively.

In addition, a solar-vibration hybrid energy harvester has been reported.[533] PZT cantilever arrays (piezoelectric) were laminated with Si solar cells (photovoltaic) for the simultaneously harvesting of vibration and indoor ambient light. The vibration energy was used to compensate the low intensity of the indoor light. A hierarchical nano/micro-architectured PDMS-dye sensitized solar cell (triboelectric-photovoltaic) hybrid structure was also developed for concurrently harvesting solar, pressure and wind energy.[534] ZnO nanowires were utilized to improve the efficiency. The cymbal design of the triboelectric part of the hybrid harvester responded to wind-induced pressure, thus harvesting the wind energy via the triboelectric effect.

3.3.4. Thermal and kinetic energy

A particular occasion of the co-existence of thermal and kinetic energy which may occur in nature is that heat is generated when two objects suffer relative frictional motion or one object is subject to a deformation (e.g. thermoacoustic energy). While individual triboelectric and piezoelectric energy harvesters only focus on harvesting the friction and the deformation, respectively, the accompanied heat is then wasted. Therefore, hybrid energy harvesters combining a conventional thermoelectric generator and the triboelectric[535] or piezoelectric[536] configuration were reported to simultaneously harvest the thermal and the kinetic energy described in the above situations. The thermoelectric-triboelectric hybrid structure employed a PTFE film as the triboelectric generator. A 13 % output power improvement was achieved by the hybrid harvester compared to its individual triboelectric counterpart. The thermoelectric-piezoelectric hybrid structure utilized ZnO nanowires to exhibit the piezoelectric effect. The two energy conversion effects in the hybrid structure compensated each other, with the thermoelectric component providing high output current whilst the piezoelectric part generated

a high output voltage. This hybrid harvester was proposed for the application of harvesting skin heat and human body movement simultaneously.

There is a temperature gradient between the human body and the environment. At the same time, as people are frequently changing their location, e.g. going indoors and outdoors many times per day, temperature fluctuations also exist in the ambient in which case the pyroelectric effect is needed. The pyroelectric effect has also been used in some thermal-kinetic hybrid energy harvesters. **Figure 12** provides two representatives.[537, 538] Both structures integrated piezoelectric, pyroelectric and triboelectric effects. The integration of piezoelectric and pyroelectric effects using ferroelectric materials (e.g. PVDF in the structures shown in Figure 12) is not treated as the hybridization of different structures but as the multi-functional route for multi-source energy harvesting. Details will be given in Section 4. In the structure shown in Figure 12 (a) and (c), the PVDF exhibited both the piezoelectric and pyroelectric effects, while the PTFE was used as the triboelectric material. The PVDF and PTFE were laminated with other supportive layers e.g. electrodes. Figure 12 (b) is the output response of the hybrid harvester shown in Figure 12 (a) when subject to a temperature change and contact-separation motion between the PVDF and PTFE layers. The wide and sharp peaks were generated from the pyroelectric and piezoelectric-triboelectric effects, respectively. This hybrid harvester proved practical for use in a self-powered cathodic protection system for metal corrosion prevention.[537]

The working principles of the hybrid harvester in Figure 12 (c) are shown in Figure 12 (d)-(f). The sliding motion (in and out) of the triboelectric energy harvester also induced a compressive force and heat. While the sliding motion was harvested via the triboelectric effect, the temperature variation caused by the heat and the applied compression were harvested by the pyroelectric and piezoelectric effects of the PVDF, respectively. This hybrid configuration contributed to a 26 % energy conversion efficiency improvement compared to the individual triboelectric counterpart.

3.3.5. Thermal, Kinetic and Solar energy

Because piezoelectric and pyroelectric effects can co-exist in the same ferroelectric material for kinetic and thermal energy harvesting, as mentioned above, they can be further hybridized with a photovoltaic configuration thus harvesting triple energy sources. **Figure 13** shows the structure and output profiles of a thermal-kinetic-solar hybrid energy harvester integrating the pyroelectric, piezoelectric and photovoltaic effects.[539] As shown in Figure 13 (a), the hybrid structure contained aligned ZnO nanowire arrays grown on a polyester substrate and P3HT to form a heterojunction solar cell, a PVDF layer acting as a piezoelectric and pyroelectric component, and electrodes such as ITO and Ag. Figure 13 (b) and (c) are the output of the hybrid harvester with thermal-kinetic energy and thermal-solar energy inputs, respectively. It can be clearly seen that the piezoelectric and pyroelectric outputs exhibited add-on effects to the pyroelectric and photovoltaic outputs, correspondingly. The benefit of harvesting multiple energy sources via this all-in-one hybrid energy harvesting configuration are well illustrated. This hybrid harvester was used to charge a Li-ion battery and could illuminate 4 LED bulbs. The main advantage is that the harvester can always be functional thus successively generating electricity with no interuptions, as long as any or all of the three richest most common energy sources – thermal, kinetic and solar – are present.

In terms of the hybridization of the three above-mentioned energy sources, Lee et al. has written a comprehensive review[540] focusing mainly on nanogenerators where more details can be found.

3.3.6. Other hybrid energy harvesters

A biomechanical-biochemical hybrid energy harvester[541] was reported for potential in-vivo applications. In this harvester, a piezoelectric nanogenerator made from PVDF nanofibers was combined with a flexible enzymatic biofuel cell. The piezoelectric part was able to harvest

kinetic energy generated from a human's breathing or heartbeat. The biofuel cell was used to harvest biochemical energy, e.g. glucose/O_2 in a biofluid. The open-circuit voltage and short-circuit current of the piezoelectric component was reported to be 15-20 mV and 0.2-0.3 nA, respectively. The output power density of the biofuel cell was about 2.2 nW cm^{-2}. The energy harvesting capability and feasibility of this hybrid harvester was demonstrated with a self-powered nanosystem – a ZnO nanowire UV light sensor.

A wind-solar-chemical hybrid energy harvester[542] was developed by combining a triboelectric nanogenerator, a solar cell and an electrochemical cell. The wind was harvested through the triboelectric effect. The PTFE and Al films were assembled in a rotor configuration which had blades and could be driven by the wind. The wind-driven rotary motion caused a relative movement and friction between the FTFE and Al films, thus triggering the triboelectric energy conversion effect, providing a maximum power density of 16 mW m^{-2}. The solar and chemical energy were harvested by the solar and electrochemical cells, respectively. The generated electricity was stored in a Li-ion battery and used for powering wind speed and temperature sensors. For these hybrid harvesters involving chemical energy, applications should be properly defined.

3.4. Summary

Table 1 also lists the structures/configurations, output voltage, power, power density and energy conversion efficiency of the representative hybrid multi-source energy harvesters. As described in Section 3, there are many possibilities to combine different energy conversion effects into a hybrid energy harvester. However, there remains a major physical challenge; all of the hybrid energy harvesters to date are basically only simple combinations of different individual energy harvesters made from different materials/structures. No matter how the structures are optimized, because the used energy conversion materials are single-functional, it is necessary to employ an additional material if there is a need to add an extra harvestable energy source. Thus, a

sacrifice of space and size is always the case in order to employ an increased number of harvestable sources. This means that, due to the increase in size, the efficiency per unit volume stays the same or may even decrease compared to the individual counterparts. In order for the hybrid structures to be as compact as their individual counterparts as possible, smart structural optimization is always needed for any combination.

The hybridization of the current individual energy harvesters provides endless opportunities for self-powered and battery-less solutions in practical applications. However, a wide range of combination possibilities at the same time means tedious repetitions of the structural optimization loop for each new application, i.e. for each newly identified energy harvesting scenario it is necessary to go through energy source analysis, selection of energy conversion, hybridization and structural optimization. This is another major challenge for hybrid energy harvesters. This makes the hybridization very complicated when integrating all the energy conversion effects to cover the richest and most common energy sources, i.e. it is challenging to obtain an all-in-one solution. Therefore, together with the necessary structural optimization, investigations must be expanded into the materials, i.e. composition, microstructure, etc., in order to realize multi-source energy harvesting from the very beginning of the development loop mentioned above. If a material can accomplish the task of converting multiple energy sources such thermal, kinetic and solar into electricity simultaneously based on a single piece of this material, the structural optimization stage will be simplified. In such a case, more advanced structural optimization will be enabled without the concerns of materials selection and the hybridization of different individual energy harvesting principles. This is the view to be presented in Section 4 below.

The hybrid energy harvesters presented in this section should be distinguished from the multi-source energy harvesters made from multi-functional materials to be presented in Section 4. The fundamental difference is that a hybrid harvester is made by incorporating different energy conversion materials with each being responsible for harvesting a specific energy source. A

multi-source harvester contains only one energy conversion material which can simultaneously harvest different sources. In hybrid harvesters, the materials may consist of the best piezoelectric, pyroelectric, photovoltaic, etc. energy conversion components in order to achieve the best possible efficiency. In multi-source harvesters, the multi-functional properties as a whole are crucial for the efficiency. Different energy conversion effects co-existing in the material should be optimized simultaneously. They should not degrade each other. Therefore, material investigation and optimization is the core of such harvesters. This is the focus of Section 4.

4. Multi-functional materials for multi-source energy harvesting

4.1. Ferroelectric materials co-exhibiting piezoelectric and pyroelectric effects

As mentioned in Sections 2.3.3 and 3.3.4, poled ferroelectric materials can exhibit piezoelectric and pyroelectric effects simultaneously. This naturally provides a family of multi-functional materials for multi-source (kinetic and thermal) energy harvesting. Two sub-groups of ferroelectric materials have been discovered and widely used – ABO_3 perovskite structured single- or polycrystals (e.g. PZT, BT, KNN, BNT-BT, PMN-PT and their doped compositions) and ferroelectric polymers (e.g. PVDF, P(VDF-TrFE)). The ferroelectricity in the ABO_3 sub-group (ionically bonded materials) is realized by the switching and alignment of domains – the nano- or micro-sized areas with spontaneous polarizations in the same orientation. In ferroelectric polymers, the ferroelectricity is attributed to aligned molecular chains due to the alignment of polarized covalent bonds in such crystalline polymers. In particular, for an un-poled ferroelectric material, e.g. a newly fabricated material which has not been exposed to any external electric field, the electric domains are non-aligned. The orientations of the polarizations of the domains are randomly distributed, thus counteracting each other. In this case, the macro-scale remanent polarization of the entire material is zero, so the material cannot exhibit piezoelectricity or pyroelectricity. After poling, i.e. applying an external electric field which is

large enough to re-orient and align the domains into the same direction, there will be a macro-scale remanent polarization for the entire material even when the external field is removed. In this case, the material will display both piezoelectric and pyroelectric properties.

The use of ferroelectric materials for the simultaneous harvesting of kinetic and thermal energy has already been realized. **Figure 14** shows an example of a practical application using a micro-patterned PMN-PT single crystal flexible ribbon to harvest kinetic and thermal (temperature fluctuation) energies concurrently.[543] PMN-PT single crystals were first grown. After wet etching, they were transferred onto a flexible PET substrate and then deposited with Au electrodes, as shown in Figure 14 (a). The fabricated harvester was attached to a human wrist for the kinetic energy harvesting test. AC piezoelectric output signals were detected from the wrist movement, as shown in Figure 14 (b). The same harvester was used for a thermal energy harvesting test. When the harvester was immersed in warm water (temperature increasing) and then removed, pyroelectric output signals were detected, as shown in Figure 14 (c). Such a multi-source energy harvester could provide a peak output power density of about 25 mW cm^{-2}.[543] The harvested energy was used to power monitoring sensors.

For piezoelectric-pyroelectric multi-functional materials used for the simultaneous harvesting kinetic of energy and temperature fluctuations, it is crucial that the two energy conversion effects do not conflict each other. In a case study work with PVDF, it was confirmed that the piezoelectric-pyroelectric multi-energy conversion effect is equivalent to the algebraic sum of the two individual effects.[544] This implies that in ferroelectric materials, the potential piezoelectric and pyroelectric effects do not couple and degrade each other, providing the possibility of maintaining the efficiency of each effect in the multi-functional working mode comparable to that in the individual mode. This is an important advantage of using ferroelectric materials in practice since the piezoelectric and pyroelectric effects can give truly add-on value to each other in terms of overall efficiency and output power.

There is a major physical challenge for ferroelectric materials for use as piezoelectric-pyroelectric multi-functional energy harvesting materials. According to Equation 3 and 4, a large pyroelectric figure of merit requires a large pyroelectric coefficient, which further requires a significant change of spontaneous polarization with temperature. Therefore, in practice ferroelectric-based pyroelectric materials are expected to operate near and below their Curie temperatures where most ferroelectric materials exhibit the most obvious change of spontaneous polarization with temperature.[410, 545] However, the permittivity increases drastically at around the Curie temperature[545], leading to a potential decrease of the figure of merit. This increase of permittivity also leads to a decrease of the piezoelectric voltage coefficient, according to Equation 1. Furthermore, there may also be a significant drop in the piezoelectric charge coefficient when the temperature approaches the Curie point.[546, 547] The simultaneous decrease of piezoelectric charge and voltage coefficients degrads the piezoelectric figure of merit and thus the kinetic energy harvesting capability.

There are two potential methods to overcome this dilemma – compositional and structural optimization. In terms of the compositional optimization route, through doping a modified ferroelectric composition may exhibit a more stable piezoelectric charge coefficient compared to its undoped parental composition. For instance, a ferroelectric composition, 0.08 wt.% Ga_2O_3 doped $(Ba_{0.99}Ca_{0.01})(Zr_{0.02}Ti_{0.98})O_3$ (BCZT) could exhibit up to ~ 25 % change of the spontaneous polarization in the temperature range of 40-100 ˚C. Meanwhile, at 100 ˚C the composition only lost 2-3 % of the piezoelectric charge coefficient compared to the value at 40 ˚C. The permittivity also remained almost unchanged. In comparison, the undoped BCZT suffered a ~ 40 % decrease of the piezoelectric charge coefficient under the same conditions, despite a relatively stable permittivity as in the doped composition.[547] A similar effect was reported on a Tb-doped BCZT.[546]

In terms of the structural optimization route, introducing porosity into the dense ferroelectric ceramic structures can also help to improve and balance the piezoelectric-pyroelectric multi-

functional energy harvesting capabilities. For instance, a highly aligned porosity was created in PZT ceramics with a freeze-casting fabrication method. The microstructural pores were aligned in parallel, giving a decreased permittivity and volume specific heat. According to Equation 1 and 4, such a decrease can potentially increase the piezoelectric and pyroelectric figures of merit. The maximum thermal energy density of the aligned porous PZT was measured to be 374 % higher than that of the dense PZT ceramics.[424] The boost of the pyroelectric performance may provide an opportunity for compromise, i.e. to shift the working temperature away from the Curie temperature in order to avoid the significant degradation of the piezoelectric charge coefficient.

Other structural optimization methods include textural engineering of the ferroelectric ceramics. This method is able to increase the piezoelectric properties by creating textured crystallographic orientations in the microstructure. With the high texture levels (up to 90 %), significant enhancements in piezoelectric properties compared to those of randomly oriented ceramics can be achieved. The piezoelectric charge coefficients can be increased by 2-3 times, approaching the values of the corresponding single-crystals.[548-552] However, there can be exceptions. For instance, textured $(Ba_{0.85}Ca_{0.15})(Ti_{0.9}Zr_{0.1})O_3$ only achieved the same level of piezoelectric charge coefficient compared to that of randomly oriented ceramics with the same composition.[160, 553]

In a brief summary, for the further development of the use of a ferroelectric materials' multifunctional nature, i.e. simultaneous harvesting of kinetic and thermal energies through piezoelectric and pyroelectric effects in the same material, both compositional and structural optimizations need to be carried out. This will enable demonstration devices to be fabricated with the highest possible piezoelectric and pyroelectric figures of merit at the same time, in anticipation of practical applications.

4.2. Non-ferroelectric multi-functional materials

It has been mentioned in Section 2.3.3 that ferroelectric materials form only on group of those materials that can exhibit piezoelectricity and pyroelectricity. There are also non-ferroelectric materials which can be multi-functional. Moreover, it would be very advantagious if more than two energy conversion effects (e.g. thermoelectric and/or photovoltaic effects in addition to piezoelectric and pyroelectric effects) could be exhibited simultaneously in the same material. Inorganic compositions such as GaN, AlN, CdS, ZnO can also exhibit simultaneous piezoelectric and pyroelectric effects.[291] Although they have much weaker piezoelectric and pyroelectric responses than those of poled ferroelectrics, what makes them of interest is their semiconducting characteristics. This provides them with the possibility to exhibit photovoltaic and thermoelectric effects in addition to piezoelectric and pyroelectric ones. ZnO is the most researched composition among these inorganic compositions. It has been widely used in piezoelectric nanogenerators. Details have been given throughout this paper and more information can be found in other reviews[161, 164].

ZnO has also been used in photovoltaic energy harvesters. Although it has a wide band gap of 3.37 eV[164], ZnO has a number of benefits if used in dye-sensitized, bulk heterojunction organic and inorganic p-n junction solar cells. A typical dye-sensitized solar cell based on TiO_2 possesses the record photovoltaic efficiency to date for this type of solar cells. However, although the ZnO based dye-sensitized solar cells performed worse than the TiO_2 based counterparts, the ZnO's significantly higher electron mobility and its feasibility for creating flexible structures has attracted some attention. Increased electron mobility in ZnO compared to that in TiO_2 can, in theory, induce more efficient electron collection in theory. Therefore, there have been a number of research projects utilizing ZnO nanostructures as the photoanode of dye-sensitized solar cells.[554] In bulk heterojunction organic solar cells, ZnO can be used as a novel anode and interface layer.[555, 556] This is because in typical bulk heterojunction organic solar cells, ITO modified with PEDOT:PSS (poly(3,4-ethylene dioxythiophene):poly(styrene sulfonate) is used as the anode. However, the use of this acidic water based solution leads to

instability of the interface in the photoactive layer and the corrosion of the ITO.[557, 558] Due to its high electron mobility as well as its transparency in the visible range, a ZnO anode can improve the interface stability and suppress device degradation. In inorganic p-n junction solar cells, n-type ZnO and p-type Cu_2O are used to form a heterojunction. This type of solar cell is excitonic, in which excitons are generated, compared to that in conventional p-n junction solar cells where electrons and holes are generated. The advantage of excitonic solar cells is that the open circuit voltage can be greater than the band bending, while in conventional cells it is limited to the level of the band bending.[559-562]

More details of the ZnO used in solar cells, piezoelectric nanogenerators and hybrid/multi-source energy harvesters can be found in an extensive review[164]. Unfortunately, due to its wide band gap ZnO cannot effectively absorb the visible light in the solar spectrum and is thus not able to be used as the direct conversion component in solar cells through the photovoltaic effect. Furthermore, the pyroelectric coefficients of ZnO and other inorganic semiconducting counterparts (<10 $\mu C\ m^{-2}\ K^{-1}$) are negligible compared to those of conventionally strong pyroelectric materials such as PZT (260 $\mu C\ m^{-2}\ K^{-1}$), BT (200 $\mu C\ m^{-2}\ K^{-1}$) and PMN-PT (1790 $\mu C\ m^{-2}\ K^{-1}$), and are much smaller than those of PVDF (33 $\mu C\ m^{-2}\ K^{-1}$).[563-567] All these drawbacks make ZnO and its other inorganic counterparts not the ideal candidates for the multi-functional materials used in the simultaneous harvesting of multiple energy sources. This is the reason why a multi-source energy harvester solely based on these materials has not been reported. Therefore, a multi-functional material exhibiting a narrow band gap and strong piezoelectric and pyroelectric responses – to be an ideal candidate for multi-source energy harvesting based on a single material – needs to be developed.

4.3. Organic-halide perovskites

ZnO and other corresponding materials presented above have wide band gaps, but they provide an easy fabrication route for nano-scale and flexible structures which are suitable for MEMS

and wearable devices. Similarly, the organic-halide perovskites can also provide nano-scale and flexible structures, e.g. thin-films made by the wet-chemical methods. More importantly, the organic-halide perovskites have tunable and much narrower band gaps compared to ZnO, etc., making them more advantageous to be potential multi-functional materials which co-exhibit piezoelectric, pyroelectric and visible-range photovoltaic effects. Organic-halide perovskites are also called organic-inorganic halide perovskites, organic-inorganic hybrid perovskites or organometal halide perovskites. Since 2014, the observation of ferroelectric behavior in some organic-halide perovskites has been claimed.[568-575] However, it seems that not all of them can exhibit ferroelectricity. It depends very much on their composition and microstructure. For instance, while most of the evidence of ferroelectricity was reported in $MAPbI_3$ with a non-centrosymmetric microstructure, $MAPbBr_3$ was found to be centrosymmetric and non-polar, and thus was not being able to be ferroelectric.[59] This situation is similar to that in ABO_3 perovskites, although their unit cell structures differ differ from those of the organic-halide perovskites to some extent, as shown in Figure 1. In ABO_3 perovskites, the tolerance factor ($\boldsymbol{tol.}$) defined in **Equation 5** determines the symmetry of the unit cell. In the equation, $\boldsymbol{R_A}$, $\boldsymbol{R_B}$ and $\boldsymbol{R_O}$ are the radii of A, B site ions and oxygen ions, respectively, assuming the ions to be perfect spheres.[55] When $\boldsymbol{tol.} = \mathbf{1}$, the unit cell will be in the cubic phase which is centrosymmetric, making the bulk material constructed by such unit cells unable to exhibit any ferroelectricity. When $\mathbf{0.9} < \boldsymbol{tol.} < \mathbf{1}$, the unit cells will be in non-cubic phase (e.g. tetragonal, orthorhombic, rhombohedral) which is non-centrosymmetric, making the corresponding bulk materials to be polar and able to exhibit ferroelectricity. Although the microstructure of organic-halide perovskites, which involves not only inorganic atom/ion sites but also molecular chains, is not well understood compared to that of the ABO_3 counterparts, the atoms/ions on the X sites (e.g. I or Br) must determine the microstructural symmetry. This can be clearly seen in tetragonal $CH_3NH_3PbI_3$ which is claimed to be ferroelectric[574] and $CH_3NH_3PbBr_3$ which is centrosymmetric and non-ferroelectric[59].

$$\boldsymbol{tol.} = \frac{\boldsymbol{R_A + R_O}}{\sqrt{\boldsymbol{2}} \cdot (\boldsymbol{R_B + R_O})} \quad (13)$$

It is in fact complex and complicated to examine the ferroelectricity in organic-halide perovskites, as they are usually made in the form of thin-films with high leakage currents which can screen the long-range dipolar interactions and thus lead to fake ferroelectric hysteresis loops being obtained.[576] In other cases, the fake ferroelectricity was misunderstood by the detected pyroelectric- or piezoelectric-like signals which could be due to trapped charges at the interface between the perovskites and metallic electrodes.[59] Even though in those experimental and theoretical studies the ferroelectric nature of non-centrosymmetric organic-halide perovskites such as non-centrosymmetric $CH_3NH_3PbI_3$ was suggested, the reported data were often considered to be conflicting and inconclusive.[572, 574, 577] A brief history of proving the existence of ferroelectricity in $CH_3NH_3PbI_3$ is summarized here with some very recent publications.

In 2014, the presence of ferroelectric domains was observed in high-quality β-$CH_3NH_3PbI_3$ using PFM (piezoforce microscopy).[568] The β-$CH_3NH_3PbI_3$ thin-films were fabricated through a novel solution-processing route. The ferroelectric domains were found to be of a similar size to that of the grains, which was about 100 nm. Evidence of the reversibility of the ferroelectric domains with external electric fields – the fundamental definition of ferroelectricity – was also reported. The observation of ferroelectricity was considered to aid the understanding of the photovoltaic behavior in organic-halide perovskites, as it was believed that the polarization was able to affect their photovoltaic performance.[568] Such evidence triggered an increased number of relevant researches reported in 2015. It was found that both charged and uncharged ferroelectric domain walls can be formed in $CH_3NH_3PbI_3$ because of the flexible orientation order of the organic molecules.[578] Both 180˚ and 90˚ domain walls were found to exist in the structure, as in tetragonal ABO_3 perovskites. The most important observation was that the charged domain walls were able to reduce the band gap by 20-40 % while uncharged domain walls were not able to do this. Meanwhile, it was found that a positive electric poling in

$CH_3NH_3PbI_3$ improved the charge separation inside the perovskite, but a negative poling did the opposite.[569] This evidence confirmed the interaction between the photovoltaic and ferroelectric effects in organic-halide perovskites. However, controversy occurred when it was reported that no permanent polarization exists at room temperature in $CH_3NH_3PbI_3$[570] and spontaneous polarization exists in $CH_3NH_3PbI_3$ without an external electric field which was not significantly dependent on the grain size[571]. After a short one-year standstill, in 2017 a combination of microscopic and macroscopic methods was used to probe the spontaneous polarization and ferroelectricity in $CH_3NH_3PbI_3$.[572] In addition, the orientation of the polarization was reported not only to be switched by an external electric field but also by light illumination in the absence of an electric field. The photo-induced polarization switching was caused by the combination of ionic motions and photovoltaic field. With further freshly published evidences[573-575], $CH_3NH_3PbI_3$ can now be convincingly considered to be ferroelectric. This provides a unique opportunity to optimize these two effects (plus the piezoelectric and pyroelectric effects induced by ferroelectricity) simultaneously.

While the existence of ferroelectricity was in the process of being proved, there has not been much research focusing on the use of $CH_3NH_3PbI_3$'s piezoelectricity and pyroelectricity for kinetic and thermal energy conversion/harvesting. Nevertheless, compared to the long debating history of the organic-halide perovskites' ferroelectricity, their piezoelectricity has been reliably observed and extensively investigated. In 2015 the piezoelectric response of $CH_3NH_3PbI_3$ was first reported to be significantly enhanced under illumination.[570] This implies that if the perovskite was used for simultaneously harvesting of kinetic and solar energy via piezoelectric and photovoltaic effects, respectively, the piezoelectric output could be improved by the presence of solar energy. In this case, the benefits of using the multi-functional organic-halide perovskites for multi-source energy harvesting would not only be the structural simplification but also the further stimulation of output power or efficiency. In 2016, the use of the piezoelectric properties of $CH_3NH_3PbI_3$ for kinetic energy harvesting was first proposed.[579]

The $MAPbI_3$ perovskite crystalline thin-films (500 nm thick) were deposited on FTO (fluorine-doped SnO_2)/glass and Au/Ti/PET substrates. The films were poled in an 80 kV cm^{-1} electric field. Under 0.5 MPa pressure, an open-circuit voltage of 2.7 V and a short-circuit current density of 140 nA cm^{-2} were generated via the piezoelectric effect. Although the photovoltaic effect was not studied in this particular device, using it to concurrently harvest solar and kinetic energy for wearable electronics was proposed.

In the last couple of years, recognizable or strong piezoelectric responses were successively reported[58, 580-582], most of which were photo-induced or photo-enhanced. Liu et al. have quantified the piezoelectric effect of a broad range of organic-halide perovskites via first principle calculation as well as by experimental validation.[58] In a polar structural model, the $\boldsymbol{d_{33}}$ of the $MAMX_3$ perovskites can vary from 4 pC/N obtained with $MASnCl_3$ to 101 pC/N of $MASnI_3$. A further improved $\boldsymbol{d_{33}}$ (248 pC/N) can be achieved with $CF_3NH_3PbI_3$.

However, although organic-halide perovskites can exhibit extraordinary photovoltaic behavior as presented in Section 2.1, and the ferroelectricity and piezoelectricity of some compositions have been proved, instability is still a major physical challenge to be overcome for their application in multi-source energy harvesting. In Section 2.1, it has been mentioned that ambient conditions e.g. light exposure, humidity and elevated temperature can cause instability in most organic-halide perovskite compositions. What is worse, it has been found that strain can also lead to degradation of the fabricated organic-halide perovskites.[583] With the conventional spin coating and thermal annealing fabrication process, lattice strain may exist in the fabricated perovskite thin-films which can be caused by a thermal expansion mismatch between the substrate and the thin-film. Such lattice strain may lead to a decomposition of $MAPbI_3$ into PbI_2. The accelerated degradation is caused by the easier migration of MA^+ and I^- ions, as the free energy of the systems is increased by the strain. Ion migration can reduce the free energy by relaxing the lattice strain. The instability caused by strain is further confirmed by introducing additional tensile strain to the entire film. This issue brings a serious concern to

multi-source energy harvesting co-utilizing the piezoelectricity and photovoltaic effects of the organic-halide perovskites, because for kinetic energy harvesting with the piezoelectric effect bending or compression has to occur in the material. This is very likely to accelerate the degradation. Considering that instability also occurs with temperature variation, it is still hard to conclude whether the piezoelectric, pyroelectric and photovoltaic effects co-existing in the organic-halide perovskites are mutually beneficial or detrimental. This challenge may hinder the practical applications of the organic-halide perovskite multi-functional materials used for kinetic-thermal-solar multi-source energy harvesting.

For further development, an extensive research into the relationships of strain, illumination, temperature variation, stability and their influence on the multi-functional performance should be carried out to understand the mechanisms in greater detail. Different organic-halide compositions as well as a range of optimized fabrication methods should also be studied in order to achieve good multi-functional properties and stability by improving the intrinsic stability in compositions and releasing any residual strain after fabrication. In the present state of the art, there has not been any report focusing on the performance/stability improvement of the photovoltaic and ferroelectric effects simultaneously or as a whole.

4.4. ABO_3 structured photovoltaic-ferroelectric perovskites

4.4.1. Overview

As presented above, the ZnO and other relevant materials exhibit weak piezoelectric and pyroelectric responses and a wide band gap, meaning that they are unsuitable for efficient kinetic, thermal and solar energy harvesting. The organic-halide perovskites may show strong piezoelectricity and a narrow band gap, but they are hindered by instability. Consequently, these two groups of materials seem unlikely to become ideal piezoelectric-pyroelectric-photovoltaic multi-functional materials used for kinetic-thermal-solar multi-source energy harvesting. As a result, the focus must go back to those ferroelectric materials with strong piezoelectric and

pyroelectric responses as well as stability under strain, illumination and temperature variation. In fact, the photovoltaic effect can also be observed in ABO_3 structured ferroelectric ceramics, despite their wide band gaps which are mostly located out of the visible-range. There are theories being established, i.e. bulk photovoltaic effect and photo-ferroelectrics, which support the development of the ferroelectric-photovoltaic multi-functions of these ferroelectric ceramics. It can be predicted that as long as the band gaps can be narrowed whilst the strong ferroelectricity can be maintained, these ferroelectric materials have the potential to become ideal candidates used for harvesting kinetic, thermal and visible-range solar energies with the same material.

4.4.2. Bulk photovoltaic effect

Although the ABO_3 structured perovskites are famous for their strong ferroelectricity, piezoelectricity and pyroelectricity, they can also exhibit a BPVE (bulk photovoltaic effect). The BPVE is defined as that photocurrent (short-circuit boundary condition) or photovoltage (open-circuit boundary condition) that is raised in crystals or polycrystalline media under illumination in the range of intrinsic and extrinsic absorption.[57] In practice, the BPVE (also known as the anomalous photovoltaic effect) can be observed in 20 specific point groups of crystals, which lack an inversion symmetry center (e.g. ferroelectrics and piezoelectrics).[13] For instance, the above-mentioned BTO, PZT, KNN, BNT-BTO, ZnO can all exhibit the BPVE.

It is known that the conventional photovoltaic effect (not BPVE) can be separated into two types. The first is called the Dember effect, which is caused by, for example, a strong light absorption by the crystal leading to non-uniform illumination. In this effect, the photovoltaic phenomenon is associated with the diffusion of non-equilibrium, photoexcited carriers and the mobility difference between electrons and holes. The second happens in the case of crystal inhomogeneity associated with the separation of non-equilibrium carriers, as in the well-known p-n junctions widely used in solar cells. Neither type of the conventional photovoltaic effect is

able to generate a photovoltage that exceeds the band gap of the material, i.e. it is limited to several volts. However, the BPVE allows the photovoltage to be several orders of magnitude greater than the band gap.[57] The other feature of the BPVE is that the photocurrent direction and magnitude are dependent on the light frequency and polarization.[57, 584] The BPVE was first discovered in the 1960s, although as early as 1956 a steady photocurrent in a BT at above its Curie temperature was observed which was due to space charges.[57, 585] The mechanism of the BPVE is not fully understood. There are two proposed explanations: the ballistic and shift current mechanisms.

In the ballistic mechanism the BPVE is associated with the excitation of the so-called hot carriers, i.e. the non-thermalized carriers, in a crystal. **Figure 15** helps to explain the internal photovoltaic effect of centrosymmetric and non-centrosymmetric crystals. In the intrinsic excitation of the centrosymmetric crystal, the electron distribution in the band is symmetric so that no current can be extracted. By contrast, the excitation of the non-centrosymmetric crystal has an asymmetric electron distribution with a momentum. A shift of $\boldsymbol{l_0}$ is induced with the photo-excited non-thermalized electrons losing their energy and descending to the bottom of the band.[13, 57] The steady-state photovoltaic current ($\boldsymbol{J_{photo}}$) and $\boldsymbol{l_0}$ can be expressed by **Equation 6** and **7**, where $\boldsymbol{\alpha}$ is the absorption coefficient, $\boldsymbol{I_0}$ is the light intensity, $\boldsymbol{\hbar\omega}$ is the incident photon energy, $\boldsymbol{\varphi}$ is the quantum yield, $\boldsymbol{\tau}$ is the photo-excitation asymmetry parameter and $\boldsymbol{g}$ is the piezoelectric voltage coefficient.[13]

$$\boldsymbol{J_{photo} = e \cdot \alpha \cdot I_0 \cdot (\hbar\omega)^{-1} \cdot \varphi \cdot \tau \cdot l_0} \quad (6)$$

$$\boldsymbol{l_0 = g \cdot e^{-1} \cdot (\hbar\omega) \cdot (\varphi\tau)^{-1}} \quad (7)$$

The most recent breakthrough explained by the ballistic mechanism is the photovoltaic energy conversion efficiency ($\boldsymbol{\eta_{photo}}$) exceeding the S-Q limit, as observed in a bulk BT ferroelectric crystal[13] (also briefly mentioned in Section 2.1). Under ‘‘one sun’’ illumination, the BT generated a short-circuit current ($\boldsymbol{J_{SC}}$) of 19 mA cm^{-2} and an open-circuit voltage ($\boldsymbol{V_{OC}}$) of 1.2

V, reaching an $\boldsymbol{\eta_{photo}}$ of 4.8 % which is about 1.5 times the S-Q limit for the 3.2 eV band gap. Although the $\boldsymbol{\eta_{photo}}$ is far removed from the record value (> 20 %) of the organic-halide perovskites, it still implies an important advantage because, with a potentially reduced band gap and improved S-Q limit, the efficiency of the BPVE for photovoltaic-ferroelectrics is expected to be significantly improved. For instance, with a $(PbNiO_2)_x(PbTiO_3)_{1-x}$ nanolayer (1-2 nm thick) on $PbTiO_3$, the total photocurrent was improved by 43 times compared to pure $PbTiO_3$, due to the reduced band gap (from 3.6 eV to 1.5 eV) and photocurrent direction alignment for all absorption energy.[586]

In the shift current mechanism the BPVE is naturally quantum-mechanical obtained by taking the non-diagonal elements of the density matrix into account. Details can be found in reference[584]. In this mechanism, the BPVE is caused by the carrier band-band transition followed by the shift in real space, rather than the carrier movement in the band. The BPVE in BTO and $PbTiO_3$ was studied with the shift current explanation through first principle calculation and experiments. These confirmed the expectation that the photocurrent in these photovoltaic-ferroelectric materials does not depend on the intensity of the polarization, but on electronic states with delocalized, covalent bonding which is highly asymmetric along the direction of the current.[584]

A recently published, extensive review[587] is available for details of the development of BPVE mechanisms and materials.

4.4.3. Photoferroelectrics

The BPVE can also be referred to as photoferroelectric phenomena. The difference between these therms is that the former usually focuses on the photovoltaic response (which is influenced by the non-centrosymmetric microstructure) including those exhibiting ferroelectricity, while the latter attempts to explain the photo-induced and photo-stimulated effects on the ferroelectric, physical and electric properties. The combination of the studies of the BPVE and

photoferroelectric phenomena contributes to the development of the piezoelectric-pyroelectric-photovoltaic multi-functional materials used for multi-source energy harvesting.

Photo-stimulated phase transition is one of the photoferroelectric phenomena. The illumination tends to shift the phase transition temperatures (including the Curie points) towards lower temperatures. For instance, illumination may lower the Curie point of BTO crystals by 5 ˚C compared to the value in the dark. This indicates that the filling of the bands with electrons, as well as the contribution to the free energy due to the inter-band electron-phonon interaction, can be changed by photoactive light absorption. The photoactive illumination may change not only the free electrons' concentration in the band, but also the filling of all the traps in the forbidden band due to defects or impurities.

Photo-induced deformation is another photoferroelectric phenomenon. Under illumination, ferroelectrics may deform due to the influence of the non-equilibrium carriers on the spontaneous polarization and electrostriction coefficient. The lattice deformation caused by the pressure of the non-equilibrium carriers may also lead to the deformation of the material. In addition, when the generated photovoltaic field is large enough, it may cause perceptible deformation through the inverse piezoelectric effect.

With photo-stimulated phase transition and photo-induced deformation, the illumination is also able to affect spontaneous polarization and piezoelectric properties in photoferroelectrics. Detailed discussions of the mechanisms of the photoferroelectric phenomena can be found in the books.[588, 589]

4.4.4. Bismuth ferrite and relevant materials

$BiFeO_3$ (BFO) and its relevant compositions have been extensively studied together with the development of the theories of BPVE and photoferroelectrics. More importantly, BFO yields the narrowest known band gap (2.2-2.7 eV) among the conventional ferroelectric ceramics such as BTO, PZT and KNN (> 3.5 eV).[56, 587] The relatively narrow band gap allows BFO to absorb

about 20 % of the solar spectrum. Meanwhile, pure $BiFeO_3$ exhibits a piezoelectric charge coefficient ($\boldsymbol{d_{33}}$) and pyroelectric coefficient ($\boldsymbol{p}$) of ~45 pC/N and ~90 μC m^{-2} K^{-1}, respectively[590]. BFO is also ferromagnetic, making it a multiferroic material.[591] With these multi-functional properties, BFO can be considered a potential candidate for multi-source energy harvesting.

The domain wall photovoltaic effect has been observed in BFO thin-films. Yang et al.[592] used 200-300 nm thick, (001) oriented BFO films comprising purely 71˚ domain walls to examine the domain wall photovoltaic effect. Because of the domain wall orientation, stripe domains with an average width of ~ 160 nm were obtained. A linearly polarized blue laser (405 nm, 3.06 eV) was used as the incident light source. Atomic force microscopy (AFM) and piezoresponse force microscopy (PFM) were used to detect the photocurrents and map the surface of the BFO films, respectively. **Figure 16** shows the results. It can be clearly seen that the peak photovoltaic currents were detected at the domain walls which corresponded to the valleys of the in-plane PFM amplitude signals. The enhanced photocurrent at the domain walls may be caused by the higher photoconductivity than that existing within the domains due to increased carrier density or mobility. However, this is not considered a photovoltaic effect within the domain walls.[592]

The band gap of pure BFO prevents it from effectively using a large part of the solar spectrum. As mentioned above, 1.34 eV is an ideal band gap for photovoltaic materials. As a consequence, some works focusing on further reducing BFO's band gap have been carried out. Doping is an effective method. A Ho and Mn co-doped BFO showed a reduced band gap of 1.77 eV. Such a co-doping could also increase the ferroelectric properties at the same time, e.g. spontaneous and remanent polarizations.[593] This may help the co-optimization of the ferroelectric and photovoltaic multi-functions. By partially substituting Fe with Cr, a Bi_2FeCrO_6 (BFCO) thin-film obtained a tunable band gap between 1.5-2.7 eV. Multi-layer structured solar cells were constructed using the BFCO thin-films. An 8.1 % photovoltaic energy conversion efficiency was achieved under ''one sun'' illumination, compared to only < 2 % for those wide band gap

ferroelectrics including pure BFO.[594] This result shows a possible and promising future for photoferroelectrics to reach the same level of efficiency as Si-based solar cells. **Figure 17** (a) shows the configuration of the fabricated solar cell. This cell also exhibited a giant ferroelectricity with remanent polarization larger than those of conventional ferroelectrics such as PZT, BTO and KNN, as shown in Figure 17 (b) – see hysteresis loop M1. Although it was not discussed in detail, the polarization may affect the external quantum efficiency of the photoferroelectrics by determining the separation of photogenerated charges, as can be seen in Figure 17 (b) and when comparing the efficiencies of the M1 (8.1 %) and M2 (4.3 %) cells.[594] This also provides a unique opportunity to tune the photovoltaic property and ferroelectricity (i.e. potentially piezoelectric and pyroelectric responses) simultaneously.

The piezoelectric and pyroelectric properties of pure BFO are still much worse than those of conventional counterparts, e.g. d_{33} of ~ 600 pC N^{-1} and p of ~ 260 μC m^{-2} K^{-1} for PZT.[565, 595] As for other ABO_3 structured piezoelectric materials, proper doping is able to effectively enhance the piezoelectric properties. For instance, Sm-doping could increase the d_{33} up to 110 pC N^{-1} (for composition $Bi_{0.86}Sm_{0.14}FeO_3$).[596] By creating the BFO-BTO binary system, the 0.1 wt.% Mn-doped 0.75BFO-0.25BTO and 0.35 mol.% Mn/0.6 mol.% Li-co-doped 0.725BFO-0.275BTO could exhibit d_{33} values of up to 116 pC N^{-1} and 163 pC N^{-1}, respectively.[597, 598]

The major physical challenge of the BFO used as the multi-functional material for multi-source energy harvesting is the need for the simultaneous optimization of the photovoltaic, piezoelectric and pyroelectric properties. Although BFO can exhibit spontaneous and remanent polarizations which are even larger than conventional PZT, this does not necessarily induce better piezoelectric and pyroelectric properties. Although the PZT family has been maturely and widely used in piezoelectric and pyroelectric devices for a long time, there have been only rare efforts to optimize the piezoelectric and pyroelectric properties of the BFO which seemed not to be worthwhile. Consequently, with the increasing interest in the multi-source energy

harvesting, comprehensive data are lacking for the compositional optimization methods of piezoelectric and pyroelectric properties. The examples given above are not enough; they are still unable to show properties competitive with those of PZT. In addition, the introduction of the BTO into the BFO is likely to widen the band gap, as the BTO has a much wider band gap than the BFO. Therefore, further developments need to be focused on compositional and microstructural optimizations in order to improve the piezoelectric and pyroelectric properties towards the level of PZT, whilst maintaining or even further reducing the band gap. Potential methods will be given in detail in Section 5.

4.4.5. Band gap engineering

Apart from the effort made to reduce the BFO's band gap, band gap engineering has also been applied to other compositions. There are two effective methods reported for band gap engineering of the ferroelectric materials – polarization rotation associated with phase change or strain[599-601] and compositional modification via, for example, doping[599, 602-607]. Wang et al. studied the band gap engineering of 7 types of ferroelectric crystals including $LaScO_3$, BT, $BaZrO_3$, $PbTiO_3$, $KTaO_3$, $KNbO_3$ and WO_3.[599] For each composition, when the value of the spontaneous polarization was changed because of a phase transition (rhombohedral to tetragonal) or an applied strain, the band gap was reduced correspondingly by different extents. The largest band gap decrease with a relatively small deterioration of polarization (meaning less influence on potential piezoelectric and pyroelectric effects) appeared to be for $KNbO_3$ and $KTaO_3$. For instance, the band gap in rhombohedral-phase $KNbO_3$ with a spontaneous polarization value of 57 μC cm^{-2} was about 3.7 eV. This was reduced to 2.6 eV when the phase changed to tetragonal exhibiting a spontaneous polarization of 50 μC cm^{-2}. Only a 9 % compromise in the polarization resulted in a 30 % reduction in band gap. Meanwhile, the band gap of the $KNbO_3$ was further reduced by 0.6 eV when subject to a -2 % in-plane strain.[599, 600]

Similar phenomena were also observed in other compositions such as $BaSnO_3$ and $SrSnO_3$, where tensile strain induced a significant band gap narrowing effect (from 3 eV to 2-2.8 eV).[601] However, the band gap engineering via polarization rotation is limited by the original band gap to some extent. The material has a maximum strain value it can stand, thus the band gap reduction is limited to certain extent associated with the strain limit. If a ferroelectric composition has a very wide original band gap, this method becomes restricted and unable to reduce it to a value suitable for visible range absorption. In this situation, compositional modification becomes necessary to intrinsically reduce the band gap at the unit cell level. Appropriate doping is an effective method of narrowing a band gap. Zr-doped $Pb(Zn_{1/3}Nb_{2/3})O_3$ and $Pb(Mg_{1/3}Nb_{2/3})O_3$ were able to exhibit a band gaps 0.5 eV lower than their un-doped counterparts due to the presence of oxygen vacancies after doping.[602] By partially substituting Nb^{5+} for Zn^{2+}, the composition of $0.75KNbO_3$-$0.25(Sr_{1/2}La_{1/2})(Zn_{1/2}Nb_{1/2})O_3$ exhibited a band gap of 2.1 eV compared to 3.4 eV for pure $KNbO_3$.[600] A similar phenomenon was also observed in Bi-doped $KNbO_3$ due to the introduction of low-lying intermediate bands via Bi^{5+} substitution for Nb^{5+}.[603] Other reported band gap engineering for $KNbO_3$ based ferroelectrics includes the compositions of $(KNbO_3)_{1-x}(BaCo_{1/2}Nb_{1/2}O_{3-\delta})_x$[604] and $(KNbO_3)_{1-x}(BaNb_{1/2}Fe_{1/2}O_3)_x$[605] which exhibited narrow band gaps of 2.4 eV and 1.72-2.48 eV, respectively. Apart from the $KNbO_3$ based compositions, the effect of band gap reduction was also reported for a multiferroic $CaMn_7O_{12}$ nanocrystalline structure in the presence of surface oxygen vacancies[606] and for a Ni-doped $SrBi_2Nb_2O_9$ ferroelectric ceramic[607]. The lowest band gaps achieved in these two compositions were 1.38 eV and 2.25 eV, respectively.

Further details of the history and development of the photovoltaic-ferroelectric compositions including BFO, PZT based, BTO based, etc. can be found in reference[587]. It is worth mentioning that first principle calculation is an important tool for the band gap engineering based on compositional modification. The unit cells and microstructure need to be simulated to

predict the expected performance in order to avoid tedious empirical works such as happened in the early stages of thermoelectric development history.

Unfortunately, although the ferroelectricity, piezoelectricity, pyroelectricity, band gap engineering, photovoltaic effect and photoferroelectric phenomena/BPVE, as well as their applications in single-source and hybrid energy harvesters have been extensively studied, these properties as a whole have rarely been reported in the same paper or by the same research team. Although band gap engineering methods could effectively reduce the band gaps of some compositions, those compositions rarely exhibit good piezoelectric and pyroelectric simultaneously. Until that to be presented in Section 4.5, neither the piezoelectric-pyroelectric-photovoltaic multi-functional properties of any material nor a multi-source energy harvesting prototype have been reported to demonstrate the feasibility of using photoferroelctrics for multi-source energy harvesting. More works need to be done from such a point of view.

4.5. Realization of truly multi-source energy harvesting with piezoelectric-pyroelectric-photovoltaic multi-functional materials

4.5.1. Potassium barium nickel niobate – KBNNO

While the photovoltaic and ferroelectric properties have been researched individually for the photoferroelectrics, and visible range narrow band gaps and strong ferroelectricity in these materials have been reported separately, their piezoelectric, pyroelectric and photovoltaic properties have rarely been studied simultaneously in the same material. One of the reasons may be that although the theories and methods of tuning the photovoltaic or piezoelectric/pyroelectric properties without concerns of compromising the other has been relatively well established, optimizing all of them concurrently whilst avoiding degradation of any property seems to be complicated. For example, Grinberg et al. reported a composition of Ba, Ni-co-doped $KNbO_3$ with the presence of oxygen vacancies, $(KNbO_3)_{1-x}(BaNi_{1/2}Nb_{1/2}O_{3-\delta})_x$ (KBNNO).[56] With the variation of the x value from 0.1 to 0.5, the band gap of the

composition was tunable from 1.1 eV to 2 eV. It should be particularly noted that when x = 0.1, i.e. the composition $0.9KNbO_3$-$0.1BaNi_{1/2}Nb_{1/2}O_{3-\delta}$, a direct band gap of 1.39 eV was obtained. This value is very close to 1.34 eV which gives the maximum S-Q limit and thus is considered to be the ideal band gap for photovoltaic materials. However, in the mean time it was shown that typical, saturated ferroelectric hysteresis loops could only be measured at < 0 ˚C (i.e. from -196 ˚C to -103 ˚C), exhibiting a remanent polarization of about 5 μC cm^{-2}. At above -83 ˚C, the loops became distorted and unsaturated, showing a remanent polarization of nearly zero, which was explained as being due to increased leakage and thus ineffective poling.[56] This makes this composition unlikely to exhibit substantial piezoelectricity and pyroelectricity in practice (e.g. at room temperature), which properties are in a close relationship with the remanent polarization and effectiveness of poling.

Bai et al. subsequently confirmed the narrow band gap in the same composition and characterized the piezoelectric and pyroelectric properties.[608] Although the high leakage and ineffective poling were avoided to a large extent by further fine tuning of the composition from the original $(K_{0.9}Ba_{0.1})(Nb_{0.95}Ni_{0.05})O_{3-0.025}$ to $(K_{0.8}Ba_{0.1})(Nb_{0.95}Ni_{0.05})O_{3-0.075}$, the $\boldsymbol{d_{33}}$ and $\boldsymbol{p}$ were measured to be only 23 pC/N and 26 μC m^{-2} K^{-1}, respectively, despite the narrow band gap of 1.48 eV. These values were already much more advantageous than those of non-ferroelectric semiconductors (e.g. ZnO, AlN, etc.), however, they were not as competitive as those of BTO and PZT based compositions. When considering its narrow band gap, which could not be emulated by BTO and PZT based compositions, KBNNO shows a very promising future as discovering an excellent piezoelectric-pyroelectric-photovoltaic multi-functional material. The main strategy is to narrow the band gap whilst maintaining the strong ferroelectricity.

4.5.2. Potassium sodium barium nickel niobate – KNBNNO

A candidate co-exhibiting narrow band gap and strong ferroelectricity, piezoelectricity and pyroelectricity was firstly reported by Bai et al. for the composition of $(K_{0.5}Na_{0.5})NbO_3$ doped

with 2 mol.% $Ba(Ni_{0.5}Nb_{0.5})O_{3-\delta}$ (KNBNNO).[60] Compared to the matrix composition, $KNbO_3$, in the KBNNO the $(K_{0.5}Na_{0.5})NbO_3$ in the KNBNNO offered a more reliable fabrication route (i.e. easier sintering, less hygroscopic, etc.). It had already been known that the Ni^{2+} ions doped into the B site in combination with the introduced oxygen vacancies were able to significantly reduce the band gap, due to easier electron transfer from the oxygen 2p states at the maximum level of the valence band to the transition-metal (Nb) d states at the minimum level of the conduction band. However, it was practically not necessary to introduce a large concentration of Ni^{2+}-oxygen vacancy combinations, because a non-monotonic relationship between the band gap and Ni^{2+}-oxygen vacancy concentration was found to exist.[56] Excessive oxygen vacancy was likely to degrade the ferroelectricity and poling effectiveness due to the introduction of the pinning effect. It was finally found that with only 2 mol.% doping the KNBNNO could exhibit a narrow band gap (1.6 eV) together with strong ferroelectric (remanent polarization of 11 μC cm^{-2}), piezoelectric ($\boldsymbol{d_{33}} \approx 100$ pC N^{-1}) and pyroelectric ($\boldsymbol{p} \approx 130$ μC m^{-2} K^{-1}) properties. Although the piezoelectric and pyroelectric properties were still not as good as those of BTO and PZT based compositions, the properties in the matrix composition were successfully maintained in the doped composition whilst simultaneously achieving a narrow band gap simultaneously. These results, which had never been reported previously, provided a guideline to further develop such ideal multi-functional materials for multi-source energy harvesting.

Figure 18 demonstrates the feasibility and a potential example of a practical application of using KNBNNO as the multi-functional material for multi-source energy harvesting. Figure 18 (a) explains that there was no degradation between the pyroelectric and photovoltaic effects. As can be seen in the figure, the output current signals of the material under illumination and with temperature fluctuation simultaneously are the sum of those under illumination only and those with temperature fluctuation only. This implies that the photovoltaic and pyroelectric effects in the KNBNNO can work both independently and simultaneously without counteracting each other. Figure 18 (b) shows the output current of the KNBNNO subject to light, kinetic and

thermal energies, both individually and simultaneously. The energy sources used to obtain the data were very practical, i.e. a desk lamp as the light source, a hairdryer as the heat source and mechanical impact as the kinetic source. It has been discussed in Section 4.1 that the piezoelectric and pyroelectric effects can also work independently and simultaneously without counteracting each other. Therefore, the feasibility of making a multi-source energy harvester using KNBNNO as the only energy conversion component can be proved. Figure 18 (c) shows three cantilever structures. Potential examples of the hybrid and multi-source energy harvesters are proposed. It can be clearly seen that with only a piece of a multi-functional energy conversion material attached to the cantilever, the multi-source energy harvester is significantly simplified compared to the hybrid structures where different energy conversion components need to be laminated.

As a summary, Table 2 lists the piezoelectric and pyroelectric properties of different compositions (including oxides, inorganic compositions, polymers and perovskites) together with their band gaps. Considering the factors listed in Table 2 as a whole, the perovskite structured KNBNNO shows the most promising performance for solar-thermal-kinetic multi-source energy harvesting.

5. Conclusion and perspectives

The development of energy harvesting research from single-source to multi-source has been reviewed in this paper. The single-source energy harvesters have been relatively well-developed, showing their capability of practically powering low power consumption WSN with ample and stable ambient input energy. The development progress of energy harvesting technology has come to the stage of a broad investigation of multi-source energy harvesters based on structural hybridizations or multi-functional energy conversion materials. This is a compulsory stage in order to deal with the insufficient, unstable and even random input energy available to energy harvesters in most cases of a real ambient environment. Compared to structurally hybrid multi-

source energy harvesters, which have attracted much attention and generated many prototypes aimed for certain applications, the development of those based on multi-functional materials has only just begun. It is still at the stage of exploring ideal material candidates to be used for further structural optimization. This will require a great deal of effort in the research related to physics, chemistry and materials science.

In the current state of the art, only piezoelectric, pyroelectric and photovoltaic effects can be integrated into the same multi-functional material. However, other possibilities also exist but remain to be investigated. As with the co-existence of the photovoltaic effect and ferroelectricity in photoferroelectrics, ferroelectric-thermoelectricity has also been discussed[609], although the focus has only been on the thermoelectric aspect. With deeper investigation of the thermoelectric properties in ferroelectrics, an opportunity might occur in the future that allows the piezoelectric, pyroelectric, photovoltaic and even thermoelectric effects to be co-exhist in the same multi-functional material.

In summary, as single-source energy harvesting research has created many research results and outcomes, new research directions need to be set for a continuous development. The new directions may include (but are not limited to):

1) More advanced structural hybridization of more than three energy harvesting effects/materials/configurations. The major challenge of the hybrid energy harvesters is the increased structural complexity and device size associated with the increased number of energy conversion materials for different energy sources. Although the structure can still be made compact by laminating a layer of piezoelectric-pyroelectric material and a layer of photovoltaic solar cell, more compact structures need to be designed and fabricated with more coupled energy sources. There has not been a hybrid harvester reported to integrate more than three energy harvesting effects. For instance, a three-layer lamination could be designed with piezoelectric-pyroelectric, photovoltaic and thermoelectric materials. Triboelectric materials and electrets coukld also be further integrated to enhance the kinetic energy conversion

efficiency. These materials can be fabricated into a multi-layer film structure layer by layer (e.g. with pulsed laser deposition), and do not require relatively moving parts.

2). Improved piezoelectric and pyroelectric properties in narrow band gap photoferroelectrics. The major challenge of the use of multi-functional materials for multi-source energy harvesting is that the piezoelectric, pyroelectric and photovoltaic properties have not simultaneously reached the levels of their individual counterparts. The newly developed KNBNNO exhibits a narrow band gap which is comparable to those of conventional photovoltaic materials. However, its piezoelectric and pyroelectric properties are still far below those of conventional counterparts. On the other hand, the band gaps of those conventional piezoelectric and pyroelectric materials are too wide to effectively absorb the visible-range of the solar spectrum. According to the previous experience with ferroelectric materials co-exhibiting strong piezoelectric and pyroelectric effects as well as non-ferroelectric materials which are narrow band gap semiconductors and weak piezoelectrics/pyroelectrics, two strategies can be established for developing multi-functional materials with strong piezoelectric and pyroelectric responses together with the narrow bandgaps required for efficient multi-source energy harvesting. One strategy is to employ the platform of a good photovoltaic material (narrow bandgap, high photovoltaic energy conversion efficiency) and then investigate the possibility of the introduction/discovery of strong piezoelectric and/or pyroelectric phenomena in the material's microstructure, i.e. to increase the asymmetry of the unit cells. The other strategy is to use the frame of strong piezoelectric/pyroelectric materials (e.g. poled ferroelectrics with large spontaneous polarizations) and to explore the possibilities of narrowing the band gaps, e.g. by introducing Ni^{2+} and oxygen vacancy combinations, as used for the development of KNBNNO.

3) Fabrication and characterization of multi-source energy harvesters. As the studies of the piezoelectric-pyroelectric-photovoltaic effects as a whole multi-functional property have emerged only very recently, there has not been any investigation conducted at the device level.

A multi-source energy harvesting demonstrator made with a multi-functional material, e.g. KNBNNO, needs to be fabricated and characterized. The inter-influence of the kinetic, thermal and solar energy harvesting behaviors should be studied, e.g. the effect of strain on the photovoltaic effect. A cantilever attached with a piece of KNBNNO can be a straightforward start of such an investigation. Multi-functional modeling can be a supportive tool for the device design and performance prediction.

The energy harvesting research has come to the era of multi-source energy harvestings based on hybrid structures and/or multi-functional materials which will widen the feasibility of energy harvesters. The future of the energy harvesting will see more novel multi-source harvesters.

Acknowledgements

The authors would like to acknowledge the funding from the European Union's Horizon 2020 research and innovation program under the Marie Sklodowska-Curie grant agreement number 705437. Author J.J. acknowledges the funding of the Academy of Finland (project numbers 267573 and 304033).

References

[1] J. Manuel Carrasco, L. G. Franquelo, J. T. Bialasiewicz, E. Galvan, R. Portillo, M. Martin Prats, J. Ignacio Leon, N. Moreno-Alfonso, , *IEEE Trans. Ind. Electron.* **2006**, *53*(4), 1002-1016.

[2] E. Haeusler, L. Stein, G. Harbauer, , *Ferroelectrics.* **1984**, *60*(1), 277-282.

[3] S. Roundy, P. Wright, J. Rabaey, , *Comput. Commun.* **2003**, *26*(11), 1131-1144.

[4] H. Sodano, D. Inman, G. Park, , *The shock and vibration digest.* **2004**, *36*, 197.

[5] S. R. Anton, H. A. Sodano, , *Smart Mater. Struct.* **2007**, *16*(3), R1-R21.

[6] F. Edler, E. Lenz, , *9th European Conference on Thermoelectrics (Ect2011).* **2012**, *1449*, 369-372.

[7] A. A. Babayo, M. H. Anisi, I. Ali, , *Renew. Sust. Energ. Rev.* **2017**, *76*, 1176-1184.

[8] G. D. Szarka, B. H. Stark, S. G. Burrow, , *IEEE Trans. Power Electron.* **2012**, *27*(2), 803-815.

[9] C. Wei, X. Jing, , *Renew. Sust. Energ. Rev.* **2017**, *74*, 1-18.

[10] M. A. Green, Y. Hishikawa, E. D. Dunlop, D. H. Levi, J. Hohl-Ebinger, A. W. Y. Ho-Baillie, , *Prog. Photovoltaics.* **2018**, *26*(1), 3-12.

[11] K. A. Cook-Chennault, N. Thambi, A. M. Sastry, , *Smart Mater. Struct.* **2008**, *17*(4), 043001.

[12] J. H. Heo, S. H. Im, , *Adv Mater.* **2016**, *28*(25), 5121-5125.

[13] J. E. Spanier, V. M. Fridkin, A. M. Rappe, A. R. Akbashev, A. Polemi, Y. Qi, Z. Gu, S. M. Young, C. J. Hawley, D. Imbrenda, G. Xiao, A. L. Bennett-Jackson, C. L. Johnson, , *Nat. Photonics.* **2016**, *10*(10), 688-688.

[14] A. Polman, M. Knight, E. C. Garnett, B. Ehrler, W. C. Sinke, , *Science.* **2016**, *352*(6283), aad4424.

[15] G. K. Singh, , *Energy.* **2013**, *53*, 1-13.

[16] A. Goetzberger, C. Hebling, H. Schock, , *Mater. Sci. Eng. R-Rep.* **2003**, *40*(1), 1-46.

[17] Q. Tai, F. Yan, , *Adv Mater.* **2017**, *29*(34), 1700192.

[18] J. Rath, , *Solar Energy Mater. Solar Cells.* **2003**, *76*(4), 431-487.

[19] A. Hagfeldt, G. Boschloo, L. Sun, L. Kloo, H. Pettersson, , *Chem. Rev.* **2010**, *110*(11), 6595-6663.

[20] M. Gratzel, , *J. Photochem. Photobiol. C-Photochem. Rev.* **2003**, *4*(2), 145-153.

[21] M. Graetzel, , *Acc. Chem. Res.* **2009**, *42*(11), 1788-1798.

[22] B. E. Hardin, H. J. Snaith, M. D. McGehee, , *Nat. Photonics.* **2012**, *6*(3), 162-169.

[23] Y. Cheng, S. Yang, C. Hsu, , *Chem. Rev.* **2009**, *109*(11), 5868-5923.

[24] S. Guenes, H. Neugebauer, N. S. Sariciftci, , *Chem. Rev.* **2007**, *107*(4), 1324-1338.

[25] B. C. Thompson, J. M. J. Frechet, , *Angew. Chem. -Int. Edit.* **2008**, *47*(1), 58-77.

[26] G. Dennler, M. C. Scharber, C. J. Brabec, , *Adv Mater.* **2009**, *21*(13), 1323-1338.

[27] G. Li, R. Zhu, Y. Yang, , *Nat. Photonics.* **2012**, *6*(3), 153-161.

[28] K. Coakley, M. McGehee, , *Chem. Mat.* **2004**, *16*(23), 4533-4542.

[29] H. Hoppe, N. Sariciftci, , *J. Mater. Res.* **2004**, *19*(7), 1924-1945.

[30] C. J. Brabec, S. Gowrisanker, J. J. M. Halls, D. Laird, S. Jia, S. P. Williams, , *Adv Mater.* **2010**, *22*(34), 3839-3856.

[31] L. Lu, T. Zheng, Q. Wu, A. M. Schneider, D. Zhao, L. Yu, , *Chem. Rev.* **2015**, *115*(23), 12666-12731.

[32] P. V. Kamat, , *J. Phys. Chem. C.* **2008**, *112*(48), 18737-18753.

[33] W. S. Yang, B. Park, E. H. Jung, N. J. Jeon, Y. C. Kim, D. U. Lee, S. S. Shin, J. Seo, E. K. Kim, J. H. Noh, S. I. Seok, , *Science.* **2017***, 356*(6345), 1376-+.

[34] G. Hodes, , *Science.* **2013***, 342*(6156), 317-318.

[35] M. A. Green, A. Ho-Baillie, H. J. Snaith, , *Nat. Photonics.* **2014***, 8*(7), 506-514.

[36] S. D. Stranks, H. J. Snaith, , *Nat. Nanotechnol.* **2015***, 10*(5), 391-402.

[37] P. Gao, M. Graetzel, M. K. Nazeeruddin, , *Energy Environ. Sci.* **2014***, 7*(8), 2448-2463.

[38] H. S. Jung, N. Park, , *Small.* **2015***, 11*(1), 10-25.

[39] W. Yin, J. Yang, J. Kang, Y. Yan, S. Wei, , *J. Mater. Chem. A.* **2015***, 3*(17), 8926-8942.

[40] T. Salim, S. Sun, Y. Abe, A. Krishna, A. C. Grimsdale, Y. M. Lam, , *J. Mater. Chem. A.* **2015***, 3*(17), 8943-8969.

[41] P. P. Boix, K. Nonomura, N. Mathews, S. G. Mhaisalkar, , *Mater. Today.* **2014***, 17*(1), 16-23.

[42] T. Ibn-Mohammed, S. C. L. Koh, I. M. Reaney, A. Acquaye, G. Schileo, K. B. Mustapha, R. Greenough, , *Renew. Sust. Energ. Rev.* **2017***, 80*, 1321-1344.

[43] U. Mehmood, A. Al-Ahmed, M. Afzaal, F. A. Al-Sulaiman, M. Daud, , *Renew. Sust. Energ. Rev.* **2017***, 78*, 1-14.

[44] S. Yang, W. Fu, Z. Zhang, H. Chen, C. Li, , *J. Mater. Chem. A.* **2017***, 5*(23), 11462-11482.

[45] M. I. Asghar, J. Zhang, H. Wang, P. D. Lund, , *Renew. Sust. Energ. Rev.* **2017***, 77*, 131-146.

[46] D. Wang, M. Wright, N. K. Elumalai, A. Uddin, , *Solar Energy Mater. Solar Cells.* **2016**, *147*, 255-275.

[47] C. R. Osterwald, T. J. McMahon, , *Prog. Photovoltaics.* **2009**, *17*(1), 11-33.

[48] S. Maniarasu, T. B. Korukonda, V. Manjunath, E. Ramasamy, M. Ramesh, G. Veerappan, , *Renew. Sust. Energ. Rev.* **2018**, *82*, 845-857.

[49] W. Chen, Y. Wu, Y. Yue, J. Liu, W. Zhang, X. Yang, H. Chen, E. Bi, I. Ashraful, M. Graetzel, L. Han, , *Science.* **2015**, *350*(6263), 944-948.

[50] EU-Directive 2002/96/EC, , *Off. J. Eur. Union.* **2003**, *46*(L37), 24.

[51] EU-Directive 2002/95/EC, , *Off. J. Eur. Union.* **2003**, *46*(L37), 19.

[52] N. K. Noel, S. D. Stranks, A. Abate, C. Wehrenfennig, S. Guarnera, A. Haghighirad, A. Sadhanala, G. E. Eperon, S. K. Pathak, M. B. Johnston, A. Petrozza, L. M. Herz, H. J. Snaith, , *Energy Environ. Sci.* **2014**, *7*(9), 3061-3068.

[53] S. J. Lee, S. S. Shin, Y. C. Kim, D. Kim, Tae Kyu Ahn, J. H. Noh, J. Seo, S. I. Seok, , *J. Am. Chem. Soc.* **2016**, *138*(12), 3974-3977.

[54] Z. Zhao, F. Gu, Y. Li, W. Sun, S. Ye, H. Rao, Z. Liu, Z. Bian, C. Huang, , *Adv. Sci.* **2017**, *4*(11), 1700204.

[55] J. Roedel, W. Jo, K. T. P. Seifert, E. Anton, T. Granzow, D. Damjanovic, , *J Am Ceram Soc.* **2009**, *92*(6), 1153-1177.

[56] I. Grinberg, D. V. West, M. Torres, G. Gou, D. M. Stein, L. Wu, G. Chen, E. M. Gallo, A. R. Akbashev, P. K. Davies, J. E. Spanier, A. M. Rappe, , *Nature.* **2013**, *503*(7477), 509-+.

[57] V. M. Fridkin, , *IEEE Trans. Ultrason. Ferroelectr. Freq. Control.* **2013**, *60*(8), 1551-1555.

[58] S. Liu, F. Zheng, I. Grinberg, A. M. Rappe, , *J. Phys. Chem. Lett.* **2016**, *7*(8), 1460-1465.

[59] Y. Rakita, E. Meirzadeh, T. Bendikov, V. Kalchenko, I. Lubomirsky, G. Hodes, D. Ehre, D. Cahen, , *APL Mater.* **2016**, *4*(5), 051101.

[60] Y. Bai, P. Tofel, J. Palosaari, H. Jantunen, J. Juuti, , *Adv Mater.* **2017**, *29*(29), 1700767.

[61] C. Sue, N. Tsai, , *Appl. Energy.* **2012**, *93*, 390-403.

[62] H. Kalantarian, M. Sarrafzadeh, , *IEEE Sens. J.* **2016**, *16*(23), 8314-8321.

[63] L. Mateu, F. Moll, , *J Intell Mater Syst Struct.* **2005**, *16*(10), 835-845.

[64] Y. Xin, X. Li, H. Tian, C. Guo, C. Qian, S. Wang, C. Wang, , *Ferroelectrics.* **2016**, *493*(1), 12-24.

[65] J. Zhao, Z. You, , *Sensors.* **2014**, *14*(7), 12497-12510.

[66] M. Leinonen, J. Juuti, H. Jantunen, J. Palosaari, , *Energy Technol.* **2016**, *4*(5), 620-624.

[67] S. Almouahed, M. Gouriou, C. Hamitouche, E. Stindel, C. Roux, , *IEEE-ASME Trans. Mechatron.* **2011**, *16*(5), 799-807.

[68] M. Deterre, S. Risquez, B. Bouthaud, R. Dal Molin, M. Woytasik, E. Lefeuvre, , *13th International Conference on Micro and Nanotechnology for Power Generation and Energy Conversion Applications (Powermems 2013).* **2013**, *476*, UNSP 012039.

[69] K. Pancharoen, D. Zhu, S. P. Beeby, , *14th International Conference on Micro and Nanotechnology for Power Generation and Energy Conversion Applications (Powermems 2014).* **2014**, *557*, 012038.

[70] A. Sudano, D. Accoto, M. T. Francomano, F. Salvinelli, E. Guglielmelli, , *2011 Annual International Conference of the Ieee Engineering in Medicine and Biology Society (Embc).* **2011**, 7678-7681.

[71] D. A. Porter, T. A. Berfield, , *Smart Mater. Struct.* **2014**, *23*(7), 075003.

[72] T. Xue, X. Ma, C. Rahn, S. Roundy, , *14th International Conference on Micro and Nanotechnology for Power Generation and Energy Conversion Applications (Powermems 2014).* **2014**, *557*, 012090.

[73] Y. Bai, P. Pofel, Z. Hadas, J. Smilek, P. Losak, P. Skarvada, R. Macku, , *Mechanical Systems and Signal Processing.* **2018**, *106*, 303.

[74] J. Smilek, Z. Hadas, , *Microsyst. Technol.* **2016**, *22*(7), 1535-1547.

[75] A. Chandrasekhar, N. R. Alluri, V. Vivekananthan, Y. Purusothaman, S. Kim, , *J. Mater. Chem. C.* **2017**, *5*(6), 1488-1493.

[76] J. Feenstra, J. Granstrom, H. Sodano, , *Mech. Syst. Signal Proc.* **2008**, *22*(3), 721-734.

[77] J. Granstrom, J. Feenstra, H. A. Sodano, K. Farinholt, , *Smart Mater. Struct.* **2007**, *16*(5), 1810-1820.

[78] C. Dagdeviren, Z. Li, Z. L. Wang, , *Annu. Rev. Biomed. Eng.* **2017**, *19*, 85-108.

[79] F. Invernizzi, S. Dulio, M. Patrini, G. Guizzetti, P. Mustarelli, , *Chem. Soc. Rev.* **2016**, *45*(20), 5455-5473.

[80] P. D. Mitcheson, E. M. Yeatman, G. K. Rao, A. S. Holmes, T. C. Green, , *Proc IEEE.* **2008**, *96*(9), 1457-1486.

[81] A. Proto, M. Penhaker, S. Conforto, M. Schmid, , *Trends Biotechnol.* **2017**, *35*(7), 610-624.

[82] R. Riemer, A. Shapiro, , *J. NeuroEng. Rehabil.* **2011**, *8*, 22.

[83] A. Moure, M. A. Izquierdo Rodriguez, S. Hernandez Rueda, A. Gonzalo, F. Rubio-Marcos, D. Urquiza Cuadros, A. Perez-Lepe, J. F. Fernandez, , *Energy Conv. Manag.* **2016**, *112*, 246-253.

[84] Y. Chen, H. Zhang, Y. Zhang, C. Li, Q. Yang, H. Zheng, C. Lu, , *J. Appl. Mech. -Trans. ASME.* **2016**, *83*(8), 081001.

[85] F. Duarte, A. Ferreira, , *Proc. Inst. Civ. Eng. -Energy.* **2016**, *169*(2), 79-90.

[86] X. Jiang, Y. Li, J. Li, J. Wang, J. Yao, , *J. Renew. Sustain. Energy.* **2014**, *6*(4), 043110.

[87] F. Duarte, A. Ferreira, P. Fael, , *J. Renew. Sustain. Energy.* **2017**, *9*(3), 034701.

[88] A. du Plessis, M. Huigsloot, F. Discenzo, , *Smart Structures and Materials 2005: Industrial and Commercial Applications of Smart Structures Technologies.* **2005**, *5762*, 224-235.

[89] X. Shan, S. Guan, Z. Liu, Z. Xu, T. Xie, , *J. Zhejiang Univ. -SCI A.* **2013**, *14*(12), 890-897.

[90] X. D. Xie, Q. Wang, , *Energy.* **2015**, *86*, 385-392.

[91] L. Zuo, B. Scully, J. Shestani, Y. Zhou, , *Smart Mater. Struct.* **2010**, *19*(4), 045003.

[92] P. Cahill, N. A. N. Nuallain, N. Jackson, A. Mathewson, R. Karoumi, V. Pakrashi, , *J. Bridge Eng.* **2014**, *19*(9), 04014034.

[93] M. Peigney, D. Siegert, , *Smart Mater. Struct.* **2013**, *22*(9), 095019.

[94] Y. Zhang, S. C. S. Cai, L. Deng, , *J Intell Mater Syst Struct.* **2014**, *25*(12), 1414-1428.

[95] M. Karimi, A. H. Karimi, R. Tikani, S. Ziaei-Rad, , *Int. J. Mech. Sci.* **2016**, *119*, 1-11.

[96] C. Maruccio, G. Quaranta, L. De Lorenzis, G. Monti, , *Smart Mater. Struct.* **2016**, *25*(8), 085040.

[97] F. U. Khan, I. Ahmad, , *Shock Vibrat.* **2016**, 1340402.

[98] C. R. Bowen, M. H. Arafa, , *Adv. Energy Mater.* **2015**, *5*(7), 1401787.

[99] Y. Hu, C. Xu, Y. Zhang, L. Lin, R. L. Snyder, Z. L. Wang, , *Adv Mater.* **2011**, *23*(35), 4068-+.

[100] J. Lee, B. Choi, , *Energy Conv. Manag.* **2014**, *78*, 32-38.

[101] K. H. Mak, S. McWilliam, A. A. Popov, , *Proc. Inst. Mech. Eng. Part D-J. Automob. Eng.* **2013**, *227*(6), 842-852.

[102] K. B. Singh, V. Bedekar, S. Taheri, S. Priya, , *Mechatronics.* **2012**, *22*(7), 970-988.

[103] A. T. Eshghi, S. Lee, M. K. Sadoughi, C. Hu, Y. Kim, J. Seo, , *Smart Mater. Struct.* **2017**, *26*(10), 105037.

[104] J. Lee, J. Oh, H. Kim, B. Choi, , *J Intell Mater Syst Struct.* **2015**, *26*(11), 1404-1416.

[105] F. Amoroso, R. Pecora, M. Ciminello, A. Concilio, , *Smart. Struct. Syst.* **2015***, 16*(3), 383-399.

[106] A. Cammarano, D. Spenza, C. Petrioli, , *2013 Ieee Conference on Computer Communications Workshops (Infocom Wkshps).* **2013**, 75-76.

[107] J. Y. Cho, S. Jeong, H. Jabbar, Y. Song, J. H. Ahn, J. H. Kim, H. J. Jung, H. H. Yoo, T. H. Song, , *Sens. Actuator A-Phys.* **2016***, 250*, 210-218.

[108] G. De Pasquale, A. Soma, N. Zampieri, , *J. Comput. Nonlinear Dyn.* **2012***, 7*(4), 041011.

[109] D. Song, H. Jang, S. B. Kim, T. H. Sung, , *J. Electroceram.* **2013***, 31*(1-2), 35-41.

[110] P. Cahill, N. Jackson, A. Mathewson, V. Pakrashi, , *Damage Assessment of Structures X, Pts 1 and 2.* **2013***, 569-570*, 335-341.

[111] M. Y. Gao, P. Wang, Y. Cao, R. Chen, C. Liu, , *J. Vibroeng.* **2016***, 18*(7), 4647-4663.

[112] W. Wang, R. Huang, C. Huang, L. Li, , *Acta Mech. Sin.* **2014***, 30*(6), 884-888.

[113] Z. Hadas, V. Vetiska, R. Huzlik, V. Singule, , *Microsyst. Technol.* **2014***, 20*(4-5), 831-843.

[114] M. Akbar, J. L. Curiel-Sosa, , *Compos. Struct.* **2016***, 153*, 193-203.

[115] Y. Lu, Al Savvaris, A. Tsourdos, M. Bevilacqua, , *2016 Ieee Metrology for Aerospace (Metroaerospace).* **2016**, 25-32.

[116] Y. Shi, S. R. Hallett, M. Zhu, , *Compos. Struct.* **2017***, 160*, 1279-1286.

[117] A. Somov, Z. J. Chew, T. Ruan, Q. Li, M. Zhu, , *2016 15th Acm/ieee International Conference on Information Processing in Sensor Networks (Ipsn).* **2016**.

[118] D. Li, Y. Wu, A. Da Ronch, J. Xiang, , *Prog. Aerospace Sci.* **2016**, *86*, 28-62.

[119] S. P. Beeby, M. J. Tudor, N. M. White, , *Meas Sci Technol.* **2006**, *17*(12), R175-R195.

[120] R. L. Harne, K. W. Wang, , *Smart Mater. Struct.* **2013**, *22*(2), 023001.

[121] H. S. Kim, J. Kim, J. Kim, , *Int. J. Precis. Eng. Manuf.* **2011**, *12*(6), 1129-1141.

[122] S. Saadon, O. Sidek, , *Energy Conv. Manag.* **2011**, *52*(1), 500-504.

[123] D. Zhu, M. J. Tudor, S. P. Beeby, , *Meas Sci Technol.* **2010**, *21*(2), 022001.

[124] F. U. Khan, , *J. Renew. Sustain. Energy.* **2016**, *8*(4), 044702.

[125] F. U. Khan, M. U. Qadir, , *J Micromech Microengineering.* **2016**, *26*(10), 103001.

[126] T. Yildirim, M. H. Ghayesh, W. Li, G. Alici, , *Renew. Sust. Energ. Rev.* **2017**, *71*, 435-449.

[127] Z. L. Wang, , *ACS Nano.* **2013**, *7*(11), 9533-9557.

[128] F. Fan, Z. Tian, Z. L. Wang, , *Nano Energy.* **2012**, *1*(2), 328-334.

[129] R. Hinchet, W. Seung, S. Kim, , *ChemSusChem.* **2015**, *8*(14), 2327-2344.

[130] Y. Li, G. Cheng, Z. Lin, J. Yang, L. Lin, Z. L. Wang, , *Nano Energy.* **2015**, *11*, 323-332.

[131] S. Wang, L. Lin, Z. L. Wang, , *Nano Energy.* **2015**, *11*, 436-462.

[132] Z. L. Wang, J. Chen, L. Lin, , *Energy Environ. Sci.* **2015**, *8*(8), 2250-2282.

[133] M. W. Williams, , *AIP Adv.* **2012**, *2*(1), 010701.

[134] Y. Yu, X. Wang, , *Extreme Mech. Lett.* **2016**, *9*, 514-530.

[135] X. Zhang, M. Han, B. Meng, H. Zhang, , *Nano Energy.* **2015**, *11*, 304-322.

[136] Z. Lin, J. Chen, J. Yang, , *J. Nanomater.* **2016**, 5651613.

[137] Z. L. Wang, T. Jiang, L. Xu, , *Nano Energy.* **2017**, *39*, 9-23.

[138] N. Zhang, C. Tao, X. Fan, J. Chen, , *J. Mater. Res.* **2017**, *32*(9), 1628-1646.

[139] Q. Zheng, B. Shi, Z. Li, Z. L. Wang, , *Adv. Sci.* **2017**, *4*(7), 1700029.

[140] W. Seung, H. Yoon, T. Y. Kim, H. Ryu, J. Kim, J. Lee, J. H. Lee, S. Kim, Y. K. Park, Y. J. Park, S. Kim, , *Adv. Energy Mater.* **2017**, *7*(2), 1600988.

[141] Y. Suzuki, , *IEEJ Trans. Electr. Electron. Eng.* **2011**, *6*(2), 101-111.

[142] S. Boisseau, G. Despesse, A. Sylvestre, , *Smart Mater. Struct.* **2010**, *19*(7), 075015.

[143] Y. Chiu, Y. Lee, , *J Micromech Microengineering.* **2013**, *23*(1), 015012.

[144] M. P. Perez, S. Boisseau, P. Gasnier, J. Willemin, J. L. Reboud, , *Smart Mater. Struct.* **2015**, *24*(3), 035004.

[145] M. Perez, S. Boisseau, P. Gasnier, J. Willemin, M. Geisler, J. L. Reboud, , *Smart Mater. Struct.* **2016**, *25*(4), 045015.

[146] Xiao Huiming, Chen Gangjin, Chen Xuming, Chen Zhi, , *Sci Rep.* **2017**, *7*, 8443.

[147] G. Chen, Y. Li, H. Xiao, X. Zhu, , *J. Mater. Chem. A.* **2017***, 5*(8), 4150-4155.

[148] A. Crovetto, F. Wang, O. Hansen, , *J Micromech Microengineering.* **2013***, 23*(11), 114010.

[149] F. Belhora, D. Guyomar, M. Mazroui, A. Hajjaji, Y. Boughaleb, , *Eur. Phys. J. Plus.* **2015***, 130*(2), 20.

[150] R. Chen, Y. Suzuki, , *J Micromech Microengineering.* **2013***, 23*(12), 125015.

[151] Y. Chiu, M. H. Lee, S. Wu, , *J Micromech Microengineering.* **2015***, 25*(10), 104007.

[152] Y. Feng, K. Hagiwara, Y. Iguchi, Y. Suzuki, , *Appl. Phys. Lett.* **2012***, 100*(26), 262901.

[153] Y. Lu, M. Capo-Chichi, Y. Leprince-Wang, P. Basset, , *Smart Mater. Struct.* **2018***, 27*(1), 014001.

[154] S. Ahmed, V. Kakkar, , *IEEE Access.* **2017***, 5*, 19631-19643.

[155] M. Bi, S. Wang, X. Wang, X. Ye, , *Nano Energy.* **2017***, 41*, 434-442.

[156] I. Seo, Y. Cha, I. Kang, J. Choi, S. Nahm, T. Seung, J. Paik, , *J Am Ceram Soc.* **2011***, 94*(11), 3629-3631.

[157] I. Seo, C. Choi, I. Kang, S. Nahm, S. Bin Kim, D. Song, J. Lee, T. H. Sung, J. Paik, , *J. Ceram. Process. Res.* **2012***, 13*(6), 739-743.

[158] C. J. Jeon, H. N. Hwang, Y. H. Jeong, J. S. Yun, J. H. Nam, J. H. Cho, J. H. Paik, J. B. Lim, S. Nahm, E. S. Kim, , *J. Korean Phys. Soc.* **2013***, 63*(9), 1772-1776.

[159] M. Zheng, Y. Hou, L. Zhang, M. Zhu, , *Eur. J. Inorg. Chem.* **2016**(19), 3072-3075.

[160] Y. Bai, A. Matousek, P. Tofel, V. Bijalwan, B. Nan, H. Hughes, T. W. Button, , *J. Eur. Ceram. Soc.* **2015***, 35*(13), 3445-3456.

[161] J. Briscoe, S. Dunn, , *Nano Energy.* **2015***, 14*, 15-29.

[162] F. R. Fan, W. Tang, Z. L. Wang, , *Adv Mater.* **2016***, 28*(22), 4283-4305.

[163] F. Hu, Q. Cai, F. Liao, M. Shao, S. Lee, , *Small.* **2015***, 11*(42), 5611-5628.

[164] B. Kumar, S. Kim, , *Nano Energy.* **2012***, 1*(3), 342-355.

[165] S. Crossley, R. A. Whiter, S. Kar-Narayan, , *Mater. Sci. Technol.* **2014***, 30*(13A), 1613-1624.

[166] H. J. Song, Y. Choi, N. M. Wereley, A. S. Purekar, , *J Intell Mater Syst Struct.* **2010***, 21*(6), 647-658.

[167] S. Ju, S. H. Chae, Y. Choi, C. Ji, , *Sens. Actuator A-Phys.* **2015***, 226*, 126-136.

[168] K. Kim, C. Kim, Y. H. Jeong, Y. Lee, J. Cho, J. Paik, S. Nahm, , *J. Eur. Ceram. Soc.* **2013***, 33*(2), 305-311.

[169] M. Renaud, P. Fiorini, C. van Hoof, , *Smart Mater. Struct.* **2007***, 16*(4), 1125-1135.

[170] A. Jemai, F. Najar, M. Chafra, , *J. Vibrat. Control.* **2017***, 23*(15), 2538-2553.

[171] H. Maiwa, W. Sakamoto, , *Ferroelectrics.* **2013***, 446*(1), 67-77.

[172] A. Erturk, D. J. Inman, , *Smart Mater. Struct.* **2009***, 18*(2), 025009.

[173] G. Wang, , *J Intell Mater Syst Struct.* **2013***, 24*(2), 226-239.

[174] R. Xu, A. Lei, C. Dahl-Petersen, K. Hansen, M. Guizzetti, K. Birkelund, E. V. Thomsen, O. Hansen, , *Sens. Actuator A-Phys.* **2012**, *188*, 383-388.

[175] C. Kuo, S. Lin, W. Wu, , *Smart Mater. Struct.* **2016**, *25*(10), 105016.

[176] I. Kim, H. Joo, S. Jeong, M. Kim, J. Song, , *Ferroelectrics.* **2010**, *409*, 100-107.

[177] X. Gao, W. Shih, W. Y. Shih, , *Appl. Phys. Lett.* **2010**, *97*(23), 233503.

[178] A. L. Avsar, M. Sahin, , *Smart. Struct. Syst.* **2016**, *18*(2), 249-265.

[179] M. Salim, H. Salleh, E. W. K. Loh, M. Khir, D. Salim, , *Microsyst. Technol.* **2017**, *23*(6), 2097-2106.

[180] F. Goldschmidtboeing, P. Woias, , *J Micromech Microengineering.* **2008**, *18*(10), 104013.

[181] A. G. A. Muthalif, N. H. D. Nordin, , *Mech. Syst. Signal Proc.* **2015**, *54-55*, 417-426.

[182] R. Hosseini, M. Hamedi, , *Microsyst. Technol.* **2016**, *22*(5), 1127-1134.

[183] R. Hosseini, M. Hamedi, , *J Micromech Microengineering.* **2015**, *25*(12), 125008.

[184] S. Kirubaveni, S. Radha, B. S. Sreeja, T. Sivanesan, , *Microsyst. Technol.* **2015**, *21*(10), 2165-2173.

[185] M. Guan, Y. Li, Y. Zhao, , *Ferroelectrics.* **2015**, *478*(1), 96-105.

[186] J. Han, J. Hu, S. X. Wang, J. He, , *Appl. Phys. Lett.* **2014**, *104*(9), 093901.

[187] M. Han, Y. C. Chan, W. Liu, S. Zhang, H. Zhang, *Low Frequency PVDF Piezoelectric Energy Harvester with Combined d31 and d33 Operating Modes*, IEEE, NEW YORK; 345 E 47TH ST, NEW YORK, NY 10017 USA **2013**.

[188] M. Kim, B. Hwang, J. Jeong, N. K. Min, K. Kwon, *, J. Nanosci. Nanotechnol.* **2012**, *12*(7), 6011-6015.

[189] W. J. Choi, Y. Jeon, J. -. Jeong, R. Sood, S. G. Kim, *, J. Electroceram.* **2006**, *17*(2-4), 543-548.

[190] J. C. Park, J. Y. Park, Y. Lee, *, J Microelectromech Syst.* **2010**, *19*(5), 1215-1222.

[191] H. Miyabuchi, T. Yoshimura, S. Murakami, N. Fujimura, *, Jpn. J. Appl. Phys.* **2011**, *50*(9), 09ND17.

[192] G. Tang, B. Yang, J. Liu, B. Xu, H. Zhu, C. Yang, , *Sens. Actuator A-Phys.* **2014**, *205*, 150-155.

[193] T. Xu, E. J. Siochi, J. H. Kang, L. Zuo, W. Zhou, X. Tang, X. Jiang, , *Smart Mater. Struct.* **2013**, *22*(6), 065015.

[194] H. Kim, A. Batra, S. Priya, K. Uchino, D. Markley, R. Newnham, H. Hofmann, *, Jpn. J. Appl. Phys. Part 1 - Regul. Pap. Short Notes Rev. Pap.* **2004**, *43*(9A), 6178-6183.

[195] H. Kim, S. Priya, K. Uchino, *, Jpn. J. Appl. Phys. Part 1 - Regul. Pap. Brief Commun. Rev. Pap.* **2006**, *45*(7), 5836-5840.

[196] C. Mo, D. Arnold, W. C. Kinsel, W. W. Clark, *, J Intell Mater Syst Struct.* **2013**, *24*(7), 828-836.

[197] B. Ren, S. W. Or, X. Zhao, H. Luo, *, J. Appl. Phys.* **2010**, *107*(3), 034501.

[198] M. Leinonen, J. Palosaari, J. Juuti, H. Jantunen, , *J Intell Mater Syst Struct.* **2014**, *25*(4), 391-400.

[199] J. Yuan, X. Shan, T. Xie, W. Chen, , *J Intell Mater Syst Struct.* **2010**, *21*(8), 765-771.

[200] Y. Kuang, A. Daniels, M. Zhu, , *J. Phys. D-Appl. Phys.* **2017**, *50*(34), 345501.

[201] G. Yesner, M. Kuciej, A. Safari, A. Jasim, H. Wang, A. Maher, , *2016 Joint Ieee International Symposium on the Applications of Ferroelectrics, European Conference on Application of Polar Dielectrics, and Piezoelectric Force Microscopy Workshop (Isaf/ecapd/pfm).* **2016**.

[202] J. Palosaari, M. Leinonen, J. Hannu, J. Juuti, H. Jantunen, , *J. Electroceram.* **2012**, *28*(4), 214-219.

[203] X. Li, M. Guo, S. Dong, , *IEEE Trans. Ultrason. Ferroelectr. Freq. Control.* **2011**, *58*(4), 698-703.

[204] W. Wang, T. Yang, X. Chen, X. Yao, , *IEEE Trans. Ultrason. Ferroelectr. Freq. Control.* **2012**, *59*(9), 2022-2026.

[205] X. Chen, T. Yang, W. Wang, X. Yao, , *Ceram. Int.* **2012**, *38*, S271-S274.

[206] Kan Junwu, Qiu Jinhao, Tang Kehong, Zhu Kongjun, Shao Chenghui, , *Int. J. Appl. Electromagn. Mech.* **2009**, *30*(1-2), 95-106.

[207] E. Minazara, D. Vasic, F. Costa, G. Poulin, , *Ultrasonics.* **2006**, *44*, E699-E703.

[208] C. Mo, L. J. Radziemski, W. W. Clark, , *Smart Mater. Struct.* **2010**, *19*(2), 025016.

[209] Z. Xiao, T. Q. Yang, Y. Dong, X. C. Wang, , *Appl. Phys. Lett.* **2014**, *104*(22), 223904.

[210] B. Guiffard, Y. Guichon, H. W. Gundel, , *Electron. Lett.* **2012**, *48*(19), 1196-U45.

[211] Y. Yang, S. Wang, P. Stein, B. Xu, T. Yang, , *Smart Mater. Struct.* **2017**, *26*(4), 045011.

[212] Y. Dong, T. Yang, Z. Xiao, Y. Liu, X. Wang, , *J. Mater. Sci. -Mater. Electron.* **2015**, *26*(10), 7921-7926.

[213] Z. Shen, S. Liu, J. Miao, L. S. Woh, Z. Wang, , *26th Ieee International Conference on Micro Electro Mechanical Systems (Mems 2013).* **2013**, 821-824.

[214] Z. Shen, S. Liu, J. Miao, L. S. Woh, Z. Wang, , *J Micromech Microengineering.* **2015**, *25*(3), 035004.

[215] A. Aladwani, O. Aldraihem, A. Baz, , *J. Vib. Acoust. -Trans. ASME.* **2013**, *135*(5), 051011.

[216] L. Zhou, J. Sun, X. J. Zheng, S. F. Deng, J. H. Zhao, S. T. Peng, Y. Zhang, X. Y. Wang, H. B. Cheng, , *Sens. Actuator A-Phys.* **2012**, *179*, 185-192.

[217] C. Majidi, M. Haataja, D. J. Srolovitz, , *Smart Mater. Struct.* **2010**, *19*(5), 055027.

[218] B. Ren, S. W. Or, Y. Zhang, Q. Zhang, X. Li, J. Jiao, W. Wang, D. Liu, X. Zhao, H. Luo, , *Appl. Phys. Lett.* **2010**, *96*(8), 083502.

[219] D. Wang, N. Liu, , *Sens. Actuator A-Phys.* **2011**, *167*(2), 449-458.

[220] T. Fan, G. Zou, L. Yang, , *Compos. Pt. B-Eng.* **2015**, *74*, 166-170.

[221] V. Kulkarni, R. Ben-Mrad, S. E. Prasad, S. Nemana, , *IEEE-ASME Trans. Mechatron.* **2014**, *19*(3), 801-807.

[222] M. H. Malakooti, H. A. Sodano, , *Smart Mater. Struct.* **2015***, 24*(5), 055005.

[223] L. Persano, A. Catellani, C. Dagdeviren, Y. Ma, X. Guo, Y. Huang, A. Calzolari, D. Pisignano, , *Adv Mater.* **2016***, 28*(35), 7633-+.

[224] X. Zheng, Z. Zhang, Y. Zhu, J. Mei, S. Peng, L. Li, Y. Yu, , *IEEE-ASME Trans. Mechatron.* **2015***, 20*(2), 728-739.

[225] J. H. Ahn, M. S. Woo, D. Song, S. K. Hong, K. H. Baek, S. J. Hwang, T. H. Sung, , *J. Korean Phys. Soc.* **2014***, 65*(11), 1943-1950.

[226] Y. Chen, X. Mu, T. Wang, W. Ren, Y. Yang, Z. L. Wang, C. Sun, A. Y. Gu, , *Sci Rep.* **2016***, 6*, 35180.

[227] F. Guido, A. Qualtieri, L. Algieri, E. D. Lemma, M. De Vittorio, M. T. Todaro, , *Microelectron. Eng.* **2016***, 159*, 174-178.

[228] Y. Liu, T. Yang, F. Shu, , *Funct. Mater. Lett.* **2016***, 9*(5), 1650069.

[229] H. Kim, S. Priya, K. Uchino, R. Newnham, , *J. Electroceram.* **2005***, 15*(1), 27-34.

[230] G. Manla, N. M. White, M. J. Tudor, , *IEEE Sens. J.* **2012***, 12*(6), 1785-1794.

[231] S. Wang, K. H. Lam, C. L. Sun, K. W. Kwok, H. L. W. Chan, M. S. Guo, X. Zhao, , *Appl. Phys. Lett.* **2007***, 90*(11), 113506.

[232] K. Park, S. Xu, Y. Liu, G. Hwang, S. L. Kang, Z. L. Wang, K. J. Lee, , *Nano Lett.* **2010***, 10*(12), 4939-4943.

[233] K. Park, J. H. Son, G. Hwang, C. K. Jeong, J. Ryu, M. Koo, I. Choi, S. H. Lee, M. Byun, Z. L. Wang, K. J. Lee, , *Adv Mater.* **2014***, 26*(16), 2514-2520.

[234] S. Shin, Y. Kim, M. H. Lee, J. Jung, J. Nah, , *ACS Nano.* **2014**, *8*(3), 2766-2773.

[235] Z. Wang, J. Song, , *Science.* **2006**, *312*(5771), 242-246.

[236] Y. Xi, J. Song, S. Xu, R. Yang, Z. Gao, C. Hu, Z. L. Wang, , *J. Mater. Chem.* **2009**, *19*(48), 9260-9264.

[237] A. Khan, M. A. Abbasi, M. Hussain, Z. H. Ibupoto, J. Wissting, O. Nur, M. Willander, , *Appl. Phys. Lett.* **2012**, *101*(19), 193506.

[238] H. B. Kang, J. Chang, K. Koh, L. Lin, Y. S. Cho, , *ACS Appl. Mater. Interfaces.* **2014**, *6*(13), 10576-10582.

[239] P. X. Gao, J. Song, J. Liu, Z. L. Wang, , *Adv Mater.* **2007**, *19*(1), 67-+.

[240] M. Lee, C. Chen, S. Wang, S. N. Cha, Y. J. Park, J. M. Kim, L. Chou, Z. L. Wang, , *Adv Mater.* **2012**, *24*(13), 1759-1764.

[241] M. Yuan, L. Cheng, Q. Xu, W. Wu, S. Bai, L. Gu, Z. Wang, J. Lu, H. Li, Y. Qin, T. Jing, Z. L. Wang, , *Adv Mater.* **2014**, *26*(44), 7432-7437.

[242] J. Yan, Y. G. Jeong, , *ACS Appl. Mater. Interfaces.* **2016**, *8*(24), 15700-15709.

[243] H. B. Kang, C. S. Han, J. C. Pyun, W. H. Ryu, C. Kang, Y. S. Cho, , *Composites Sci. Technol.* **2015**, *111*, 1-8.

[244] X. Chen, S. Xu, N. Yao, Y. Shi, , *Nano Lett.* **2010**, *10*(6), 2133-2137.

[245] C. Dagdeviren, P. Joe, O. L. Tuzman, K. Park, K. J. Lee, Y. Shi, Y. Huang, J. A. Rogers, , *Extreme Mech. Lett.* **2016**, *9*, 269-281.

[246] H. Wu, Y. Huang, F. Xu, Y. Duan, Z. Yin, , *Adv Mater.* **2016**, *28*(45), 9881-9919.

[247] J. Kwon, B. K. Sharma, J. Ahn, , *Jpn. J. Appl. Phys.* **2013**, *52*(6), UNSP 06GA02.

[248] Z. Wang, X. Pan, Y. He, Y. Hu, H. Gu, Y. Wang, , *Adv. Mater. Sci. Eng.* **2015**, 165631.

[249] Z. L. Wang, W. Wu, , *Angew. Chem. -Int. Edit.* **2012**, *51*(47), 11700-11721.

[250] T. Gao, J. Liao, J. Wang, Y. Qiu, Q. Yang, M. Zhang, Y. Zhao, L. Qin, H. Xue, Z. Xiong, L. Chen, Q. Wang, , *J. Mater. Chem. A.* **2015**, *3*(18), 9965-9971.

[251] Y. Yang, Q. Shen, J. Jin, Y. Wang, W. Qian, D. Yuan, , *Appl. Phys. Lett.* **2014**, *105*(5), 053901.

[252] H. J. Jung, Y. Song, S. K. Hong, C. H. Yang, S. J. Hwang, S. Y. Jeong, T. H. Sung, , *Sens. Actuator A-Phys.* **2015**, *222*, 314-321.

[253] C. M. T. Tien, N. S. Goo, , *Aircraft Eng. Aerospace Technol.* **2010**, *82*(6), 376-381.

[254] J. Zhang, J. Zhang, C. Shu, Z. Fang, , *Appl. Phys. Lett.* **2017**, *110*(18), 183903.

[255] J. Zhang, Z. Fang, C. Shu, J. Zhang, Q. Zhang, C. Li, , *Sens. Actuator A-Phys.* **2017**, *262*, 123-129.

[256] J. X. Tao, N. V. Viet, A. Carpinteri, Q. Wang, , *Eng. Struct.* **2017**, *133*, 74-80.

[257] M. A. Karami, J. R. Farmer, D. J. Inman, , *Renewable Energy.* **2013**, *50*, 977-987.

[258] Y. Uzun, S. Demirbas, E. Kurt, , *Elektron. Elektrotech.* **2014**, *20*(10), 35-39.

[259] H. T. Luong, N. S. Goo, , *Smart Mater. Struct.* **2012**, *21*(2), 025017.

[260] R. A. Kishore, D. Vuckovic, S. Priya, , *Ferroelectrics.* **2014**, *460*(1), 98-107.

[261] E. Kurt, F. Cottone, Y. Uzun, F. Orfei, M. Mattarelli, D. Ozhan, , *Int J Hydrogen Energy.* **2017***, 42*(28), 17813-17822.

[262] D. Avirovik, R. Kishore, S. Bressers, D. J. Inman, S. Priya, , *Integrated Ferroelectr.* **2015***, 159*(1), 1-13.

[263] Y. Bai, Z. Havranek, P. Tofel, C. Meggs, H. Hughes, T. W. Button, , *Eur. Phys. J. - Spec. Top.* **2015***, 224*(14-15), 2675-2685.

[264] J. Sirohi, R. Mahadik, , *J Intell Mater Syst Struct.* **2011***, 22*(18), 2215-2228.

[265] J. Sirohi, R. Mahadik, , *J. Vib. Acoust. -Trans. ASME.* **2012***, 134*(1), 011009.

[266] S. J. Oh, H. J. Han, S. B. Han, J. Y. Lee, W. G. Chun, , *Int. J. Energy Res.* **2010***, 34*(5), 431-437.

[267] J. Ji, F. Kong, L. He, Q. Guan, Z. Feng, , *Jpn. J. Appl. Phys.* **2010***, 49*(5), 050204.

[268] V. J. Ovejas, A. Cuadras, , *Smart Mater. Struct.* **2011***, 20*(8), 085030.

[269] N. Wu, Q. Wang, X. Xie, , *Smart Mater. Struct.* **2013***, 22*(9), 095023.

[270] H. Liu, S. Zhang, T. Kobayashi, T. Chen, C. Lee, , *Micro Nano Lett.* **2014***, 9*(4), 286-289.

[271] D. J. Li, S. Hong, S. Gu, Y. Choi, S. Nakhmanson, O. Heinonen, D. Karpeev, K. No, , *Appl. Phys. Lett.* **2014***, 104*(1), 012902.

[272] J. Zhao, J. Yang, Z. Lin, N. Zhao, J. Liu, Y. Wen, P. Li, , *Sens. Actuator A-Phys.* **2015***, 236*, 173-179.

[273] X. He, Z. Shang, Y. Cheng, Y. Zhu, , *J Micromech Microengineering.* **2013***, 23*(12), 125009.

[274] S. Orrego, K. Shoele, A. Ruas, K. Doran, B. Caggiano, R. Mittal, S. H. Kang, , *Appl. Energy.* **2017***, 194*, 212-222.

[275] Zhao Xingqiang, Wen Zhiyu, , *Sens. Lett.* **2013***, 11*(2), 328-332.

[276] S. P. Matova, R. Elfrink, R. J. M. Vullers, R. van Schaijk, , *J Micromech Microengineering.* **2011***, 21*(10), 104001.

[277] Y. Tsujiura, E. Suwa, T. Nishi, F. Kurokawa, H. Hida, I. Kanno, , *Sens. Actuator A-Phys.* **2017***, 261*, 295-301.

[278] J. D. Hobeck, D. J. Inman, *Energy Harvesting from Turbulence-Induced Vibration in Air Flow: Artificial Piezoelectric Grass Concept*, AMER SOC MECHANICAL ENGINEERS, NEW YORK; THREE PARK AVENUE, NEW YORK, NY 10016-5990 USA **2011**.

[279] H. D. Akaydin, N. Elvin, Y. Andreopoulos, , *J Intell Mater Syst Struct.* **2010***, 21*(13), 1263-1278.

[280] S. Kwon, , *Appl. Phys. Lett.* **2010***, 97*(16), 164102.

[281] H. J. Lee, S. Sherrit, L. P. Tosi, P. Walkemeyer, T. Colonius, , *Sensors.* **2015***, 15*(10), 26039-26062.

[282] D. Shen, Wikle,Howard C.,,III, S. Choe, D. Kim, , *Appl. Phys. Express.* **2008***, 1*(9), 098002.

[283] Y. Yu, Y. Liu, , *J. Fluids Struct.* **2016***, 65*, 381-397.

[284] V. Vivekananthan, N. R. Alluri, Y. Purusothaman, A. Chandrasekhar, S. Kim, , *Nanoscale.* **2017***, 9*(39), 15122-15130.

[285] H. Xiong, L. Wang, , *Appl. Energy.* **2016***, 174*, 101-107.

[286] C. H. Yang, Y. Song, M. S. Woo, J. H. Eom, G. J. Song, J. H. Kim, J. Kim, T. H. Lee, J. Y. Choi, T. H. Sung, , *Sens. Actuator A-Phys.* **2017***, 261*, 317-324.

[287] I. Jung, Y. Shin, S. Kim, J. Choi, C. Kang, , *Appl. Energy.* **2017***, 197*, 222-229.

[288] Y. Song, C. H. Yang, S. K. Hong, S. J. Hwang, J. H. Kim, J. Y. Choi, S. K. Ryu, T. H. Sung, , *Int J Hydrogen Energy.* **2016***, 41*(29), 12563-12568.

[289] L. Guo, Q. Lu, , *Renew. Sust. Energ. Rev.* **2017***, 72*, 761-773.

[290] H. Zhao, J. Ling, J. Yu, , *J Ceram Soc Jpn.* **2012***, 120*(1404), 317-323.

[291] C. R. Bowen, H. A. Kim, P. M. Weaver, S. Dunn, , *Energy Environ. Sci.* **2014***, 7*(1), 25-44.

[292] R. Calio, U. B. Rongala, D. Camboni, M. Milazzo, C. Stefanini, G. de Petris, C. M. Oddo, , *Sensors.* **2014***, 14*(3), 4755-4790.

[293] M. Kang, W. Jung, C. Kang, S. Yoon, , *Actuators.* **2016***, 5*(1), 5.

[294] A. Khan, Z. Abas, H. S. Kim, I. Oh, , *Smart Mater. Struct.* **2016***, 25*(5), 053002.

[295] R. Ahmed, F. Mir, S. Banerjee, , *Smart Mater. Struct.* **2017***, 26*(8), 085031.

[296] S. W. Ibrahim, W. G. Ali, , *J. Renew. Sustain. Energy.* **2012***, 4*(6), 062703.

[297] H. Li, C. Tian, Z. D. Deng, , *Appl. Phys. Rev.* **2014***, 1*(4), 041301.

[298] X. Zhao, Z. Shang, G. Luo, L. Deng, , *Microelectron. Eng.* **2015***, 142*, 47-51.

[299] A. Toprak, O. Tigli, , *Appl. Phys. Rev.* **2014***, 1*(3), 031104.

[300] S. P. Beeby, R. N. Torah, M. J. Tudor, P. Glynne-Jones, T. O'Donnell, C. R. Saha, S. Roy, , *J Micromech Microengineering.* **2007***, 17*(7), 1257-1265.

[301] Y. Yang, J. Yeo, S. Priya, , *Sensors.* **2012***, 12*(8), 10248-10258.

[302] S. D. Moss, O. R. Payne, G. A. Hart, C. Ung, , *Smart Mater. Struct.* **2015***, 24*(2), 023001.

[303] Y. Tan, Y. Dong, X. Wang, , *J Microelectromech Syst.* **2017***, 26*(1), 1-16.

[304] C. Cepnik, R. Lausecker, U. Wallrabe, , *Micromachines.* **2013***, 4*(2), 168-196.

[305] https://perpetuum.com/technology/, , *2017*(November).

[306] https://www.enocean.com/en/technology/energy-harvesting/, , *2017*(November).

[307] X. He, Q. Wen, Y. Sun, Z. Wen, , *Nano Energy.* **2017***, 40*, 300-307.

[308] V. R. Challa, M. G. Prasad, F. T. Fisher, , *Smart Mater. Struct.* **2009***, 18*(9), 095029.

[309] Y. Tadesse, S. Zhang, S. Priya, , *J Intell Mater Syst Struct.* **2009***, 20*(5), 625-632.

[310] H. Guo, Z. Wen, Y. Zi, M. Yeh, J. Wang, L. Zhu, C. Hu, Z. L. Wang, , *Advanced Energy Materials.* **2016***, 6*(6), 1501593.

[311] B. Yang, C. Lee, W. L. Kee, S. P. Lim, , *J. Micro-Nanolithogr. MEMS MOEMS.* **2010***, 9*(2), 023002.

[312] M. Lallart, P. Cottinet, D. Guyomar, L. Lebrun, , *J. Polym. Sci. Pt. B-Polym. Phys.* **2012**, *50*(8), 523-535.

[313] P. Cottinet, D. Guyomar, B. Guiffard, C. Putson, L. Lebrun, , *IEEE Trans. Ultrason. Ferroelectr. Freq. Control.* **2010**, *57*(4), 774-784.

[314] M. Lallart, P. Cottinet, L. Lebrun, B. Guiffard, D. Guyomar, , *J. Appl. Phys.* **2010**, *108*(3), 034901.

[315] C. Putson, L. Lebrun, D. Guyomar, N. Muensit, P. -. Cottinet, L. Seveyrat, B. Guiffard, , *J. Appl. Phys.* **2011**, *109*(2), 024104.

[316] P. Cottinet, D. Guyomar, B. Guiffard, L. Lebrun, C. Putson, , *J. Polym. Eng.* **2011**, *31*(2-3), 133-140.

[317] D. Jaaoh, C. Putson, N. Muensit, , *Composites Sci. Technol.* **2016**, *122*, 97-103.

[318] A. Eddiai, M. Meddad, K. Sbiaai, Y. Boughaleb, A. Hajjaji, D. Guyomar, , *Opt. Mater.* **2013**, *36*(1), 13-17.

[319] J. Park, G. Lee, J. Yang, C. Kim, S. Ahn, , *J. Composite Mater.* **2016**, *50*(12), 1573-1579.

[320] S. Bauer, S. Bauer-Gogonea, I. Graz, M. Kaltenbrunner, C. Keplinger, R. Schwoediauer, , *Adv Mater.* **2014**, *26*(1), 149-162.

[321] J. Noh, , *Polymers.* **2016**, *8*(4), UNSP 123.

[322] X. Yin, M. Lallart, P. Cottinet, D. Guyomar, J. Capsal, , *Appl. Phys. Lett.* **2016**, *108*(4), 042901.

[323] C. Tugui, C. Ursu, L. Sacarescu, M. Asandulesa, G. Stoian, G. Ababei, M. Cazacu, , *ACS Sustain. Chem. Eng.* **2017***, 5*(9), 7851-7858.

[324] Z. Deng, M. J. Dapino, , *Smart Mater. Struct.* **2017***, 26*(10), 103001.

[325] G. Tan, L. Zhao, M. G. Kanatzidis, , *Chem. Rev.* **2016***, 116*(19), 12123-12149.

[326] A. J. Minnich, M. S. Dresselhaus, Z. F. Ren, G. Chen, , *Energy Environ. Sci.* **2009***, 2*(5), 466-479.

[327] Z. Chen, G. Han, L. Yang, L. Cheng, J. Zou, , *Prog. Nat. Sci.* **2012***, 22*(6), 535-549.

[328] M. G. Kanatzidis, , *Chem. Mat.* **2010***, 22*(3), 648-659.

[329] K. Koumoto, Y. Wang, R. Zhang, A. Kosuga, R. Funahashi, , *Ann. Rev. Mater. Res.* **2010***, 40*, 363-394.

[330] Y. Lan, A. J. Minnich, G. Chen, Z. Ren, , *Adv. Funct. Mater.* **2010***, 20*(3), 357-376.

[331] J. Li, W. Liu, L. Zhao, M. Zhou, , *NPG Asia Mater.* **2010***, 2*(4), 152-158.

[332] K. Nielsch, J. Bachmann, J. Kimling, H. Boettner, , *Adv. Energy Mater.* **2011***, 1*(5), 713-731.

[333] P. Pichanusakorn, P. Bandaru, , *Mater. Sci. Eng. R-Rep.* **2010***, 67*(2-4), 19-63.

[334] C. J. Vineis, A. Shakouri, A. Majumdar, M. G. Kanatzidis, , *Adv Mater.* **2010***, 22*(36), 3970-3980.

[335] E. Ashalley, H. Chen, X. Tong, H. Li, Z. M. Wang, , *Front. Mater. Sci.* **2015***, 9*(2), 103-125.

[336] Fitriani, R. Ovik, B. D. Long, M. C. Barma, M. Riaz, M. F. M. Sabri, S. M. Said, R. Saidur, , *Renew. Sust. Energ. Rev.* **2016**, *64*, 635-659.

[337] Q. Jiang, J. Yang, Y. Liu, H. He, , *J. Adv. Dielectr.* **2016**, *6*(1), 1630002.

[338] W. Xie, A. Weidenkaff, X. Tang, Q. Zhang, J. Poon, T. M. Tritt, , *Nanomaterials.* **2012**, *2*(4), 379-412.

[339] G. J. Snyder, E. S. Toberer, , *Nat. Mater.* **2008**, *7*(2), 105-114.

[340] Y. Du, S. Z. Shen, K. Cai, P. S. Casey, , *Prog. Polym. Sci.* **2012**, *37*(6), 820-841.

[341] A. Shakouri, , *Ann. Rev. Mater. Res.* **2011**, *41*, 399-431.

[342] J. R. Sootsman, D. Y. Chung, M. G. Kanatzidis, , *Angew. Chem. -Int. Edit.* **2009**, *48*(46), 8616-8639.

[343] H. Alam, S. Ramakrishna, , *Nano Energy.* **2013**, *2*(2), 190-212.

[344] H. Kleinke, , *Chem. Mat.* **2010**, *22*(3), 604-611.

[345] T. M. Tritt, , *Ann. Rev. Mater. Res.* **2011**, *41*, 433-448.

[346] M. W. Gaultois, T. D. Sparks, C. K. H. Borg, R. Seshadri, W. D. Bonificio, D. R. Clarke, , *Chem. Mat.* **2013**, *25*(15), 2911-2920.

[347] J. Yang, H. Yip, A. K. -. Jen, , *Adv. Energy Mater.* **2013**, *3*(5), 549-565.

[348] J. Zheng, , *Front. Phys. China.* **2008**, *3*(3), 269-279.

[349] A. M. Dehkordi, M. Zebarjadi, J. He, T. M. Tritt, , *Mater. Sci. Eng. R-Rep.* **2015**, *97*, 1-22.

[350] X. Shi, L. Chen, C. Uher, , *Int. Mater. Rev.* **2016**, *61*(6), 379-415.

[351] C. Wan, Y. Wang, N. Wang, W. Norimatsu, M. Kusunoki, K. Koumoto, , *Sci. Technol. Adv. Mater.* **2010**, *11*(4), 044306.

[352] D. K. Aswal, R. Basu, A. Singh, , *Energy Conv. Manag.* **2016**, *114*, 50-67.

[353] J. G. Bos, R. A. Downie, , *J. Phys. -Condes. Matter.* **2014**, *26*(43), 433201.

[354] C. Xiao, Z. Li, K. Li, P. Huang, Y. Xie, , *Acc. Chem. Res.* **2014**, *47*(4), 1287-1295.

[355] C. Gayner, K. K. Kar, , *Prog. Mater. Sci.* **2016**, *83*, 330-382.

[356] T. Zhu, L. Hu, X. Zhao, J. He, , *Adv. Sci.* **2016**, *3*(7), 1600004.

[357] T. Zhu, Y. Liu, C. Fu, J. P. Heremans, J. G. Snyder, X. Zhao, , *Adv Mater.* **2017**, *29*(14), 1605884.

[358] S. Twaha, J. Zhu, Y. Yan, B. Li, , *Renew. Sust. Energ. Rev.* **2016**, *65*, 698-726.

[359] L. Huang, Q. Zhang, B. Yuan, X. Lai, X. Yan, Z. Ren, , *Mater. Res. Bull.* **2016**, *76*, 107-112.

[360] K. H. Lee, S. W. Kim, , *J. Korean Ceram. Soc.* **2017**, *54*(2), 75-85.

[361] M. S. Dresselhaus, G. Chen, M. Y. Tang, R. Yang, H. Lee, D. Wang, Z. Ren, J. Fleurial, P. Gogna, , *Adv Mater.* **2007**, *19*(8), 1043-1053.

[362] B. Sothmann, R. Sanchez, A. N. Jordan, , *Nanotechnology.* **2015**, *26*(3), 032001.

[363] G. Chen, W. Xu, D. Zhu, , *J. Mater. Chem. C.* **2017**, *5*(18), 4350-4360.

[364] Q. Zhang, Y. Sun, W. Xu, D. Zhu, , *Adv Mater.* **2014**, *26*(40), 6829-6851.

[365] N. Dubey, M. Leclerc, , *J. Polym. Sci. Pt. B-Polym. Phys.* **2011**, *49*(7), 467-475.

[366] M. He, F. Qiu, Z. Lin, , *Energy Environ. Sci.* **2013**, *6*(5), 1352-1361.

[367] R. Yue, J. Xu, , *Synth. Met.* **2012**, *162*(11-12), 912-917.

[368] Q. Wei, M. Mukaida, K. Kirihara, Y. Naitoh, T. Ishida, , *Materials.* **2015**, *8*(2), 732-750.

[369] B. Russ, A. Glaudell, J. J. Urban, M. L. Chabinyc, R. A. Segalman, , *Nat. Rev. Mater.* **2016**, *1*(10), 16050.

[370] M. A. Kamarudin, S. R. Sahamir, R. S. Datta, B. D. Long, M. F. M. Sabri, S. M. Said, , *Sci. World J.* **2013**, 713640.

[371] L. M. Cowen, J. Atoyo, M. J. Carnie, D. Baran, B. C. Schroeder, , *ECS J. Solid State Sci. Technol.* **2017**, *6*(3), N3080-N3088.

[372] A. Roncaglia, M. Ferri, , *Sci. Adv. Mater.* **2011**, *3*(3), 401-419.

[373] J. -. Niemela, A. J. Karttunen, M. Karppinen, , *J. Mater. Chem. C.* **2015**, *3*(40), 10349-10361.

[374] J. Ravichandran, , *J. Mater. Res.* **2017**, *32*(1), 183-203.

[375] F. Xiao, C. Hangarter, B. Yoo, Y. Rheem, K. Lee, N. V. Myung, , *Electrochim. Acta.* **2008**, *53*(28), 8103-8117.

[376] S. H. Zaferani, , *Renew. Sust. Energ. Rev.* **2017**, *71*, 359-364.

[377] A. J. Karttunen, L. Sarnes, R. Townsend, J. Mikkonen, M. Karppinen, , *Adv. Electron. Mater.* **2017**, *3*(6), 1600459.

[378] P. Mele, S. Saini, A. Tiwari, P. E. Hopkins, K. Miyazaki, A. Ichinose, J. Niemela, M. Karppinen, , *J. Nanosci. Nanotechnol.* **2017***, 17*(3), 1616-1621.

[379] A. Dey, O. P. Bajpai, A. K. Sikder, S. Chattopadhyay, M. A. S. Khan, , *Renew. Sust. Energ. Rev.* **2016***, 53*, 653-671.

[380] A. R. M. Siddique, S. Mahmud, B. Van Heyst, , *Renew. Sust. Energ. Rev.* **2017***, 73*, 730-744.

[381] M. Orrill, S. LeBlanc, , *J Appl Polym Sci.* **2017***, 134*(3), 44256.

[382] Y. Dong, G. S. Nolas, X. Zeng, T. M. Tritt, , *J. Mater. Res.* **2015***, 30*(17), 2558-2563.

[383] J. W. Fergus, , *J. Eur. Ceram. Soc.* **2012***, 32*(3), 525-540.

[384] R. Funahashi, T. Barbier, E. Combe, , *J. Mater. Res.* **2015***, 30*(17), 2544-2557.

[385] M. Ohtaki, , *J Ceram Soc Jpn.* **2011***, 119*(1395), 770-775.

[386] M. A. B. Bashir, S. M. Said, M. F. M. Sabri, D. A. Shnawah, M. H. Elsheikh, , *Renew. Sust. Energ. Rev.* **2014***, 37*, 569-584.

[387] R. Chetty, A. Bali, R. C. Mallik, , *J. Mater. Chem. C.* **2015***, 3*(48), 12364-12378.

[388] S. Hebert, D. Berthebaud, R. Daou, Y. Breard, D. Pelloquin, E. Guilmeau, F. Gascoin, O. Lebedev, A. Maignan, , *J. Phys. -Condes. Matter.* **2016***, 28*(1), 013001.

[389] S. Perumal, S. Roychowdhury, K. Biswas, , *J. Mater. Chem. C.* **2016***, 4*(32), 7520-7536.

[390] W. Liu, K. Yin, Q. Zhang, C. Uher, X. Tang, , *Natl. Sci. Rev.* **2017***, 4*(4), 611-626.

[391] K. Koumoto, R. Funahashi, E. Guilmeau, Y. Miyazaki, A. Weidenkaff, Y. Wang, C. Wan, , *J Am Ceram Soc.* **2013**, *96*(1), 1-23.

[392] X. Zhang, L. Zhao, , *J. Materiomics.* **2015**, *1*(2), 92-105.

[393] H. J. Goldsmid, , *Materials.* **2014**, *7*(4), 2577-2592.

[394] J. Ander Santamaria, J. Alkorta, J. Gil Sevillano, , *J. Mater. Res.* **2015**, *30*(17), 2593-2604.

[395] A. Bulusu, D. G. Walker, , *Superlattices Microstruct.* **2008**, *44*(1).

[396] P. Sundarraj, D. Maity, S. S. Roy, R. A. Taylor, , *RSC Adv.* **2014**, *4*(87), 46860-46874.

[397] B. Orr, A. Akbarzadeh, M. Mochizuki, R. Singh, , *Appl. Therm. Eng.* **2016**, *101*, 490-495.

[398] I. Temizer, C. Ilkilic, , *Renew. Sust. Energ. Rev.* **2016**, *63*, 141-151.

[399] F. Cheng, Y. Hong, W. Li, X. Guo, H. Zhang, F. Fu, B. Feng, G. Wang, C. Wang, H. Qin, , *Energy.* **2017**, *121*, 545-560.

[400] https://www.idtechex.com/research/webinars/thermoelectric-energy-harvesting-a-time-of-turmoil-00130.asp, , *2017*(November).

[401] M. Zebarjadi, K. Esfarjani, M. S. Dresselhaus, Z. F. Ren, G. Chen, , *Energy Environ. Sci.* **2012**, *5*(1), 5147-5162.

[402] J. P. Rojas, D. Singh, S. B. Inayat, G. A. T. Sevilla, H. M. Fahad, M. M. Hussain, , *ECS J. Solid State Sci. Technol.* **2017**, *6*(3), N3036-N3044.

[403] H. S. Kim, W. Liu, Z. Ren, , *Energy Environ. Sci.* **2017**, *10*(1), 69-85.

[404] G. Pennelli, , *Beilstein J. Nanotechnol.* **2014**, *5*, 1268-1284.

[405] R. Rostek, N. Stein, C. Boulanger, , *J. Mater. Res.* **2015**, *30*(17), 2518-2543.

[406] Q. H. Zhang, X. Y. Huang, S. Q. Bai, X. Shi, C. Uher, L. D. Chen, , *Adv. Eng. Mater.* **2016**, *18*(2), 194-213.

[407] D. Beretta, M. Massetti, G. Lanzani, M. Caironi, , *Rev. Sci. Instrum.* **2017**, *88*(1), 015103.

[408] D. Champier, , *Energy Conv. Manag.* **2017**, *140*, 167-181.

[409] W. He, G. Zhang, X. Zhang, J. Ji, G. Li, X. Zhao, , *Appl. Energy.* **2015**, *143*, 1-25.

[410] C. R. Bowen, J. Taylor, E. LeBoulbar, D. Zabek, A. Chauhan, R. Vaish, , *Energy Environ. Sci.* **2014**, *7*(12), 3836-3856.

[411] G. Vats, A. Kumar, N. Ortega, C. R. Bowen, R. S. Katiyar, , *Energy Environ. Sci.* **2016**, *9*(4), 1335-1345.

[412] H. R. Jo, C. S. Lynch, , *Smart Mater. Struct.* **2016**, *25*(3), 035009.

[413] F. Zhuo, Q. Li, J. Gao, Q. Yan, Y. Zhang, X. Xi, X. Chu, , *Phys. Chem. Chem. Phys.* **2017**, *19*(21), 13534-13546.

[414] X. Hao, Y. Zhao, Q. Zhang, , *J. Phys. Chem. C.* **2015**, *119*(33), 18877-18885.

[415] X. Wang, X. Hao, Q. Zhang, S. An, X. Chou, , *J. Mater. Sci. -Mater. Electron.* **2017**, *28*(2), 1438-1448.

[416] T. Yu, G. Zhang, Y. Yu, Y. Zeng, S. Jiang, , *Sens. Actuator A-Phys.* **2015**, *223*, 159-166.

[417] Q. Wang, X. Zhang, C. R. Bowen, M. Li, J. Ma, S. Qiu, H. Liu, S. Jiang, , *J. Alloys Compounds.* **2017***, 710*, 869-874.

[418] T. Yu, S. Jiang, B. Fan, Y. Zeng, G. Zhang, P. Liu, , *Ferroelectrics.* **2016***, 494*(1), 1-10.

[419] H. Karim, M. R. H. Sarker, S. Shahriar, M. A. I. Shuvo, D. Delfin, D. Hodges, T. (. Tseng, D. Roberson, N. Love, Y. Lin, , *Smart Mater. Struct.* **2016***, 25*(5), 055022.

[420] M. Vaish, N. A. Madhar, B. Ilahi, V. S. Chauhan, R. Vaish, , *Ferroelectr. Lett. Sect.* **2016***, 43*(1-3), 52-58.

[421] Y. Maeda, T. Wakamatsu, A. Konishi, H. Moriwake, C. Moriyoshi, Y. Kuroiwa, K. Tanabe, I. Terasaki, H. Taniguchi, , *Phys. Rev. Appl.* **2017***, 7*(3), 034012.

[422] N. A. Madhar, B. Ilahi, M. Vaish, , *Integrated Ferroelectr.* **2015***, 167*(1), 176-183.

[423] L. Luo, X. Jiang, Y. Zhang, K. Li, , *J. Eur. Ceram. Soc.* **2017***, 37*(8), 2803-2812.

[424] Y. Zhang, M. Xie, J. Roscow, Y. Bao, K. Zhou, D. Zhang, C. R. Bowen, , *J. Mater. Chem. A.* **2017***, 5*(14), 6569-6580.

[425] D. Zabek, K. Seunarine, C. Spacie, C. Bowen, , *ACS Appl. Mater. Interfaces.* **2017***, 9*(10), 9161-9167.

[426] D. Zabek, J. Taylor, C. R. Bowen, , *IEEE Trans. Ultrason. Ferroelectr. Freq. Control.* **2016***, 63*(10), 1681-1689.

[427] S. R. Etesami, J. Berakdar, , *Appl. Phys. Lett.* **2016***, 108*(5), 053903.

[428] S. H. Krishnan, D. Ezhilarasi, G. Uma, M. Umapathy, , *IEEE Trans. Sustain. Energy.* **2014***, 5*(1), 73-81.

[429] M. Sharma, R. Vaish, V. S. Chauhan, , *Mater. Res. Express.* **2016**, *3*(2), 025501.

[430] M. Sharma, R. Vaish, V. S. Chauhan, , *Energy Technol.* **2015**, *3*(12), 1271-1278.

[431] M. Sharma, A. Chauhan, R. Vaish, V. S. Chauhan, , *Smart Mater. Struct.* **2015**, *24*(10), 105013.

[432] T. Zhao, W. Jiang, H. Liu, D. Niu, X. Li, W. Liu, X. Li, B. Chen, Y. Shi, L. Yin, B. Lu, , *Nanoscale.* **2016**, *8*(15), 8111-8117.

[433] U. Erturun, C. Green, M. L. Richeson, K. Mossi, , *J Intell Mater Syst Struct.* **2014**, *25*(14), 1838-1849.

[434] M. Xie, D. Zabek, C. Bowen, M. Abdelmageed, M. Arafa, , *Smart Mater. Struct.* **2016**, *25*(12), 125023.

[435] P. Talemi, M. Delaigue, P. Murphy, M. Fabretto, , *ACS Appl. Mater. Interfaces.* **2015**, *7*(16), 8465-8471.

[436] M. Vaish, M. Sharma, R. Vaish, V. S. Chauhan, , *Energy Technol.* **2015**, *3*(7), 768-773.

[437] M. Kim, S. Jo, H. Ahn, Y. Kim, , *Smart Mater. Struct.* **2015**, *24*(6), 065032.

[438] A. Potnuru, Y. Tadesse, , *Integrated Ferroelectr.* **2014**, *150*(1), 23-50.

[439] R. M. Raghavendra, K. P. S. S. Praneeth, S. Dutta, , *J Electron Mater.* **2017**, *46*(1), 101-106.

[440] D. Zabek, J. Taylor, V. Ayel, Y. Bertin, C. Romestant, C. R. Bowen, , *J. Appl. Phys.* **2016**, *120*(2), 024505.

[441] M. Xie, S. Dunn, E. Le Boulbar, C. R. Bowen, , *Int J Hydrogen Energy.* **2017**, *42*(37), 23437-23445.

[442] C. Chen, T. Chung, C. Tseng, C. Hung, P. Yeh, C. Cheng, , *IEEE Trans. Magn.* **2015**, *51*(7), 9100309.

[443] T. Chung, U. Shukla, C. Tseng, C. Chen, C. Wang, , *Active and Passive Smart Structures and Integrated Systems 2013.* **2013**, *8688*, UNSP 86880M.

[444] M. Ujihara, G. P. Carman, D. G. Lee, , *Appl. Phys. Lett.* **2007**, *91*(9), 093508.

[445] M. Gueltig, H. Ossmer, M. Ohtsuka, H. Miki, K. Tsuchiya, T. Takagi, M. Kohl, , *Adv. Energy Mater.* **2014**, *4*(17), 1400751.

[446] M. Gueltig, M. Ohtsuka, H. Miki, T. Takagi, M. Kohl, , *2015 Transducers - 2015 18th International Conference on Solid-State Sensors, Actuators and Microsystems (Transducers).* **2015**, 718-721.

[447] M. Lallart, L. Wang, G. Sebald, L. Petit, D. Guyomar, , *Phys. Lett. A.* **2014**, *378*(43), 3151-3154.

[448] S. Shrestha, S. Noh, D. Choi, , *Int. J. Antennas Propag.* **2013**, 385260.

[449] W. Guo, S. Wang, , *Trans. Emerg. Telecommun. Technol.* **2013**, *24*(5), 453-457.

[450] D. Har, S. Min, T. Mladenov, Pham Ngoc Son, , *Int. J. Distrib. Sens. Netw.* **2017**, *13*(6).

[451] S. Mekid, A. Qureshi, U. Baroudi, , *Arab. J. Sci. Eng.* **2017**, *42*(7), 2673-2683.

[452] N. S. Hudak, G. G. Amatucci, , *J. Appl. Phys.* **2008**, *103*(10), 101301.

[453] J. H. Hwang, C. H. Hyoung, K. H. Park, Y. T. Kim, , *Electron. Lett.* **2013**, *49*(2), 149-150.

[454] Z. Martinovic, D. Budic, R. Malaric, D. Simunic, , *2015 Ieee International Black Sea Conference on Communications and Networking (Blackseacom).* **2015**, 117-121.

[455] F. U. K. Izhar, , *J Micromech Microengineering.* **2015**, *25*(2), 023001.

[456] M. A. Pillai, E. Deenadayalan, , *Int. J. Precis. Eng. Manuf.* **2014**, *15*(5), 949-965.

[457] T. Lafont, L. Gimeno, J. Delamare, G. A. Lebedev, D. I. Zakharov, B. Viala, O. Cugat, N. Galopin, L. Garbuio, O. Geoffroy, , *J Micromech Microengineering.* **2012**, *22*(9), 094009.

[458] A. B. A. Dow, U. Schmid, N. P. Kherani, , *Smart Mater. Struct.* **2011**, *20*(11), 115019.

[459] A. B. A. Dow, U. Schmid, N. P. Kherani, , *Microsyst. Technol.* **2014**, *20*(4-5), 933-944.

[460] A. F. Arrieta, P. Hagedorn, A. Erturk, D. J. Inman, , *Appl. Phys. Lett.* **2010**, *97*(10), 104102.

[461] D. A. W. Barton, S. G. Burrow, L. R. Clare, , *J. Vib. Acoust. -Trans. ASME.* **2010**, *132*(2), 021009.

[462] F. Cottone, H. Vocca, L. Gammaitoni, , *Phys. Rev. Lett.* **2009**, *102*(8), 080601.

[463] M. Ferrari, V. Ferrari, M. Guizzetti, B. Ando, S. Baglio, C. Trigona, , *Sens. Actuator A-Phys.* **2010**, *162*(2), 425-431.

[464] F. Cottone, L. Gammaitoni, H. Vocca, M. Ferrari, V. Ferrari, , *Smart Mater. Struct.* **2012**, *21*(3), 035021.

[465] B. P. Mann, N. D. Sims, , *J. Sound Vibrat.* **2009**, *319*(1-2), 515-530.

[466] L. Gammaitoni, I. Neri, H. Vocca, , *Appl. Phys. Lett.* **2009**, *94*(16), 164102.

[467] C. R. McInnes, D. G. Gorman, M. P. Cartmell, , *J. Sound Vibrat.* **2008**, *318*(4-5), 655-662.

[468] S. C. Stanton, C. C. McGehee, B. P. Mann, , *Physica D.* **2010**, *239*(10), 640-653.

[469] L. Tang, Y. Yang, , *Appl. Phys. Lett.* **2012**, *101*(9), 094102.

[470] S. Adhikari, M. I. Friswell, D. J. Inman, , *Smart Mater. Struct.* **2009**, *18*(11), 115005.

[471] E. Halvorsen, , *J Microelectromech Syst.* **2008**, *17*(5), 1061-1071.

[472] G. Litak, M. I. Friswell, S. Adhikari, , *Appl. Phys. Lett.* **2010**, *96*(21), 214103.

[473] S. P. Beeby, L. Wang, D. Zhu, A. S. Weddell, G. V. Merrett, B. Stark, G. Szarka, B. M. Al-Hashimi, , *Smart Mater. Struct.* **2013**, *22*(7), 075022.

[474] Y. Sang, X. Huang, H. Liu, P. Jin, , *IEEE Trans. Magn.* **2012**, *48*(11), 4495-4498.

[475] M. F. Ab Rahman, S. L. Kok, N. M. Ali, R. A. Hamzah, K. A. A. Aziz, , *2013 Ieee Conference on Clean Energy and Technology (Ceat).* **2013**, 243-247.

[476] X. Shan, Z. Xu, R. Song, T. Xie, , *Ferroelectrics.* **2013**, *450*(1), 57-65.

[477] J. A. C. Dias, C. De Marqui Jr., A. Erturk, , *Appl. Phys. Lett.* **2013**, *102*(4), 044101.

[478] P. Li, S. Gao, S. Niu, H. Liu, H. Cai, , *Smart Mater. Struct.* **2014**, *23*(6), 065016.

[479] S. Mahmoudi, N. Kacem, N. Bouhaddi, , *Smart Mater. Struct.* **2014**, *23*(7), 075024.

[480] P. Li, S. Gao, H. Cai, H. Wang, , *International Journal of Precision Engineering and Manufacturing.* **2014**, *15*(9), 1915-1924.

[481] H. Yu, J. Zhou, X. Yi, H. Wu, W. Wang, , *Microelectronic Engineering.* **2015***, 131*, 36-42.

[482] P. Li, S. Gao, H. Cai, , *Microsystem Technologies-Micro-and Nanosystems-Information Storage and Processing Systems.* **2015***, 21*(2), 401-414.

[483] J. A. C. Dias, C. De Marqui Jr., A. Erturk, , *AIAA J.* **2015***, 53*(2), 394-404.

[484] W. Chen, Y. Cao, J. Xie, , *Journal of Mechanical Science and Technology.* **2015***, 29*(10), 4313-4318.

[485] H. Xia, R. Chen, L. Ren, , *Sensors and Actuators A-Physical.* **2015***, 234*, 87-98.

[486] U. Javed, H. L. Dai, A. Abdelkefi, , *European Physical Journal-Special Topics.* **2015***, 224*(14-15), 2929-2948.

[487] Z. Xu, X. Shan, D. Chen, T. Xie, , *Applied Sciences-Basel.* **2016***, 6*(1).

[488] F. U. Khan, Izhar, , *Rev. Sci. Instrum.* **2016***, 87*(2), 025003.

[489] P. Li, S. Gao, H. Cai, L. Wu, , *Microsystem Technologies-Micro-and Nanosystems-Information Storage and Processing Systems.* **2016***, 22*(4), 727-739.

[490] B. Edwards, P. A. Hu, K. C. Aw, , *Smart Mater. Struct.* **2016***, 25*(5), 055019.

[491] L. Deng, Z. Wen, X. Zhao, , *Microsystem Technologies-Micro-and Nanosystems-Information Storage and Processing Systems.* **2017***, 23*(4), 935-943.

[492] R. Hamid, M. R. Yuce, , *Sensors and Actuators A-Physical.* **2017***, 257*, 198-207.

[493] F. Belhora, P. Cottinet, D. Guyomar, L. Lebrun, A. Hajjaji, M. Mazroui, Y. Boughaleb, , *Sensors and Actuators A-Physical.* **2012***, 183*, 50-56.

[494] F. Belhora, P. Cottinet, D. Guyomar, L. Petit, L. Lebrun, A. Hajjaji, M. Mazroui, Y. Boughaleb, , *Sensors and Actuators A-Physical.* **2013***, 189*, 390-398.

[495] F. Belhora, A. Hajjaji, M. Le, M. Mazroui, D. Guyomar, Y. Boughaleb, S. Touhtouh, L. Lebrun, , *Polym. Adv. Technol.* **2014***, 25*(9), 969-974.

[496] F. Belhora, A. Hajjaji, M. Mazroui, F. Z. El Fatnani, A. Rjafallah, D. Guyomar, , *Polym. Adv. Technol.* **2015***, 26*(6), 569-573.

[497] X. Li, Z. Lin, G. Cheng, X. Wen, Y. Liu, S. Niu, Z. L. Wang, , *Acs Nano.* **2014***, 8*(10), 10674-10681.

[498] G. Suo, Y. Yu, Z. Zhang, S. Wang, P. Zhao, J. Li, X. Wang, , *Acs Applied Materials & Interfaces.* **2016***, 8*(50), 34335-34341.

[499] G. Hassan, F. Khan, A. Hassan, S. Ali, J. Bae, C. H. Lee, , *Nanotechnology.* **2017***, 28*(17), 175402.

[500] X. Yang, W. A. Daoud, , *Journal of Materials Chemistry a.* **2017***, 5*(19), 9113-9121.

[501] X. Chen, Y. Song, Z. Su, H. Chen, X. Cheng, J. Zhang, M. Han, H. Zhang, , *Nano Energy.* **2017***, 38*, 43-50.

[502] Y. Hu, J. Yang, S. Niu, W. Wu, Z. L. Wang, , *Acs Nano.* **2014***, 8*(7), 7442-7450.

[503] Y. Wu, X. Wang, Y. Yang, Z. L. Wang, , *Nano Energy.* **2015***, 11*, 162-170.

[504] T. Quan, Y. Wu, Y. Yang, , *Nano Research.* **2015***, 8*(10), 3272-3280.

[505] Z. Wen, H. Guo, Y. Zi, M. Yeh, X. Wang, J. Deng, J. Wang, S. Li, C. Hu, L. Zhu, Z. L. Wang, , *ACS Nano.* **2016***, 10*(7), 6526-6534.

[506] X. Wang, Z. Wen, H. Guo, C. Wu, X. He, L. Lin, X. Cao, Z. L. Wang, , *Acs Nano.* **2016**, *10*(12), 11369-11376.

[507] M. Seol, S. Jeon, J. Han, Y. Choi, , *Nano Energy.* **2017**, *31*, 233-238.

[508] R. K. Gupta, Q. Shi, L. Dhakar, T. Wang, C. H. Heng, C. Lee, , *Scientific Reports.* **2017**, *7*, 41396.

[509] R. Cao, T. Zhou, B. Wang, Y. Yin, Z. Yuan, C. Li, Z. L. Wang, , *Acs Nano.* **2017**, *11*(8), 8370-8378.

[510] H. Shao, Z. Wen, P. Cheng, N. Sun, Q. Shen, C. Zhou, M. Peng, Y. Yang, X. Xie, X. Sun, , *Nano Energy.* **2017**, *39*, 608-615.

[511] Z. Saadatnia, E. Asadi, H. Askari, J. Zu, E. Esmailzadeh, , *Int. J. Energy Res.* **2017**, *41*(14), 2392-2404.

[512] M. Seol, J. Han, S. Park, S. Ron, Y. Choi, , *Nano Energy.* **2016**, *23*, 50-59.

[513] Y. Eun, D. Kwon, M. Kim, I. Yoo, J. Sim, H. Ko, K. Cho, J. Kim, , *Smart Mater. Struct.* **2014**, *23*(4), 045040.

[514] H. Madinei, H. H. Khodaparast, S. Adhikari, M. I. Friswell, M. Fazeli, , *European Physical Journal-Special Topics.* **2015**, *224*(14-15), 2703-2717.

[515] J. Yang, J. Chen, Y. Yang, H. Zhang, W. Yang, P. Bai, Y. Su, Z. L. Wang, , *Advanced Energy Materials.* **2014**, *4*(6), 1301322.

[516] A. Cornogolub, P. Cottinet, L. Petit, , *Smart Mater. Struct.* **2016**, *25*(9), 095048.

[517] A. Khaligh, P. Zeng, C. Zheng, , *IEEE Trans. Ind. Electron.* **2010**, *57*(3), 850-860.

[518] R. Bogue, , *Sens Rev.* **2015***, 35*(1), 1-5.

[519] M. Salim, H. S. S. Aljibori, D. Salim, M. H. M. Khir, A. S. Kherbeet, , *Journal of Mechanical Science and Technology.* **2015***, 29*(11), 5021-5034.

[520] M. Kim, M. Kim, K. Kim, Y. Kim, , *Smart Mater. Struct.* **2017***, 26*(9), 095046.

[521] T. Yeo, H. Hwang, D. Shin, B. Seo, W. Choi, , *Nanotechnology.* **2017***, 28*(6), 065403.

[522] Y. Nishijima, R. Komatsu, T. Yamamura, A. Balcytis, G. Seniutinas, S. Juodkazis, , *Optical Materials Express.* **2017***, 7*(10), 3484-3493.

[523] Y. Zhang, J. Fang, C. He, H. Yan, Z. Wei, Y. Li, , *Journal of Physical Chemistry C.* **2013***, 117*(47), 24685-24691.

[524] B. Luo, Y. Deng, Y. Wang, M. Gao, W. Zhu, H. T. Hashim, J. Garcia-Canadas, , *Rsc Advances.* **2016***, 6*(115), 114046-114051.

[525] Y. Li, S. Witharana, H. Cao, M. Lasfargues, Y. Huang, Y. Ding, , *Particuology.* **2014***, 15*, 39-44.

[526] L. Zheng, Z. Lin, G. Cheng, W. Wu, X. Wen, S. Lee, Z. L. Wang, , *Nano Energy.* **2014***, 9*, 291-300.

[527] S. Jeon, D. Kim, G. Yoon, J. Yoon, Y. Choi, , *Nano Energy.* **2015***, 12*, 636-645.

[528] Y. Wang, J. Duan, Y. Duan, Y. Zhao, Z. Pang, B. He, Q. Tang, , *Journal of Materials Chemistry a.* **2017***, 5*(35), 18551-18560.

[529] H. Zhong, Z. Wu, X. Li, W. Xu, S. Xu, S. Zhang, Z. Xu, H. Chen, S. Lin, , *Carbon.* **2016***, 105*, 199-204.

[530] C. Xu, Z. L. Wang, , *Adv Mater.* **2011**, *23*(7), 873-+.

[531] M. Lee, R. Yang, C. Li, Z. L. Wang, , *Journal of Physical Chemistry Letters.* **2010**, *1*(19), 2929-2935.

[532] D. Lee, H. Kim, H. Li, A. Jang, Y. Lim, S. N. Cha, Y. J. Park, D. J. Kang, W. J. Yoo, , *Nanotechnology.* **2013**, *24*(17), 175402.

[533] H. Yu, Q. Yue, J. Zhou, W. Wang, , *Sensors.* **2014**, *14*(5), 8740-8755.

[534] B. Dudem, Y. H. Ko, J. W. Leem, J. H. Lim, J. S. Yu, , *Acs Applied Materials & Interfaces.* **2016**, *8*(44), 30165-30175.

[535] M. Kim, M. Kim, S. Jo, Y. Kim, , *Smart Mater. Struct.* **2016**, *25*(12), 125007.

[536] S. Lee, S. Bae, L. Lin, S. Ahn, C. Park, S. Kim, S. N. Cha, Y. J. Park, Z. L. Wang, , *Nano Energy.* **2013**, *2*(5), 817-825.

[537] H. Zhang, S. Zhang, G. Yao, Z. Huang, Y. Xie, Y. Su, W. Yang, C. Zheng, Y. Lin, , *Acs Applied Materials & Interfaces.* **2015**, *7*(51), 28142-28147.

[538] Y. Zi, L. Lin, J. Wang, S. Wang, J. Chen, X. Fan, P. Yang, F. Yi, Z. L. Wang, , *Adv Mater.* **2015**, *27*(14), 2340-2347.

[539] Y. Yang, H. Zhang, G. Zhu, S. Lee, Z. Lin, Z. L. Wang, , *ACS Nano.* **2013**, *7*(1), 785-790.

[540] J. Lee, J. Kim, T. Y. Kim, M. S. Al Hossain, S. Kim, J. H. Kim, , *J. Mater. Chem. A.* **2016**, *4*(21), 7983-7999.

[541] B. J. Hansen, Y. Liu, R. Yang, Z. L. Wang, , *Acs Nano.* **2010**, *4*(7), 3647-3652.

[542] Y. Wu, X. Zhong, X. Wang, Y. Yang, Z. L. Wang, , *Nano Research.* **2014**, *7*(11), 1631-1639.

[543] Y. Chen, Y. Zhang, F. Yuan, F. Ding, O. G. Schmidt, , *Advanced Electronic Materials.* **2017**, *3*(3), 1600540.

[544] J. Tao, J. Hu, , *Journal of Zhejiang University-Science a.* **2016**, *17*(7), 502-511.

[545] D. Damjanovic, , *Rep. Prog. Phys.* **1998**, *61*(9), 1267-1324.

[546] J. Gao, Q. Li, H. Liu, J. Shim, Q. Yan, Y. Zhang, X. Chu, , *Ceram. Int.* **2015**, *41*(2), 2497-2501.

[547] J. Ma, X. Liu, W. Li, , *J. Alloys Compounds.* **2013**, *581*, 642-645.

[548] G. Messing, S. Trolier-McKinstry, E. Sabolsky, C. Duran, S. Kwon, B. Brahmaroutu, P. Park, H. Yilmaz, P. Rehrig, K. Eitel, E. Suvaci, M. Seabaugh, K. Oh, , *Crit. Rev. Solid State Mat. Sci.* **2004**, *29*(2), 45-96.

[549] Y. Saito, H. Takao, T. Tani, T. Nonoyama, K. Takatori, T. Homma, T. Nagaya, M. Nakamura, , *Nature.* **2004**, *432*(7013), 84-87.

[550] Y. Chang, S. F. Poterala, Z. Yang, S. Trolier-McKinstry, G. L. Messing, , *Appl. Phys. Lett.* **2009**, *95*(23), 232905.

[551] T. Richter, S. Denneler, C. Schuh, E. Suvaci, R. Moos, , *J Am Ceram Soc.* **2008**, *91*(3), 929-933.

[552] T. Kimura, , *J Ceram Soc Jpn.* **2006**, *114*(1325), 15-25.

[553] S. K. Ye, J. Y. H. Fuh, L. Lu, , *Appl. Phys. Lett.* **2012**, *100*(25), 252906.

[554] F. Xu, L. Sun, , *Energy Environ. Sci.* **2011**, *4*(3), 818-841.

[555] D. Olson, J. Piris, R. Collins, S. Shaheen, D. Ginley, , *Thin Solid Films.* **2006**, *496*(1), 26-29.

[556] Y. Sun, J. H. Seo, C. J. Takacs, J. Seifter, A. J. Heeger, , *Adv Mater.* **2011**, *23*(14), 1679-+.

[557] M. Jorgensen, K. Norrman, F. C. Krebs, , *Solar Energy Mater. Solar Cells.* **2008**, *92*(7), 686-714.

[558] L. Chen, Z. Hong, G. Li, Y. Yang, , *Adv Mater.* **2009**, *21*(14-15), 1434-1449.

[559] J. Cui, U. J. Gibson, , *J. Phys. Chem. C.* **2010**, *114*(14), 6408-6412.

[560] Y. Liu, H. K. Turley, J. R. Tumbleston, E. T. Samulski, R. Lopez, , *Appl. Phys. Lett.* **2011**, *98*(16), 162105.

[561] T. Gershon, K. P. Musselman, A. Marin, R. H. Friend, J. L. MacManus-Driscoll, , *Solar Energy Mater. Solar Cells.* **2012**, *96*(1), 148-154.

[562] K. P. Musselman, A. Wisnet, D. C. Iza, H. C. Hesse, C. Scheu, J. L. MacManus-Driscoll, L. Schmidt-Mende, , *Adv Mater.* **2010**, *22*(35), E254-+.

[563] W. S. Yan, R. Zhang, Z. L. Xie, X. Q. Xiu, Y. D. Zheng, Z. G. Liu, S. Xu, Z. H. He, , *Appl. Phys. Lett.* **2009**, *94*(24), 242111.

[564] V. Fuflyigin, E. Salley, A. Osinsky, P. Norris, , *Appl. Phys. Lett.* **2000**, *77*(19), 3075-3077.

[565] S. Lang, , *Phys Today.* **2005**, *58*(8), 31-36.

[566] G. Sebald, E. Lefeuvre, D. Guyomar, , *IEEE Trans. Ultrason. Ferroelectr. Freq. Control.* **2008**, *55*(3), 538-551.

[567] G. Sebald, D. Guyomar, A. Agbossou, , *Smart Mater. Struct.* **2009**, *18*(12), 125006.

[568] Y. Kutes, L. Ye, Y. Zhou, S. Pang, B. D. Huey, N. P. Padture, , *Journal of Physical Chemistry Letters.* **2014**, *5*(19), 3335-3339.

[569] B. Chen, X. Zheng, M. Yang, Y. Zhou, S. Kundu, J. Shi, K. Zhu, S. Priya, , *Nano Energy.* **2015**, *13*, 582-591.

[570] M. Coll, A. Gomez, E. Mas-Marza, O. Almora, G. Garcia-Belmonte, M. Campoy-Quiles, J. Bisquert, , *Journal of Physical Chemistry Letters.* **2015**, *6*(8), 1408-1413.

[571] H. Kim, S. K. Kim, B. J. Kim, K. Shin, M. K. Gupta, H. S. Jung, S. Kim, N. Park, , *Journal of Physical Chemistry Letters.* **2015**, *6*(9), 1729-1735.

[572] P. Wang, J. Zhao, L. Wei, Q. Zhu, S. Xie, J. Liu, X. Meng, J. Li, , *Nanoscale.* **2017**, *9*(11), 3806-3817.

[573] H. Roehm, T. Leonhard, M. J. Hoffmannbc, A. Colsmann, , *Energy & Environmental Science.* **2017**, *10*(4), 950-955.

[574] Y. Rakita, O. Bar-Elli, E. Meirzadeh, H. Kaslasi, Y. Peleg, G. Hodes, I. Lubomirsky, D. Oron, D. Ehre, D. Cahen, , *Proc. Natl. Acad. Sci. U. S. A.* **2017**, *114*(28), E5504-E5512.

[575] D. Seol, A. Jeong, M. H. Han, S. Seo, T. S. Yoo, W. S. Choi, H. S. Jung, H. Shin, Y. Kim, , *Advanced Functional Materials.* **2017**, *27*(37), 1701924.

[576] E. Mostafavi, A. Ataie, M. Ahmadzadeh, M. Palizdar, T. P. Comyn, A. J. Bell, , *Mater. Chem. Phys.* **2015**, *162*, 106-112.

[577] E. Strelcov, Q. Dong, T. Li, J. Chae, Y. Shao, Y. Deng, A. Gruverman, J. Huang, A. Centrone, , *Science Advances.* **2017**, *3*(4), e1602165.

[578] S. Liu, F. Zheng, N. Z. Koocher, H. Takenaka, F. Wang, A. M. Rappe, , *Journal of Physical Chemistry Letters.* **2015**, *6*(4), 693-699.

[579] Y. Kim, T. Dang, H. Choi, B. Park, J. Eom, H. Song, D. Seol, Y. Kim, S. Shin, J. Nah, S. Yoon, , *Journal of Materials Chemistry a.* **2016**, *4*(3), 756-763.

[580] Q. Zhou, Z. Bai, W. Lu, Y. Wang, B. Zou, H. Zhong, , *Adv Mater.* **2016**, *28*(41), 9163-+.

[581] Y. Lu, X. Kong, X. Chen, D. G. Cooke, H. Guo, , *Scientific Reports.* **2017**, *7*, 41860.

[582] K. Du, Q. Tu, X. Zhang, Q. Han, J. Liu, S. Zauscher, D. B. Mitzi, , *Inorg. Chem.* **2017**, *56*(15), 9291-9302.

[583] J. Zhao, Y. Deng, H. Wei, X. Zheng, Z. Yu, Y. Shao, J. E. Shield, J. Huang, , *Sci. Adv.* **2017**, *3*(11), eaao5616.

[584] S. M. Young, A. M. Rappe, , *Phys. Rev. Lett.* **2012**, *109*(11), 116601.

[585] A. Chynoweth, , *Phys. Rev.* **1956**, *102*(3), 705.

[586] F. Wang, S. M. Young, F. Zheng, I. Grinberg, A. M. Rappe, , *Nat. Commun.* **2016**, *7*, 10419.

[587] C. Paillard, X. Bai, I. C. Infante, M. Guennou, G. Geneste, M. Alexe, J. Kreisel, B. Dkhil, , *Adv Mater.* **2016**, *28*(26), 5153-5168.

[588] V. M. Fridkin, *Photoferroelectrics*, Springer, Berlin **1979**.

[589] B. I. Sturman, V. M. Fridkin, *The photovoltaic and photorefractive effects in noncentrosymmetric materials*, Bordon and Breach, Amsterdam **1992**.

[590] Y. Yao, B. Ploss, C. L. Mak, K. H. Wong, , *Appl. Phys. A-Mater. Sci. Process.* **2010**, *99*(1), 211-216.

[591] G. Catalan, J. F. Scott, , *Adv Mater.* **2009**, *21*(24), 2463-2485.

[592] M. Yang, A. Bhatnagar, Z. Luo, M. Alexe, , *Sci Rep.* **2017**, *7*, 43070.

[593] H. Hua, G. Bao, C. Li, Y. Zhu, J. Yang, X. Li, , *Journal of Materials Science-Materials in Electronics.* **2017**, *28*(22), 17283-17287.

[594] R. Nechache, C. Harnagea, S. Li, L. Cardenas, W. Huang, J. Chakrabartty, F. Rosei, , *Nat. Photonics.* **2015**, *9*(1), 61-67.

[595] G. HAYWARD, J. BENNETT, R. HAMILTON, , *J. Acoust. Soc. Am.* **1995**, *98*(4), 2187-2196.

[596] S. Fujino, M. Murakami, V. Anbusathaiah, S. -. Lim, V. Nagarajan, C. J. Fennie, M. Wuttig, L. Salamanca-Riba, I. Takeuchi, , *Appl. Phys. Lett.* **2008**, *92*(20), 202904.

[597] S. O. Leontsev, R. E. Eitel, , *J Am Ceram Soc.* **2009**, *92*(12), 2957-2961.

[598] S. Guan, H. Yang, Y. Zhao, R. Zhang, , *J. Alloys Compounds.* **2018**, *735*, 386-393.

[599] F. Wang, I. Grinberg, A. M. Rappe, , *Appl. Phys. Lett.* **2014**, *104*(15), 152903.

[600] F. Wang, I. Grinberg, A. M. Rappe, , *Physical Review B.* **2014**, *89*(23), 235105.

[601] Y. Zhang, J. Wang, M. P. K. Sahoo, T. Shimada, T. Kitamura, , *Physical Chemistry Chemical Physics.* **2017**, *19*(38), 26047-26055.

[602] T. Qi, M. T. Curnan, S. Kim, J. W. Bennett, I. Grinberg, A. M. Rappe, , *Physical Review B.* **2011**, *84*(24), 245206.

[603] F. Wang, I. Grinberg, L. Jiang, S. M. Young, P. K. Davies, A. M. Rappe, , *Ferroelectrics.* **2015**, *483*(1), 1-12.

[604] L. Yu, J. Jia, G. Yi, Y. Shan, M. Han, , *Mater Lett.* **2016**, *184*, 166-168.

[605] L. Yu, H. Deng, W. Zhou, P. Yang, J. Chu, , *Mater Lett.* **2017**, *202*, 39-43.

[606] S. Jaiswar, K. D. Mandal, , *Journal of Physical Chemistry C.* **2017**, *121*(36), 19586-19601.

[607] M. Wu, X. Lou, T. Li, J. Li, S. Wang, W. Li, B. Peng, G. Gou, , *J. Alloys Compounds.* **2017**, *724*, 1093-1100.

[608] Y. Bai, T. Siponkoski, J. Perantie, H. Jantunen, J. Juuti, , *Appl. Phys. Lett.* **2017**, *110*(6), 063903.

[609] S. Lee, J. A. Bock, S. Trolier-McKinstry, C. A. Randall, , *J. Eur. Ceram. Soc.* **2012**, *32*(16), 3971-3988.

[610] W. Wang, M. O. Tade, Z. Shao, , *Chem. Soc. Rev.* **2015**, *44*(15), 5371-5408.

[611] R. Myers, M. Vickers, H. Kim, S. Priya, , *Appl. Phys. Lett.* **2007**, *90*(5), 054106.

[612] P. T. Chiu, D. C. Law, R. L. Woo, S. B. Singer, D. Bhusari, W. D. Hong, A. Zakaria, J. Boisvert, S. Mesropian, R. R. King, N. H. Karam, *35.8% space and 38.8% terrestrial 5J direct bonded cells*, IEEE, NEW YORK; 345 E 47TH ST, NEW YORK, NY 10017 USA **2014**.

[613] J. Seo, J. Kim, U. Jeong, Y. Kim, Y. Kim, H. Lee, J. Oh, , *J. Korean Phys. Soc.* **2016**, *68*(3), 431-442.

[614] E. Dallago, M. Marchesi, G. Venchi, , *IEEE Trans. Power Electron.* **2010**, *25*(8), 1989-1997.

[615] C. Choi, I. Seo, D. Song, M. Jang, B. Kim, S. Nahm, T. Sung, H. Song, , *J. Eur. Ceram. Soc.* **2013**, *33*(7), 1343-1347.

[616] J. Kwon, W. Seung, B. K. Sharma, S. Kim, J. Ahn, , *Energy Environ. Sci.* **2012**, *5*(10), 8970-8975.

[617] J. Koenig, M. Winkler, T. Dankwort, A. -. Hansen, H. -. Pernau, V. Duppel, M. Jaegle, K. Bartholome, L. Kienle, W. Bensch, , *Dalton Trans.* **2015**, *44*(6), 2835-2843.

[618] E. Hazan, O. Ben-Yehuda, N. Madar, Y. Gelbstein, , *Adv. Energy Mater.* **2015**, *5*(11), 1500272.

[619] M. Han, X. Zhang, B. Meng, W. Liu, W. Tang, X. Sun, W. Wang, H. Zhang, , *ACS Nano.* **2013**, *7*(10), 8554-8560.

[620] F. Zheng, Y. Xin, W. Huang, J. Zhang, X. Wang, M. Shen, W. Dong, L. Fang, Y. Bai, X. Shen, J. Hao, , *J. Mater. Chem. A.* **2014**, *2*(5), 1363-1368.

[621] W. Liu, X. Ren, , *Phys. Rev. Lett.* **2009**, *103*(25), 257602.

[622] H. Birol, D. Damjanovic, N. Setter, , *J Am Ceram Soc.* **2005**, *88*(7), 1754-1759.

[623] H. Birol, D. Damjanovic, N. Setter, , *J. European Ceram. Soc.* **2006**, *26*(6), 861-866.

[624] A. P. B. Selvadurai, V. Pazhnivelu, B. K. Vasanth, C. Jagadeeshwaran, R. Murugaraj, , *J. Mater. Sci. -Mater. Electron.* **2015**, *26*(10), 7655-7665.

[625] A. P. Indolia, M. S. Gaur, , *J. Polym. Res.* **2013**, *20*(1), 43.

[626] K. Ng, H. Chan, C. Choy, , *IEEE Trans. Ultrason. Ferroelectr. Freq. Control.* **2000**, *47*(6), 1308-1315.

[627] Y. Arakawa, , *IEEE Journal of Selected Topics in Quantum Electronics.* **2002**, *8*(4), 823.

[628] W. Yim, E. Stofko, P. Zanzucchi, J. Pankove, M. Ettenberg, S. Gilbert, , *Journal of Applied Physics.* **1973**, *44*(1), 292.

[629] R. Banerjee, R. Jayakrishnan, P. Ayyub, , *J. Phys. -Condes. Matter.* **2000**, *12*(50), 10647-10654.

[630] T. M. Brenner, D. A. Egger, L. Kronik, G. Hodes, D. Cahen, , *Nat. Rev. Mater.* **2016**, *1*(1), 15007.

[631] C. C. Stoumpos, L. Frazer, D. J. Clark, Y. S. Kim, S. H. Rhim, A. J. Freeman, J. B. Ketterson, J. I. Jang, M. G. Kanatzidis, , *J. Am. Chem. Soc.* **2015**, *137*(21), 6804-6819.

[632] C. Li, J. Wei, M. Sato, H. Koike, Z. Xie, Y. Li, K. Kanai, S. Kera, N. Ueno, J. Tang, , *ACS Appl. Mater. Interfaces.* **2016**, *8*(18), 11526-11531.

[633] F. Chiarella, A. Zappettini, F. Licci, I. Borriello, G. Cantele, D. Ninno, A. Cassinese, R. Vaglio, , *Phys. Rev. B.* **2008**, *77*(4), 045129.

Figures and tables

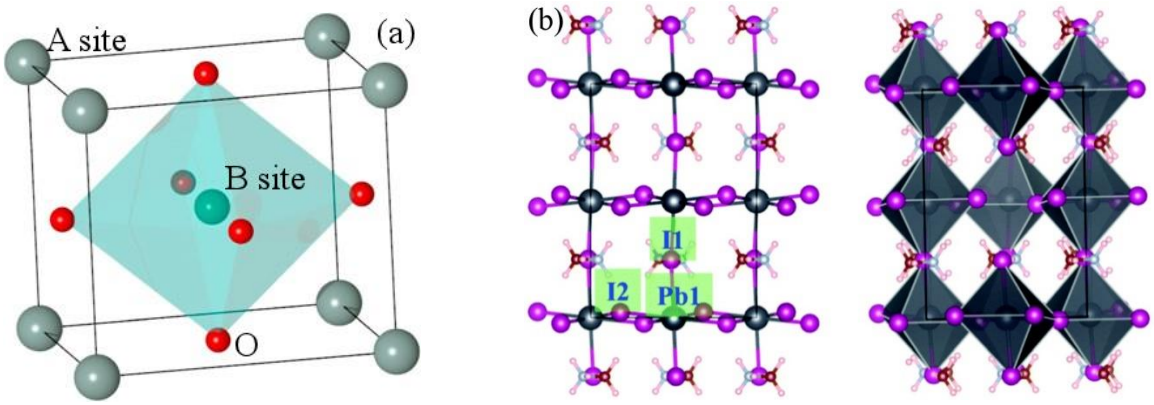

Figure 1. Schematics of the unit cells of (a) an ABO_3 structured perovskite and (b) an organic-halide perovskite ($CH_3NH_3PbI_3$ as example). Reproduced with permissions.[55, 610] (a) Copyright 2009, John Wiley and Sons; (b) Copyright 2015, Royal Society of Chemistry.

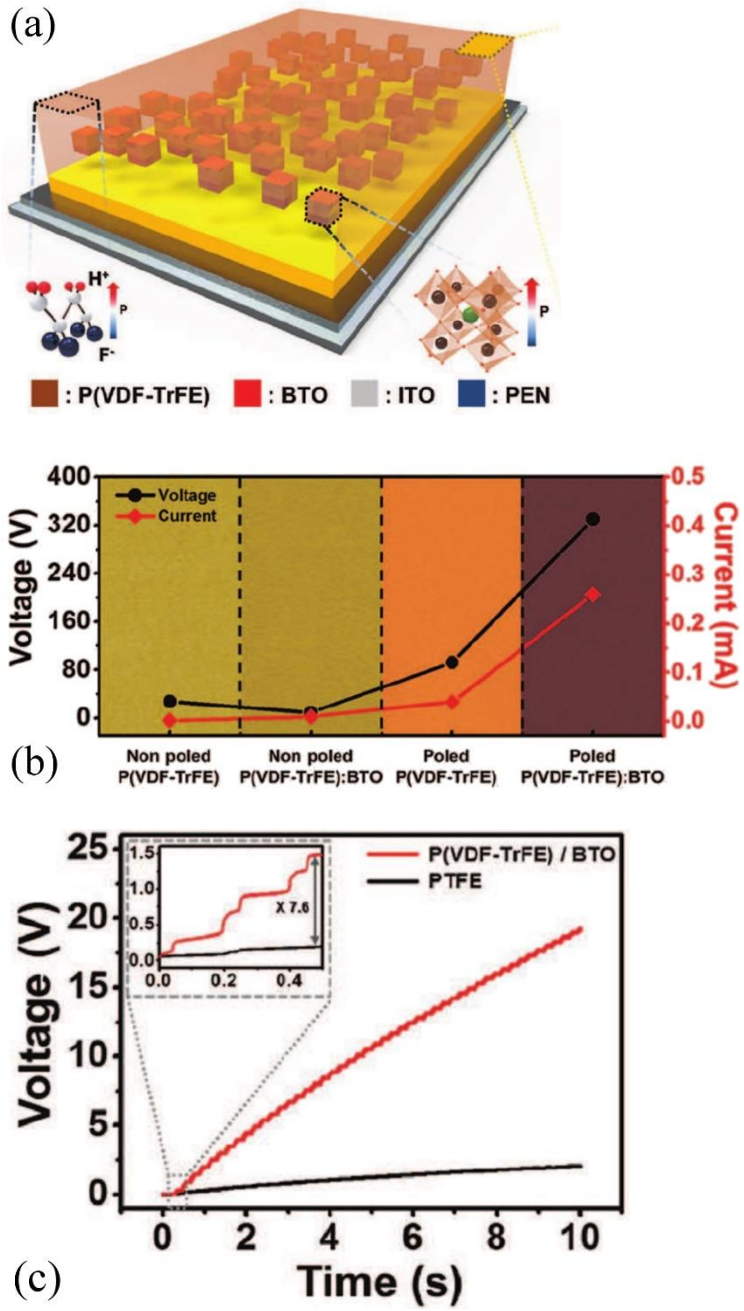

Figure 2. (a) Schematic of the BTO-P(VDF-TrFE) nanocomposite triboelectric energy harvester; (b) comparison of the output voltage and current between pure P(VDF-TrFE) and BTO-P(VDF-TrFE) nanocomposite; and (c) comparison of the charging capability of the triboelectric energy harvesters made from pure PTFE and BTO-P(VDF-TrFE) nanocomposite. ITO means indium tin oxide. PEN means polyethylene naphthalate. Reproduced with permission.[140] Copyright 2015, John Wiley and Sons.

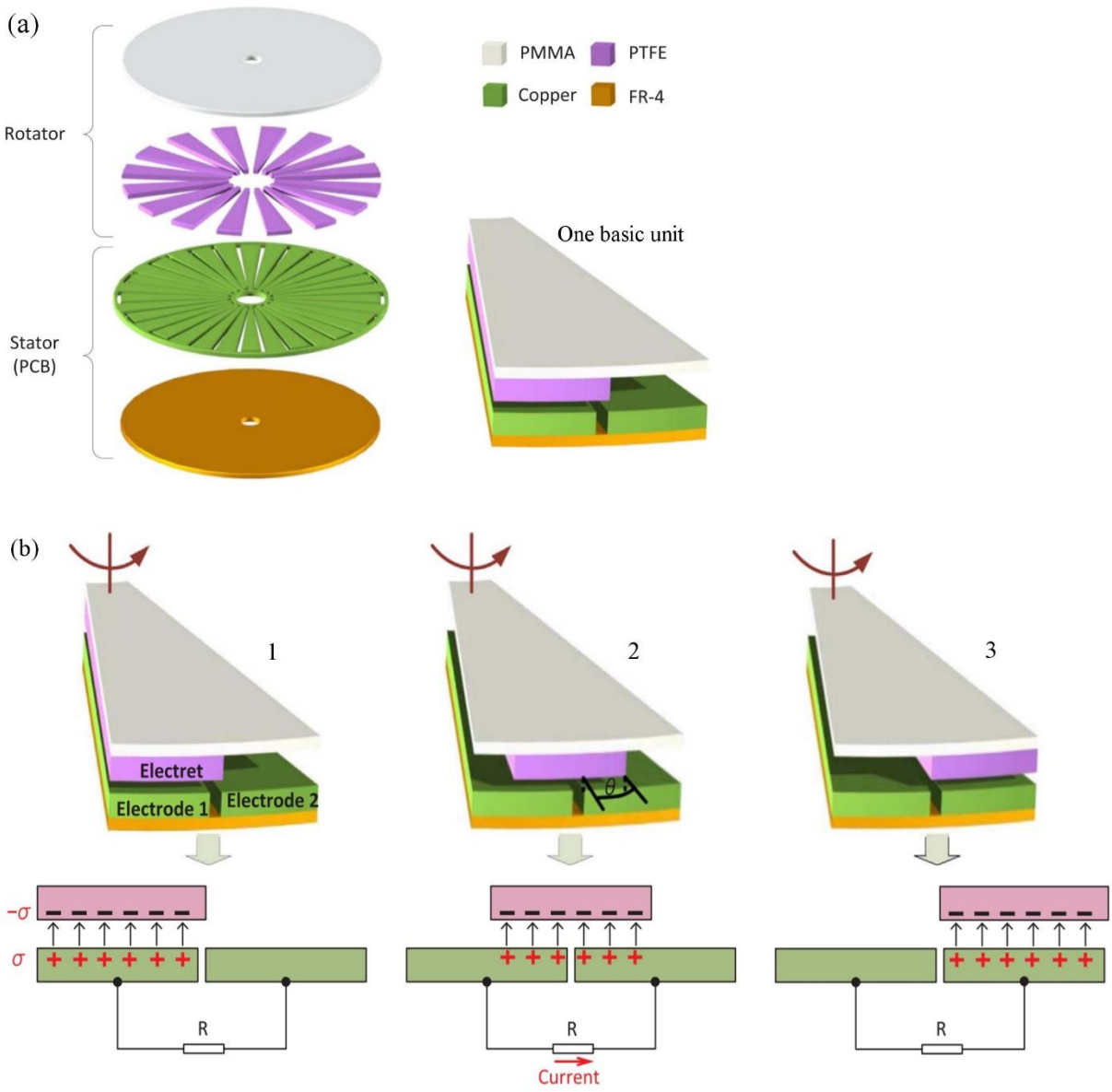

Figure 3. Schematics of a freestanding-electret rotary generator: (a) the design and structure and (b) working principle. Reproduced with permission.[155] Copyright 2017, Elsevier.

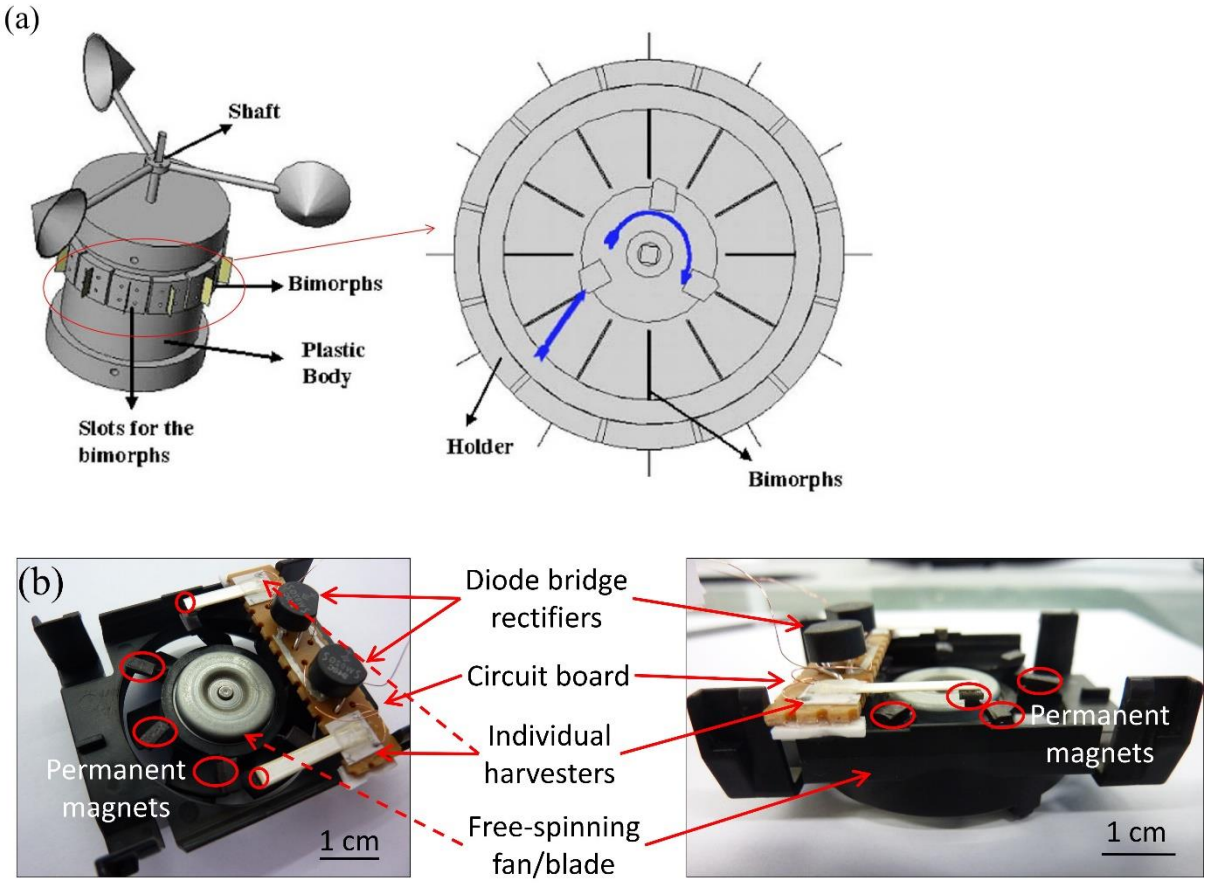

Figure 4. Schematics and pictures of wind energy harvesters combining piezoelectric materials: (a) the contact/impact design and (b) the contactless design. Reproduced with permissions.[263, 611] (a) Copyright 2007, AIP Publishing LLC; (b) Copyright 2015, Springer.

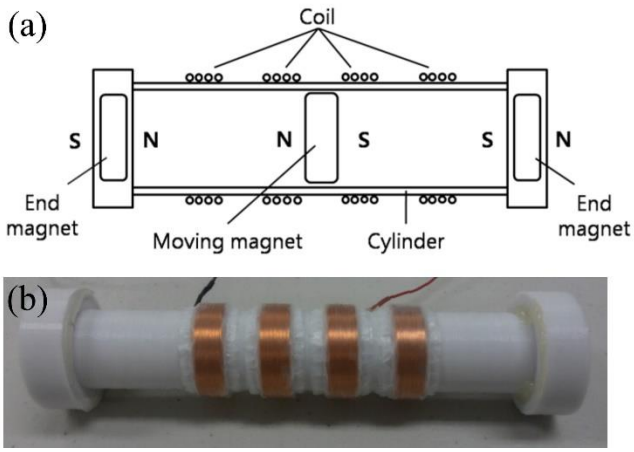

Figure 5. (a) Schematic and (b) appearance of an electromagnetic energy harvester used for bicycle handle bars. Reproduced under the terms of the Creative Commons Attribution License.[301] Copyright 2012, Multidisciplinary Digital Publishing Institute.

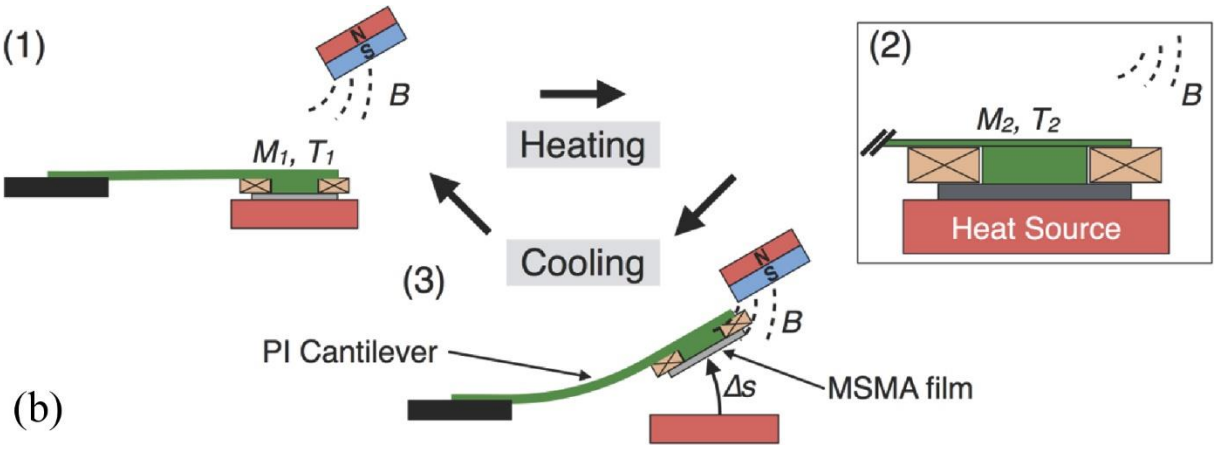

Figure 6. Schematics of the configuration and operating mechanism of a thermal energy harvester combining the electromagnetic effect and magnetic shape memory alloy (MSMA). Reproduced with permission.[445] Copyright 2014, John Wiley and Sons.

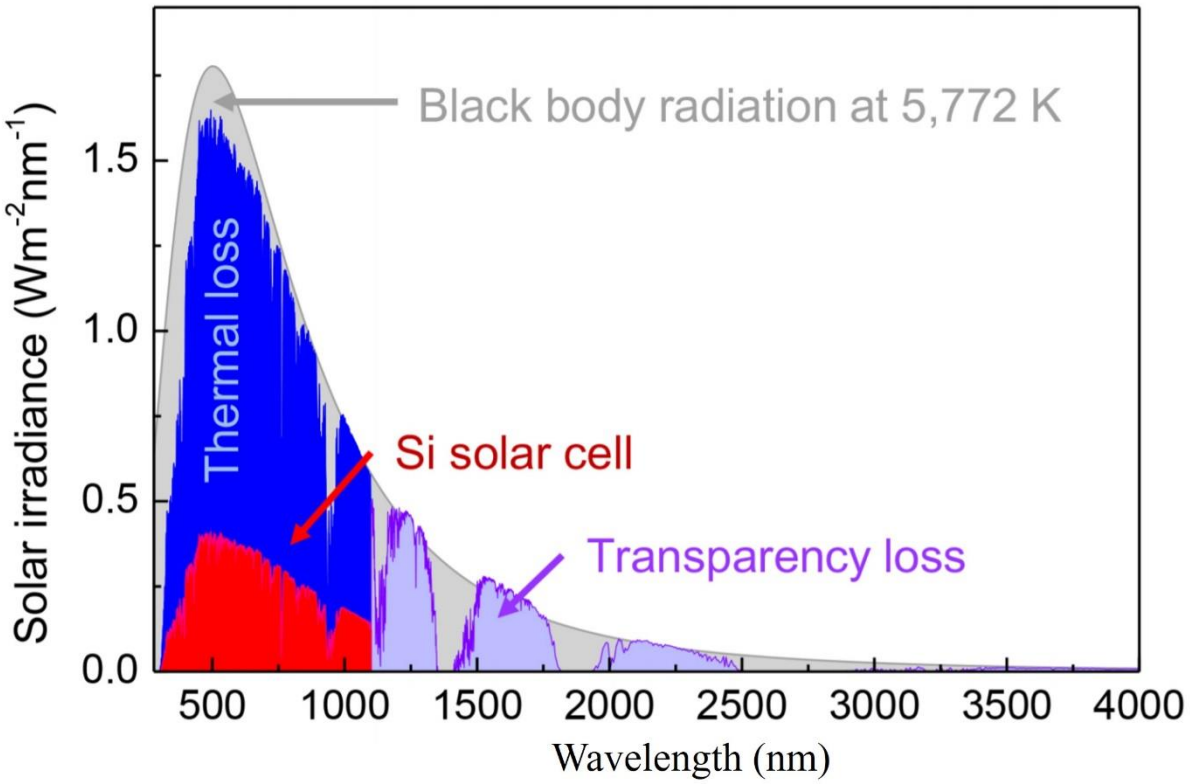

Figure 7. Illustration of the energy that can be harvested by a Si solar cell and the thermal loss in the solar irradiance spectrum. Reproduced under the terms of the Creative Commons CC BY License.[522] Copyright 2017, OSA Publishing.

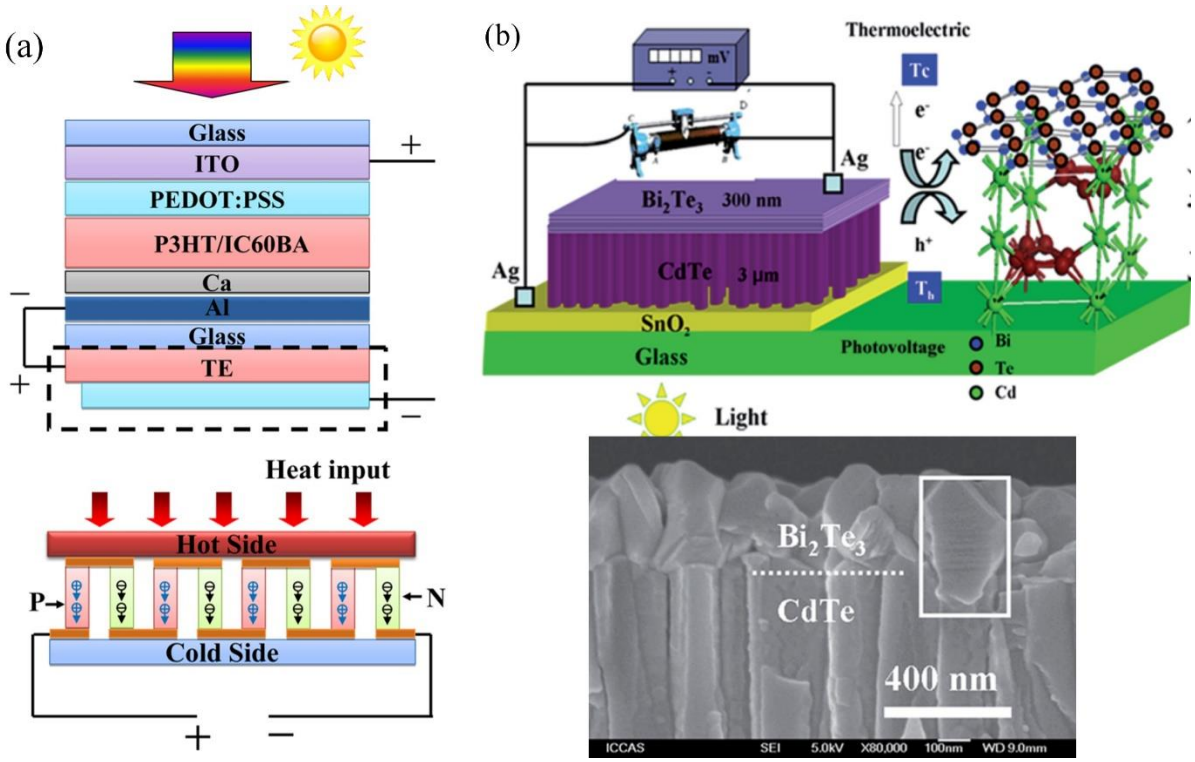

Figure 8. Two photovoltaic-thermoelectric hybrid energy harvesters: (a) a device hybridization by lamination and (b) a material hybridization using composite. Reproduced with permissions.[523, 524] (a) Copyright 2013, American Chemical Society; (b) Copyright 2016, Royal Society of Chemistry.

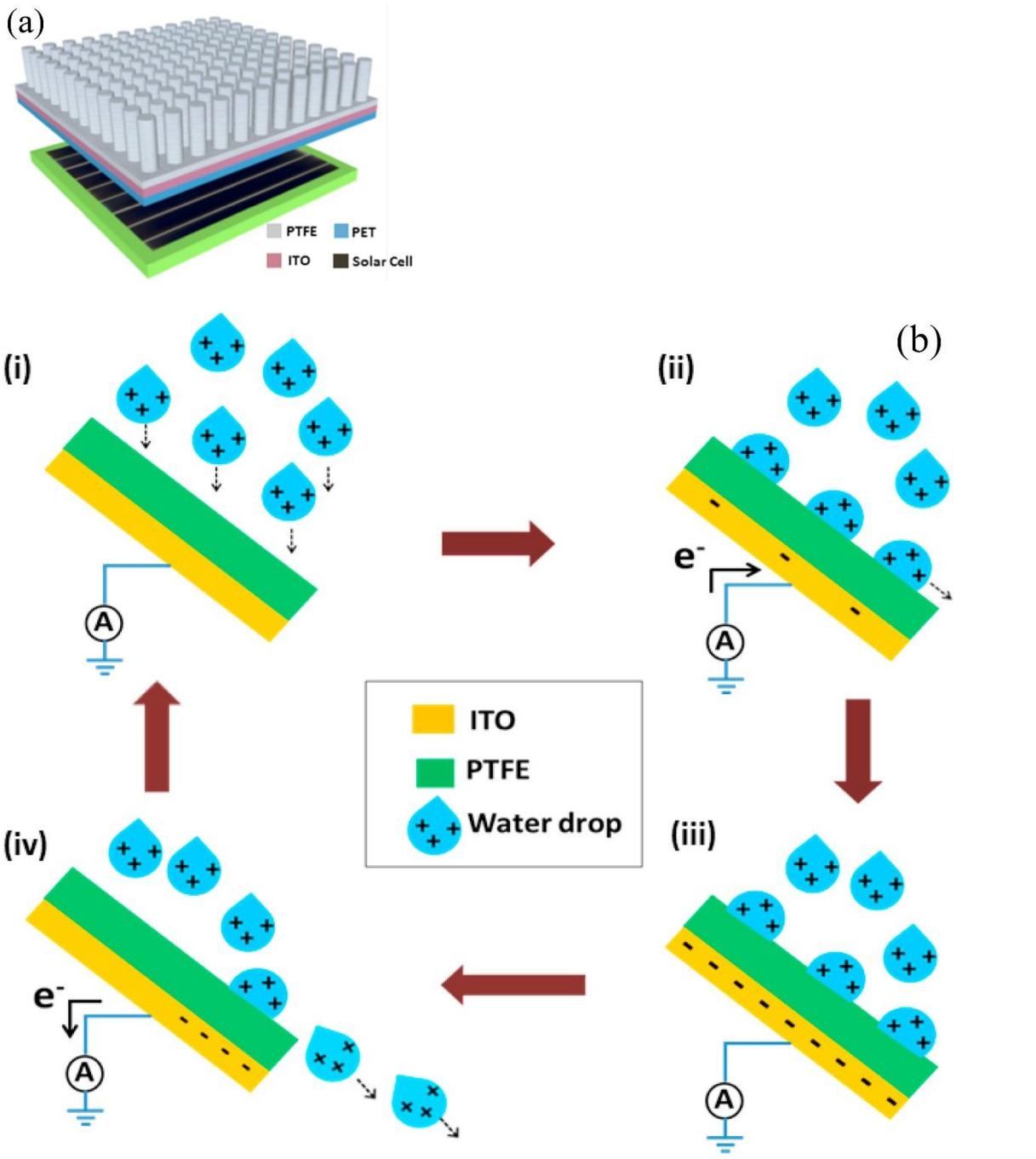

Figure 9. The schematics of (a) structure and (b) working mechanism of a photovoltaic-triboelectric hybrid energy harvester for solar and raindrop energy. Reproduced with permission.[526] Copyright 2014, Elsevier.

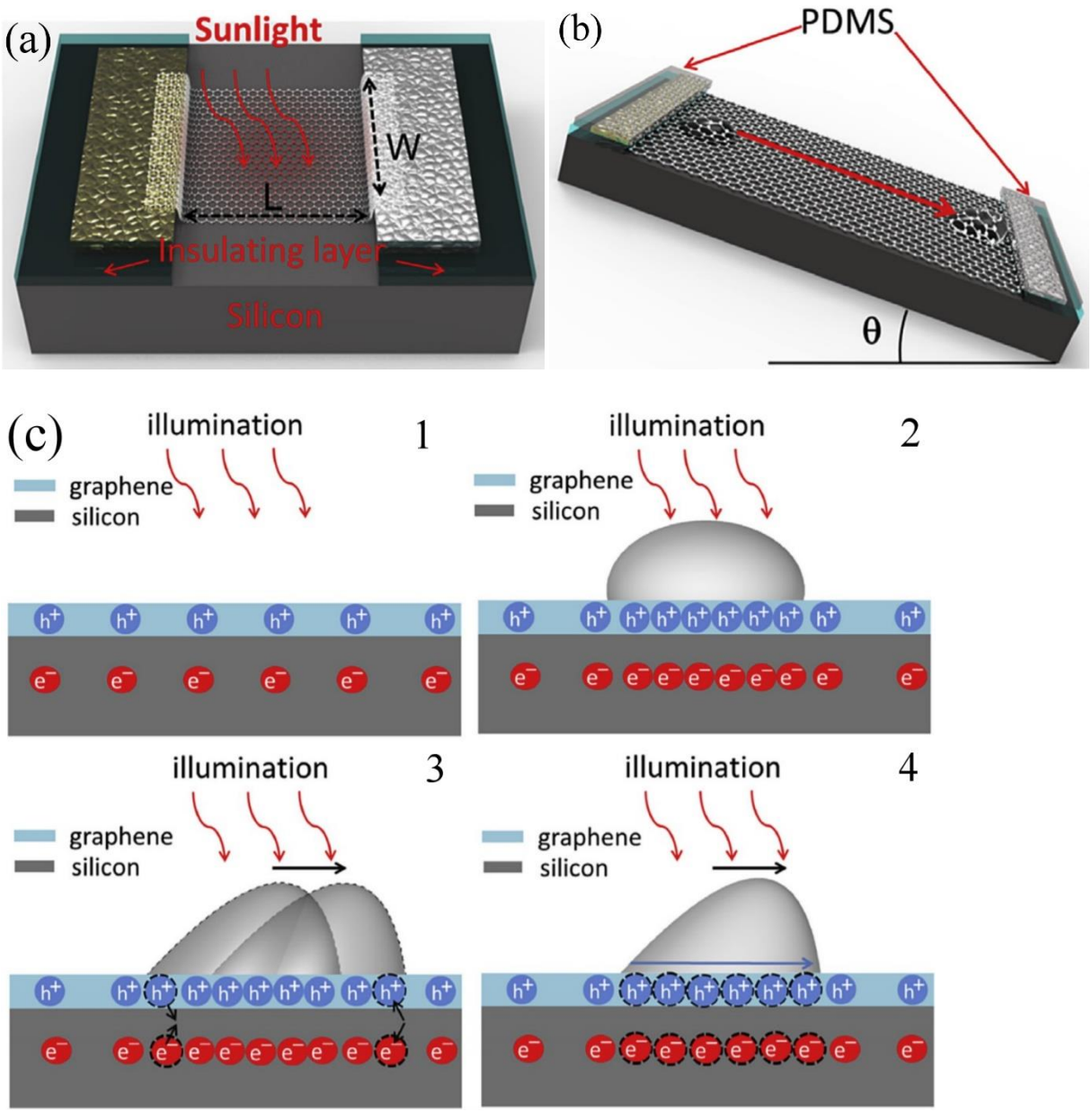

Figure 10. Schematics of a 2D hybrid nanogenerator: (a) (b) structure and (c) working principle. Reproduced with permission.[529] Copyright 2016, Elsevier.

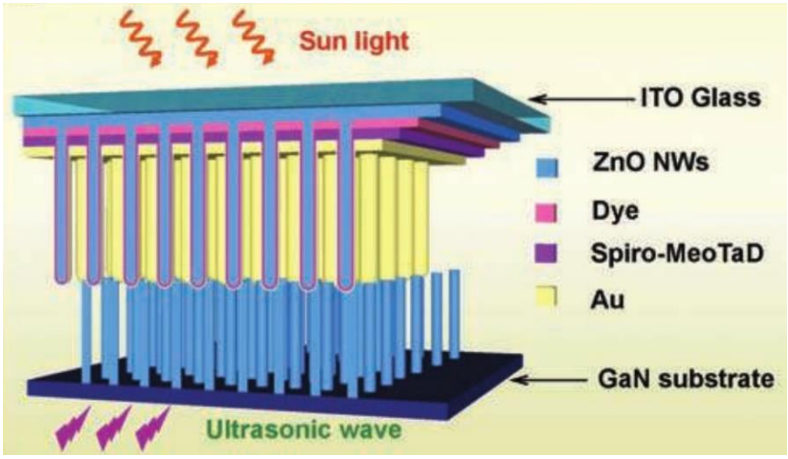

Figure 11. The structure of a photovoltaic-piezoelectric hybrid energy harvester for solar and acoustic energy. Reproduced with permission.[530] Copyright 2011, John Wiley and Sons

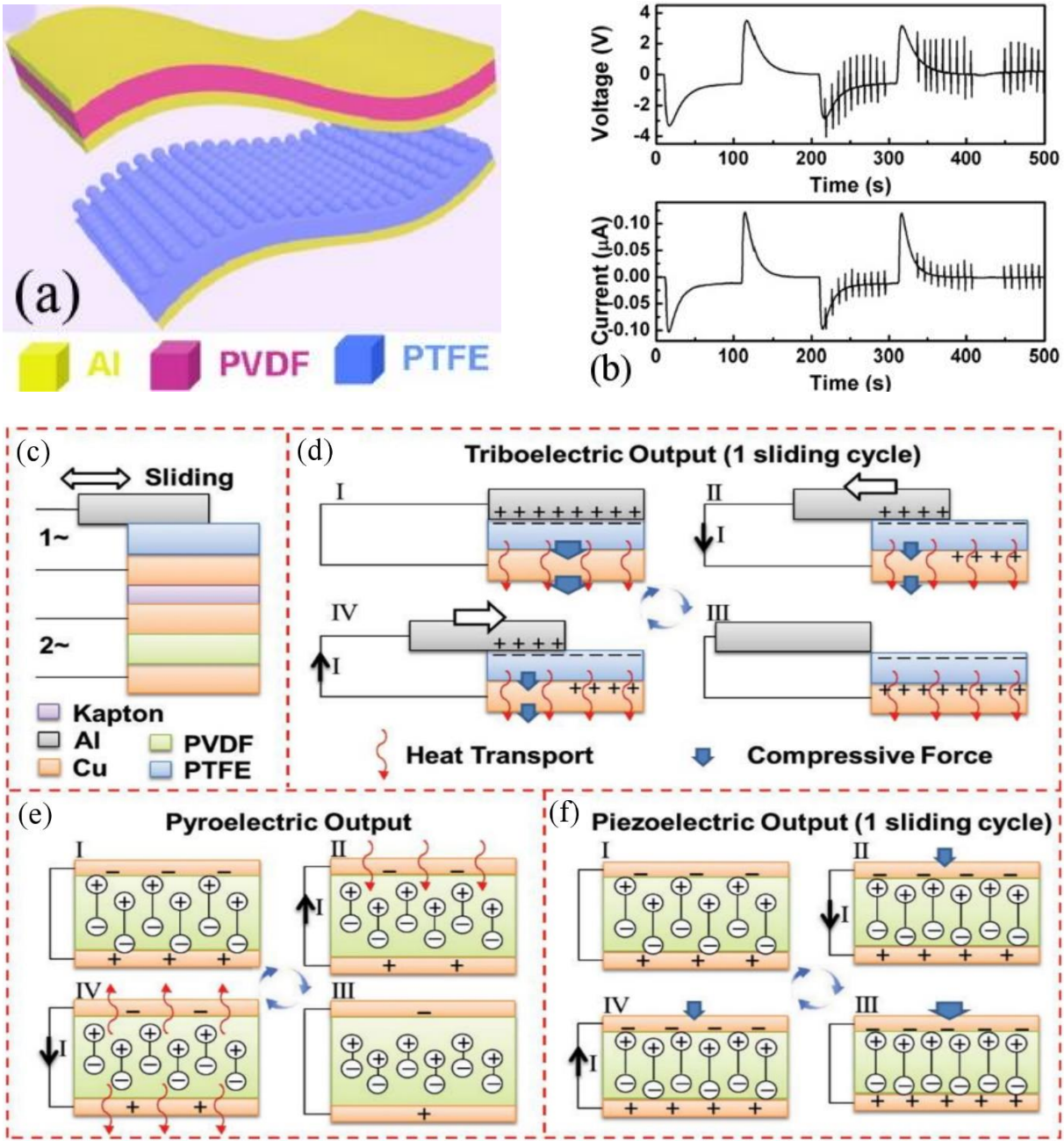

Figure 12. (a) (c) The structure, (b) output profile and (d)-(f) working principles of the piezoelectric-pyroelectric-triboelectric hybrid energy harvesters. Reproduced with permissions.[537, 538] (a) and (b) Copyright 2015, American Chemical Society; (c)-(f) Copyright 2015, John Wiley and Sons.

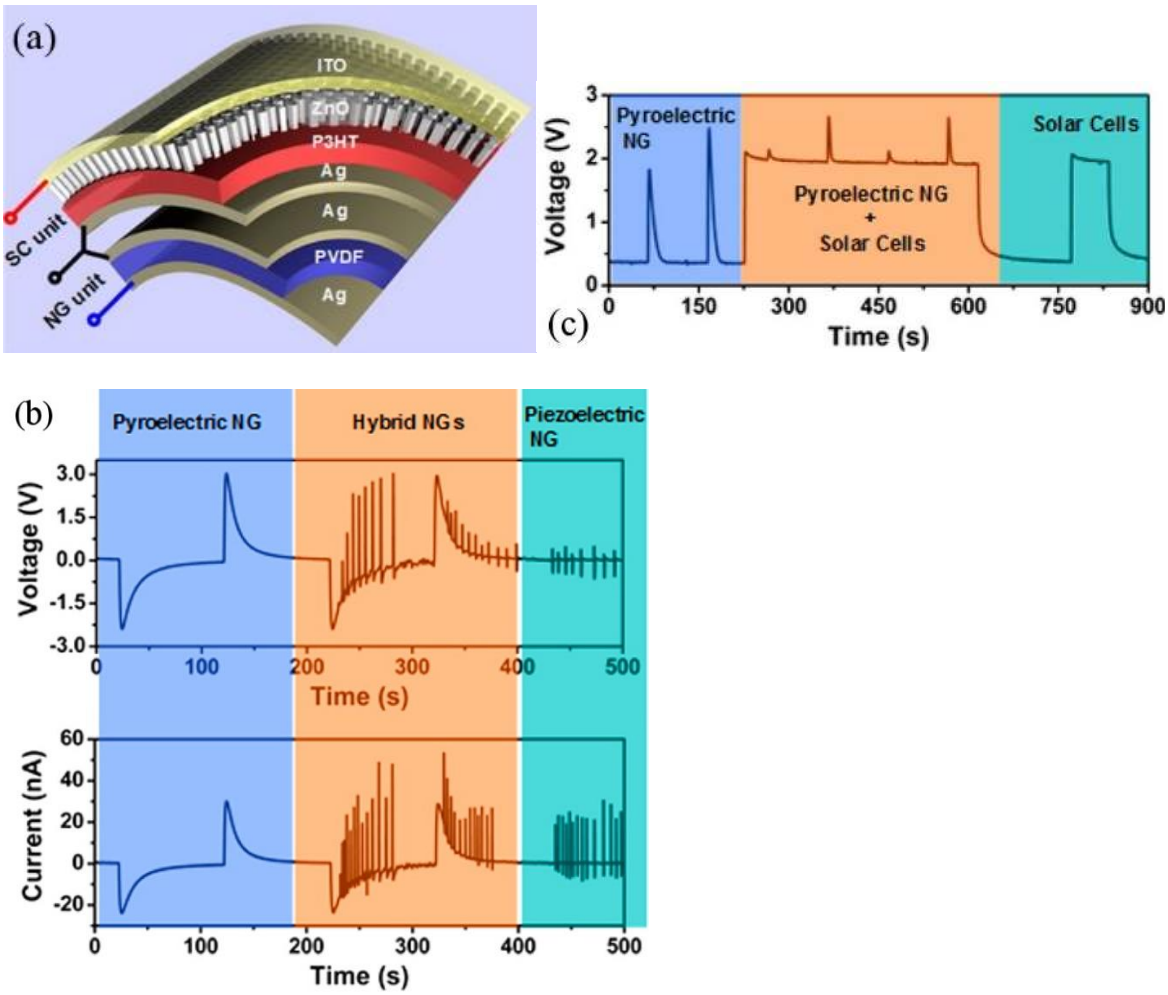

Figure 13. (a) Structure and (b), (c) output profiles of a thermal-kinetic-solar hybrid energy harvester. Reproduced with permission.[539] Copyright 2013, American Chemical Society.

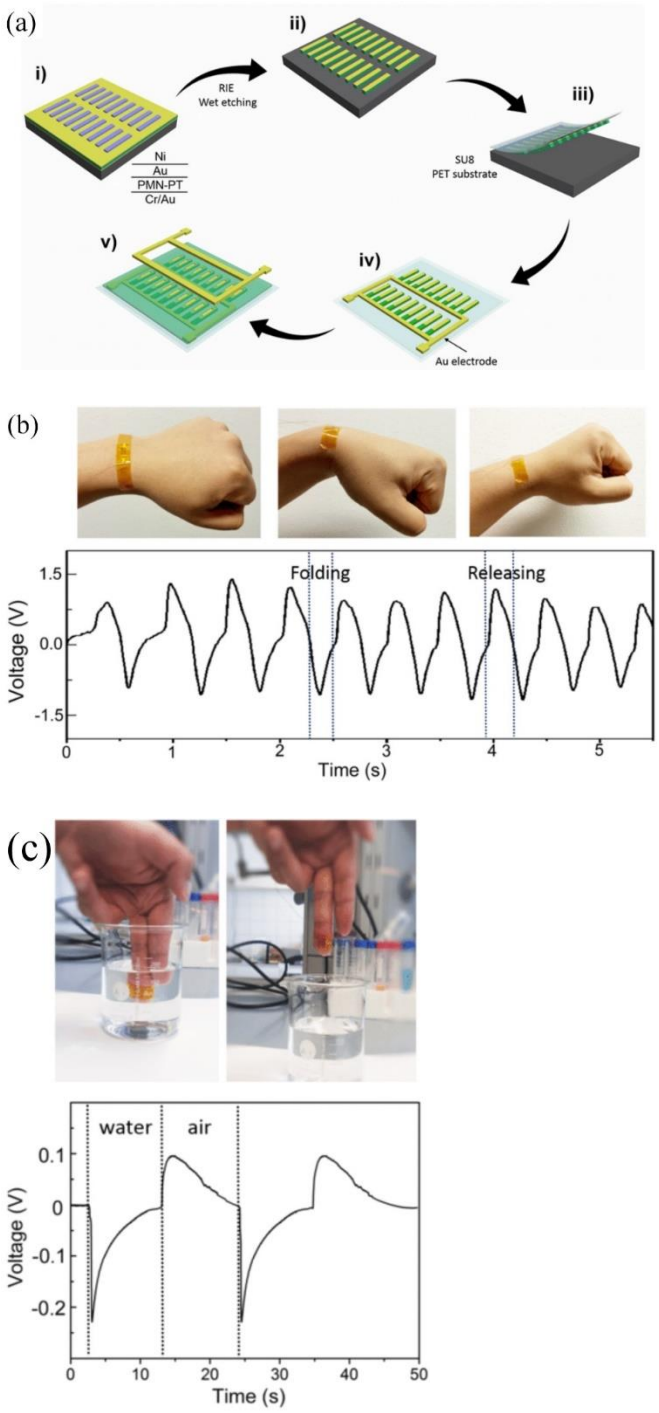

Figure 14. A flexible PMN-PT ribbon-based piezoelectric-pyroelectric multi-functional energy harvester for kinetic and thermal sources: (a) the schematic fabrication process, (b) the demonstration of kinetic energy harvesting on human body and (c) the demonstration of thermal energy harvesting using the temperature difference of the ambient environment (air) and warm water. Reproduced with permission.[543] Copyright 2017, John Wiley and Sons.

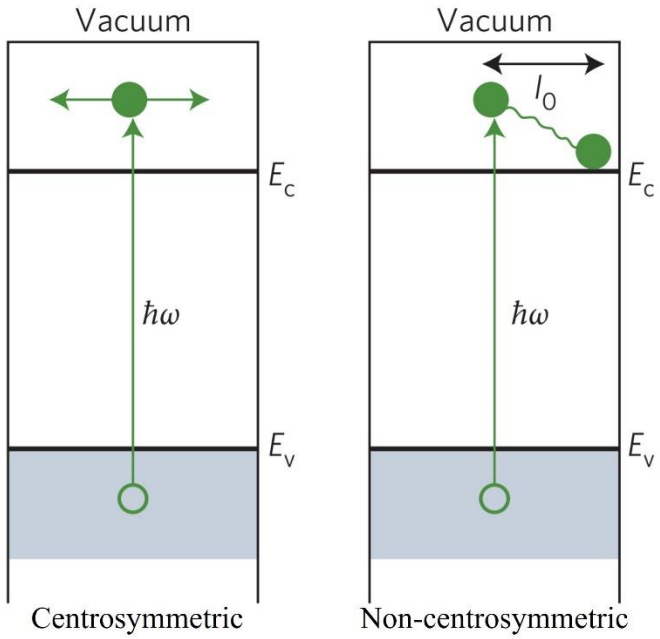

Figure 15. Schematic illustration of the photovoltaic effect in centrosymmetric and non-centrosymmetric crystals. $\hbar\omega$ is the incident photon energy, E_C is the conduction band minimum and E_V is the valence band maximum. Reproduced with permission.[13] Copyright 2016, Nature Publishing Group.

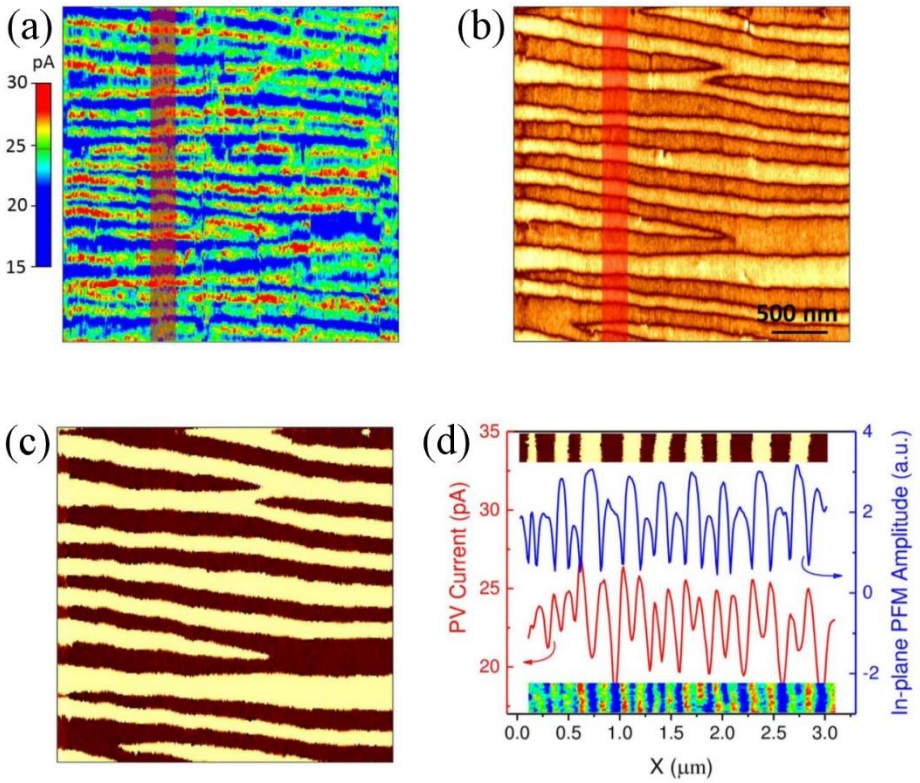

Figure 16. Spatially resolved photovoltaic current mapping with domain walls parallel to grounded electrode for the BFO thin-film. (a) Spatial distribution of the photovoltaic current detected by the AFM under illumination. (b) and (c) The in-plane PFM amplitude and phase signal, respectively. (d) Profile analysis of photovoltaic current distribution and in-plane PFM amplitude signal averaged over the area marked by red in (a) and (b), with upper and lower inserts showing the corresponding PFM phse images and the current distribution of the analyzed region, respectively. Reproduced under the terms of the Creative Commons CC BY License.[592] Copyright 2017, Springer Nature.

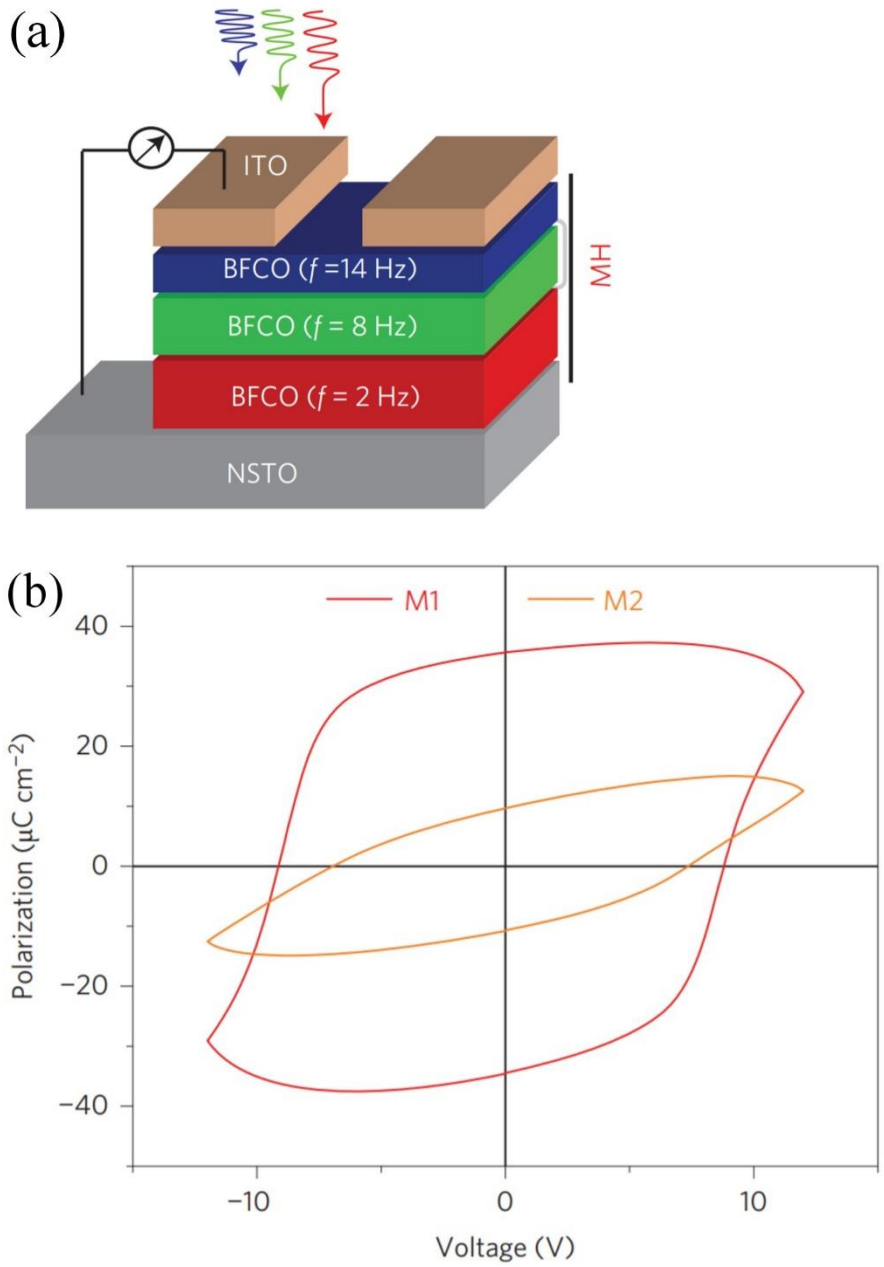

Figure 17. (a) Schematic of the structure of the multi-layer BFCO thin-film solar cell. (b) The ferroelectric hysteresis loops of two multi-layer BFCO thin-film solar cells – M1 and M2 are the ones with 8.1 % and 4.3 % photovoltaic efficiencies, respectively. Reproduced with permission.[594] Copyright 2014, Springer Nature.

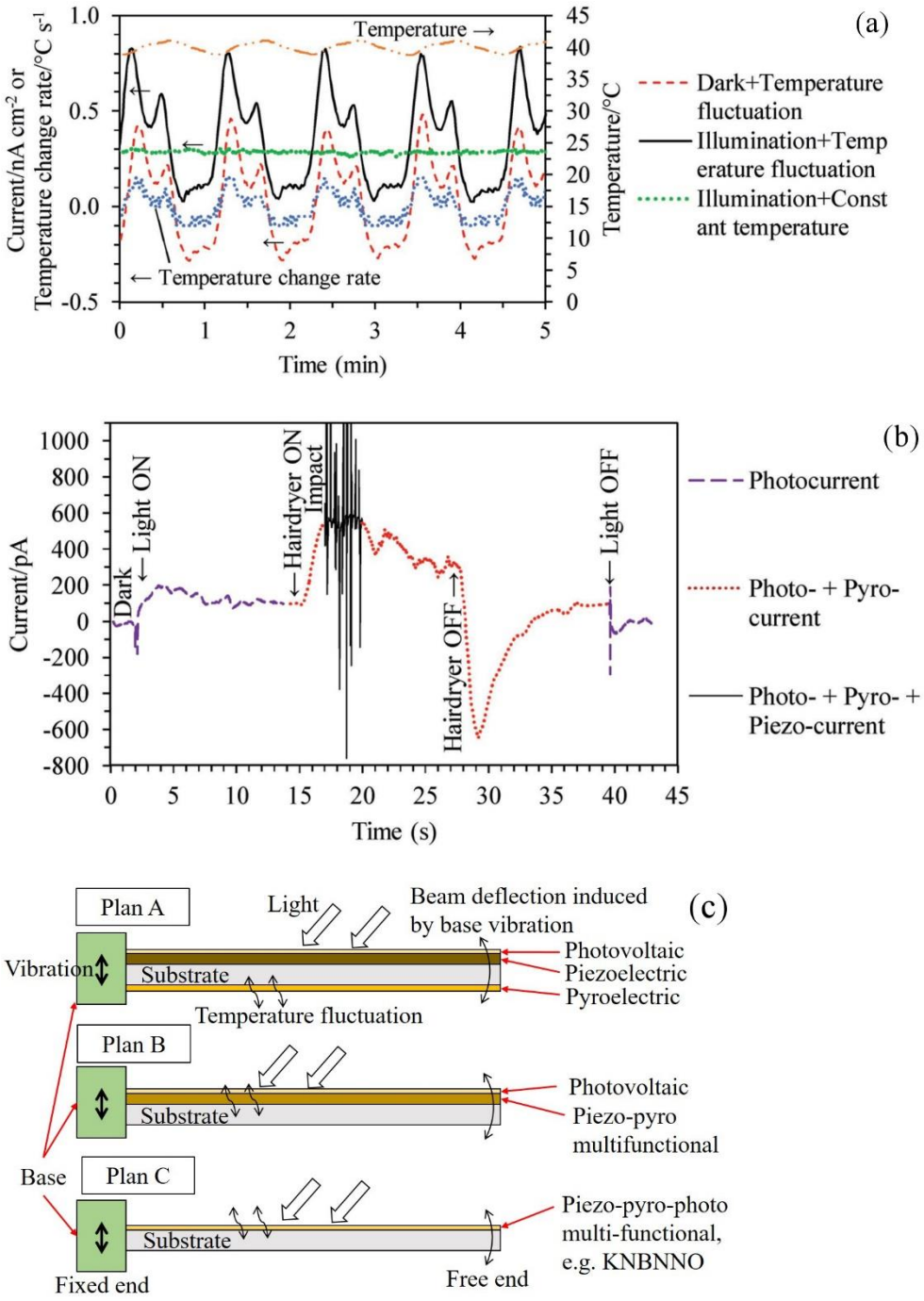

Figure 18. (a) The output current of the KNBNNO under illumination and/or with temperature fluctuation. (b) The photo-, pyro-, and piezo-currents of the KNBNNO generated individually and/or simultaneously from light, thermal and kinetic energy sources. (c) Schematics of the potential examples of hybrid and multi-source energy harvesters for practical applications. (a) and (b) are reproduced with permission.[60] Copyright 2017, John Wiley and Sons.

Table 1. Summary of single-source individual and hybrid and multi-source hybrid energy harvesters with associated record output voltage, output power, output power density or energy conversion efficiency.

Input energy source	Energy conversion principle	Material/configuration	Output voltage [V]	Output power [mW]	Output power density	Energy conversion efficiency [%]	Reference
Solar [a)]	Photovoltaic	$BaTiO_3$ ceramic, Bulk photovoltaic effect	1.2	-	4.8 mW cm^{-2}	4.8	[13]
Solar [a)]	Photovoltaic	GaAs thin-film, single-junction cell	-	-	28.8 mW cm^{-2}	28.8	[10]
Solar [a)]	Photovoltaic	$0.05MAPbBr_3$-0.95α-$FAPbI_3$ thin-film, single-junction cell	1.1	-	22.1 mW cm^{-2}	22.1	[33]

Solar [a)]	Photovoltaic	3 layers of GaAs and 2 layers of InP thin-films, 5-junction cell	4.8	33.8	38.8 mW cm^{-2}	38.8	[612]
Kinetic (6 kgf pushing force at 5 Hz)	Triboelectric	5 wt.% BTO nanoparticles-P(VDF-TrFE) nanocomposite, poled BTO and P(VDF-TrFE), contacting mode	1130	6.4	0.71 mW cm^{-2}	-	[140]
Kinetic (750 rpm rotary)	Electrostatic (electret)	Rotor (PMMA+PTFE) + stator (Cu+FR4)	324	10.5	0.42 mW cm^{-2}	56	[155]
Kinetic (vibration with 2.1 Hz frequency)	Electromagnetic	Magnet suspended by springs on both sides in a vertical tube	6.5	0.432	14.16 µW cm^{-3}	-	[613]

Kinetic (vibration with 10.4 Hz frequency and 9.8 m s^{-2} acceleration)	Electromagnetic	Magnet suspended by other magnets on both sides in a vertical tube	2.25	6	0.61 mW cm^{-3}	-	[614]
Kinetic (compression with 1 Hz frequency)	Piezoelectric	Pre-stressed multi-layer PZT diaphragms	-	11.3	10.55 mW cm^{-3}	5.5	[66]
Kinetic (vibration with 85 Hz frequency)	Piezoelectric	Cantilever, leaf spring steel substrate + 0.69PZT-0.31Pb[$(Zn_{0.4}Ni_{0.6})_{1/3}Nb_{2/3}$]$O_3$ ceramic layer	3	10.6	10.44 mW cm^{-3}	-	[615]

Kinetic (impact or movement)	Piezoelectric	Semi-transparent flexible PZT ribbon-based nanogenerator, PZT thin-film + PET stubstrate + graphene electrode	2	-	88 mW cm^{-3}	-	[616]
Thermal (temperature difference of 525 ˚C)	Thermoelectric	8 p/n leg pairs made from $(GeTe)_{0.962}(Bi_2Se_{0.2}Te_{2.8})_{0.038}$ and Bi:PbTe	-	366	1.02 W cm^{-2}	2	[617]
Thermal (temperature difference of 450 ˚C)	Thermoelectric	A p-n junction, p-type $Ge_{0.87}Pb_{0.13}Te$, two-segment n-type: 0.055 % and 0.01 % PbI_2-doped $(PbSn_{0.05}Te)_{0.92}(PbS)_{0.08}$	-	170	-	12	[618]
Thermal (temperature fluctuation from -173 ˚C to 27 ˚C)	Pyroelectric	Three stacks of PZT/$CoFe_2O_4$ multi-layered nanostructures	-	-	47.4 J cm^{-3} per cycle	-	[411]

Thermal (temperature fluctuation with 70 mHz frequency)	Pyroelectric	$Pb[(Mn_xNb_{1-x})_{1/2}(Mn_xSb_{1-x})_{1/2}]_y(Zr_{0.95}Ti_{0.5})_{1-y}O_3$ ceramics			4.86 mW cm^{-3}	-	[416]
Thermal (temperature fluctuation of 10 ˚C with 10 % duty cycle)	Magnetic shape memory film + electromagnetic	Polyimide cantilever with Cu coils and $Ni_{50.4}Co_{3.7}Mn_{32.8}In_{13.1}$ magnetic shape memory alloy film attached at the tip + a NdFeB magnet fixed above	-	-	0.5 mW cm^{-3}	-	[445]
Kinetic	Piezoelectric + electromagnetic	A cubic housing + four PZT diaphragms attached at the bottom + a NdFeB magnet suspended above the diaphragms + Cu coils attached with the housing	3.3	0.13	2.7 μW cm^{-3}	-	[492]

Kinetic	Piezoelectric + triboelectric	Arc-shaped lamination of PET/ITO, PVDF and Al layers + flat lamination of toothed PDMS and PET/ITO layers	240	-	13 mW cm^{-3}	-	[619]
Kinetic	Electrostrictive + electret	Commercial electret (Emfit film) attached on P(VDF-TrFE-CFE) filled with 1 % carbon nanoparticles [b)]	-	-	1.8 μW cm^{-3}	-	[496]
Kinetic	Electromagnetic + triboelectric	A rotator (polylactic acid + Cu + coil) + a stator (polylactic acid + Cu + FEP + magnets)	48	13	13.8 μW cm^{-3}	36.4	[509]
Kinetic	Triboelectric + electrostatic	A large acrylic disc with a small Al disc attached in the center + a Fe/Cu/PTFE laminated movable mass + 3 springs attached to the large disc and mass	120	-	0.15 mW cm^{-2}	-	[515]
Kinetic	Piezoelectric + electromagnetic + triboelectric	PET flexible picking-up vibration structures + PDMS film + Coil + Magnet + PVDF film	6.4	0.112	0.75 μW cm^{-3}	-	[307]

Thermal (temperature gradient + fluctuation)	Thermoelectric + pyroelectric	Thermoelectric generator in a circular mesh polyester knit fabric + circular-shaped pyroelectric generator + quick sweat-pickup/dry-fabric	-	-	1.5 μW m^{-2}	-	[520]
Solar + temperature gradient	Photovoltaic + thermoelectric	Commercial thermoelectric module (Micropelt) + solar cell: glass/ITO/PEDOT:PSS/P3HT/IC60BA/Ca/Al lamination	-	-	11.29 mW cm^{-2}	5.2	[523]
Solar + kinetic (raindrop)	Photovoltaic + triboelectric	Lamination of nanostructured PANi-graphene/PtCo, FTO/glass/FTO, dye-sensitized m-TiO2/LPP photoanode, redox electrolyte and counter electrode [c)]	0.73/1.8 $x10^{-4}$	-/2.3 $x10^{-6}$	8.6 mW cm^{-2}/-	8.6/25.6	[528]

Solar + kinetic (ocean wave)	Photovoltaic + electromagnetic + triboelectric	Commercial Si-based solar cell + magnet + Cu coils + PTFE + Al	150	-/0.105	5 mW cm^{-2}/0.18 μW cm^{-3}	5/-	[510]
Solar + kinetic (acoustic wave)	Photovoltaic + piezoelectric	Stack of ITO glass, vertically aligned ZnO nanowires, dye, spiro-MeOTAD [d], Au and GaN	0.243	-	34.5 μW cm^{-2}	-	[530]
Thermal (temperature fluctuation) + kinetic (compression and friction)	Pyroelectric + piezoelectric + triboelectric	Multi-layer structure of Al/PTFE/Cu/Kapton/Cu/PVDF/Cu	120/1100	-	14.6 μW cm^{-2}/-	-	[538]

Solar + temperature + fluctuation + kinetic	Photovoltaic + pyroelectric + piezoelectric	Multi-layer structure of ITO/vertically aligned ZnO nanowires/P3HT/Ag/Ag/PVDF/Ag	3	-	-	-	[539]

[a)] One-sun illumination; [b)] P(VDF-TrFE-CFE) – poly(vinylidenefluoride-trifluorethylene-chlorofluoroethylene); [c)] PANi – polyaniline, LPP – long persistence phosphor; [d)] spiro-MeOTAD – 2,2' 7,7'-tetrakis(N,N-di-p-methoxyphenylamine) 9,9'-spirobifluorene

Table 2. Summary of the piezoelectric and pyroelectric properties and band gaps of different compositions.

Composition	Piezoelectric coefficient d_{33} [pC N^{-1} or pm V^{-1}]	Piezoelectric Figure of merit $d_{33} \cdot g_{33}$ [x10^{-11} m^2 N^{-1}]	Pyroelectric coefficient p [μC m^{-2} K^{-1}]	Pyroelectric figure of merit FOM_{pyro} [x10^{-11} m^3 J^{-1}]	Band gap [eV]
PZT based	452-557[156-158]	1.65-2.03[156-158]	380[410]	0.90[410]	> 3.5[620]
BT based	149-620[621]	0.21-1.42[291,621]	200[410]	0.06[410]	> 3[13]
$KNbO_3$	90-110[622]	0.09[622]	93[622]	-	3.8[56]
$0.75KNbO_3$-$0.25(Sr_{1/2}La_{1/2})(Zn_{1/2}Nb_{1/2})O_3$	-	-	-	-	2.1[600]
Bi-doped $KNbO_3$	-	-	-	-	2-2.6[603]
$(KNbO_3)_{1-x}(BaCo_{1/2}Nb_{1/2}O_{3-\delta})_x$	-	-	-	-	2.4[604]
$(KNbO_3)_{1-x}(BaNb_{1/2}Fe_{1/2}O_3)_x$	-	-	-	-	1.7-2.5[605]
$(KNbO_3)_{0.9}(BaNi_{1/2}Nb_{1/2}O_{3-\delta})_{0.1}$	23[608]	0.009[608]	26[608]	-	1.39[56]
KNN based	100-212[623]	0.24-0.93[159,623]	140-190[410,623]	0.01-0.04[410]	> 4[60]

$[(K_{0.5}Na_{0.5})O_3]_{0.98}(BaNi_{1/2}Nb_{1/2}O_{3-\delta})_{0.02}$ (KNBNNO)	100[60]	0.12[60]	128[60]	-	1.6[60]
BNT-BT based	30-208[55]	0.28-0.49[55]	308-513[410]	0.23-0.67[410]	> 3[624]
PMN-PT	2820[291]	10.95[291]	746[410]	0.48[410]	-
$(PbNiO_2)_x(PbTiO_3)_{1-x}$	-	-	-	-	1.5[586]
PVDF	-33[291]	1.62[291]	27[410]	0.17[410]	> 4.5[625]
P(VDF-TrFE)	-37[626] a)	1.63[626] a)	40[410] b)	0.19[410] b)	-
GaN	3.7[291]	0.014[291]	4.8[410]	0.003[410]	1.8-6.2[627]
AlN	5[291]	0.024[291]	6-8[410]	0.01[410]	6.2[628]
CdS	10.3[291]	0.12[291]	4[410]	0.005[410]	2.5[629]
ZnO	12.4[291]	0.16[291]	9.4[410]	0.01[410]	3.4[164]
$(CH_3NH_3)PbI_3$	31.4[58]	0.006[579]	-	-	1.6[630]
$(CH_3NH_3)SnI_3$	100.9[58]	-	-	-	1.2[629]
$(CH_3NH_3)GeI_3$	27.4[58]	-	-	-	1.9[631]
$(CH_3NH_3)PbCl_3$	6.7[58]	-	-	-	3.1[632]

$(CH_3NH_3)SnCl_3$	4.1[58]	-	-	-	3.7[633]
$(CF_3NH_3)PbI_3$	248[58]	-	-	-	-
$BiFeO_3$	70[597]	0.31[597]	90[590]	-	2.2-2.7[56,587]
Ni-doped $SrBi_2Nb_2O_9$	-	-	-	-	2.25[607]

[a)] 70/30 copolymer; [b)] 50/50 copolymer

Received: ((will be filled in by the editorial staff))
Revised: ((will be filled in by the editorial staff))
Published online: ((will be filled in by the editorial staff))

Author biographies and photographs

Dr. Yang Bai

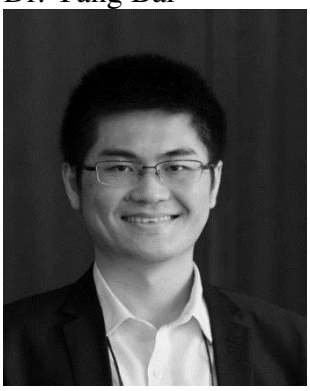

Yang Bai received his Bachelor of Engineering degree in 2011 at Tianjin University, China. He then received his Ph. D. degree in 2015 at University of Birmingham, United Kingdom. He was granted a Marie Sklodowska-Curie Individual Fellowship under European Union's Horizon 2020 research and innovation program in 2016. He is now a postdoctoral researcher and Marie Sklodowska-Curie research fellow of Microelectronics Research Unit, University of Oulu, Finland. His research interests include piezoelectric and ferroelectric materials, photovoltaic-ferroelectric materials and their applications in energy harvesting.

Prof. Heli Jantunen

Heli Jantunen received the M. Sc. Degrees 1982 and1989, University of Oulu, Finland. After being 10 years in industry she received the Dr. Science (Tech.) degree in Microelectronics (with honours) in 2001. She is Full Professor and the Leader of Microelectronics Research Unit with the focuses on novel ICT electronics, RF applications, sensors, multifunctional micromodules and printed electronics devices. Her research has been financed by Tekes, Academy of Finland, NiCe, EU, ERA.Net ERC with the Advanced Grant. She has over 208 scientific journal publications (2714 citations (without self-citations), h-index 27, WoS on June 2017, and GS: h-index 35, citations 4899).

Dr. Jari Juuti

Jari Juuti received his M.Sc. and D.Sc. degrees in mechanical and electrical engineering from University of Oulu, Finland, in 2000 and 2006, respectively. He was appointed as Docent/Adjunct professor of "Functional Materials their Components and Applications" at the university 2009. Currently he is Academy Research Fellow of Academy of Finland and has contributed/supervised dozens of research projects funded by domestic/international agencies and industry. He is author/co-author of ~80 refereed scientific journal publications, 3 book chapters and 5 patents/patent applications. His research interests include piezoelectric materials, functional composites, actuators, motors and energy harvesters for micromechanical, high frequency and printed electronics applications.